

# UNIVERSITA DEGLI STUDI DI TORINO

Doctoral School in Life and Health Sciences



**PhD in Medical Pathophysiology**

CICLO XXXV

PhD Thesis

**Determine the role of extracellular vesicles in mediating the  
therapeutic effects of mesenchymal stromal cells**

Tutor:  
**Benedetta Bussolati**

PhD Candidate  
**Dott.ssa Renata Skovronova**

**2022**

## Table of Contents

<b>Acknowledgments .....</b>	<b>3</b>
<b>Abstract .....</b>	<b>4</b>
<b><u>Introduction</u> .....</b>	<b>5</b>
<b>Kidney disease.....</b>	<b>6</b>
<b>Ischemic/reperfusion renal injury.....</b>	<b>7</b>
<b>Role of extracellular vesicles in IRI.....</b>	<b>9</b>
<b><u>Study aim</u>.....</b>	<b>33</b>
<b><u>Methods and materials</u>.....</b>	<b>34</b>
<b><u>Results</u>.....</b>	<b>43</b>
<b>Marker Expression in Small and Medium/Large Mesenchymal stromal Cell-Derived Extracellular Vesicles in Naïve or Apoptotic Condition Using Orthogonal Techniques.....</b>	<b>44</b>
<b>Functional properties of MSC EVs from different sources on ischemic renal reperfusion injury.....</b>	<b>63</b>
<b>Characterisation and functional properties of adipose tissue derived MSC products under culture in 2D and in a bioreactor.....</b>	<b>68</b>
<b>Characterisation of EVs at single EV level.....</b>	<b>74</b>
<b><u>Limitations and conclusion</u>.....</b>	<b>80</b>
<b><u>References</u>.....</b>	<b>82</b>

## Acknowledgments

I would like to thank Prof Benedetta Bussolati for the supervision, opportunities, and shared knowledge I have received during my stay in her laboratory and to thank all my thesis reviewers for their valuable suggestions.

I thank Horizon 2020 initiative and the RenalToolBox consortium for the funding. I thank all members of lab 10 in the Molecular Biotechnology Centre in Turin for all their guidance and help. I thank Dr Grange for her daily supervision.

I would specifically like to thank Dr Gebara, Dr Fallo for making my introduction to the new environment smoother, Dr Tassinari, and Dr Verta for very much appreciated support in the last months of my PhD, and to all of them for being great friends.

I would like to thank Sandra Calcat i Cervera and João Faria for their hard work during my secondment in Utrecht. To Sandra and Eleonora Scaccia, I would like to thank them for the work they did with me on the adipose tissue MSC project and their support during the RenalToolBox consortium.

Finally, I sincerely thank my family and my husband for all their moral support, help and time spent listening to my complaints and deprivation when the project didn't work.

## Abstract

Extracellular vesicles released by mesenchymal stromal cells (MSC EVs) are a rising resource for regenerative medicine. Current EVs research focuses on the small MSC EVs enriched fraction for therapeutic applications or amelioration of tissue injury.

In the theoretical part of the present thesis, I present a general introduction on the role of stem cell derived bioproducts and extracellular vesicles on kidney disease, and in particular ischemic reperfusion injury. Two reviews are presented: "Extracellular vesicles, apoptotic bodies and mitochondria: stem cell bioproducts for organ regeneration" and "Stem cell-derived extracellular vesicles and kidney regeneration".

The practical part of my thesis exposes the function and characteristic of extracellular vesicles derived from different sources of mesenchymal stromal cells. Marker Expression in small and medium/large MSC EVs will be compared in naïve or apoptotic condition using orthogonal techniques. Following characterisation, the functional properties of MSC EVs are examined in a renal reperfusion injury model based on conditionally immortalized kidney tubular epithelial cells. To better understand the properties of MSC bioproducts, we further present a functional comparison of adipose MSC EVs and their conditioned medium from different culture conditions. Lastly, the thesis is focused on EV characterisation at single EV level. Two different projects are presented: "Generation of Spike-Extracellular Vesicles (S-EVs) as a Tool to Mimic SARS-CoV-2 Interaction with Host Cells" and "Single extracellular vesicle analysis in human amniotic fluid shows evidence of phenotype alterations in preeclampsia".

# **INTRODUCTION**

# Kidney disease

Global prevalence of chronic kidney disease (Figure 1) in all five stages is currently 13,4% (Lv & Zhang, 2019). More vulnerable to kidney disease are seniors and patients with comorbidities (Charles & Ferris, 2020). Acute renal failure is one of the most common health complications, occurring in up to 24 % mortality of hospitalized patients (Doyle & Forni, 2016). Even a mild form of AKI is associated with a 50% higher risk of death. It also imposes a significant risk of chronic kidney disease and end-stage kidney failure (Abebe, Kumela, Belay, Kebede, & Wobie, 2021; Selby, Fluck, Kolhe, & Taal, 2016).

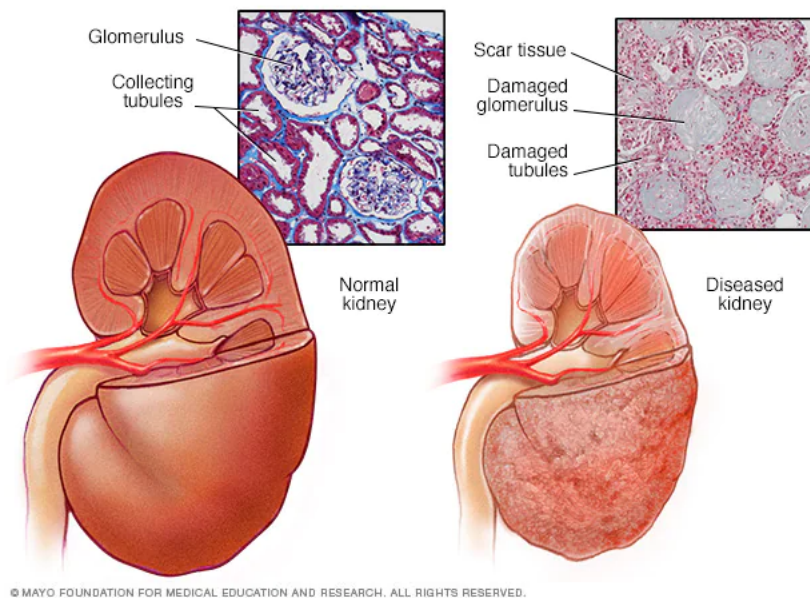


Figure 1: Healthy and diseased kidney illustration (<https://www.mayoclinic.org/diseases-conditions/chronic-kidney-disease/symptoms-causes/syc-20354521>).

# Ischemic/reperfusion renal injury

Kidney ischemia/reperfusion injury (IRI) is the leading cause of acute kidney injury (AKI), which is associated with a high morbidity and mortality rate (Shiva, Sharma, Kulkarni, Mulay, & Gaikwad, 2020). IRI is a major cause of graft failure following kidney transplantation, which is currently the only curative treatment available. The available AKI treatment options are primarily focused on supporting kidney function, necessitating more efficient and precise therapies (Li, Liu, Mao, Li, & Zhou, 2021).

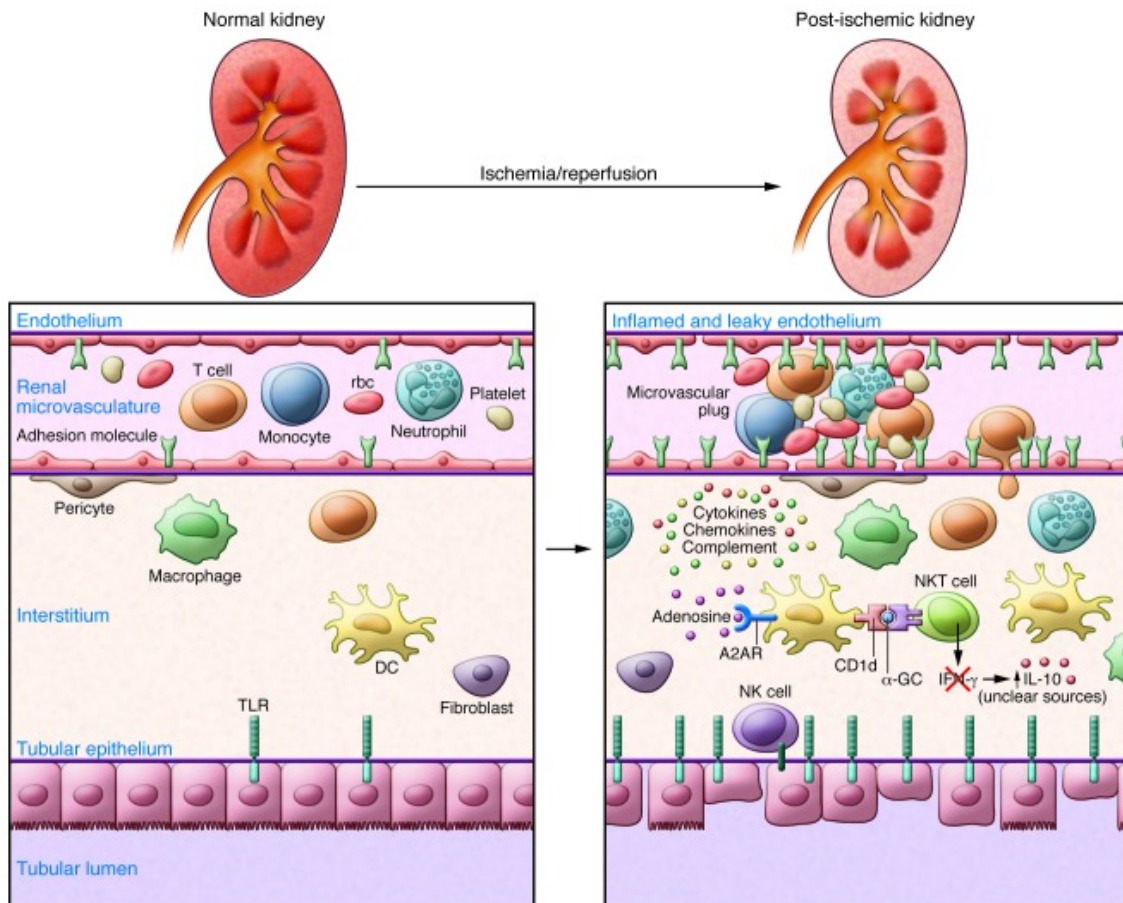


Figure 1: Scheme of normal and post-ischemic kidney and the transformation on cellular base (Rabb, 2012).

Although the pathophysiology of IRI is unknown, several cellular mechanisms that result in AKI have been identified (Figure 2) (Agarwal et al., 2016). First, ischemia occurs due to a temporary restriction in blood flow, which is associated with a decrease in ATP production and

altered metabolism as a result of the hypoxic tissue environment. Reperfusion stimulates mitochondrial oxidative phosphorylation and exacerbates the production of reactive oxygen species (ROS), contributing to oxidative stress and tissue damage (Eltzschig & Eckle, 2011; Malek & Nematbakhsh, 2015).

Within the kidney, proximal tubule cells (PTCs) have the highest mitochondrial mass and are susceptible to hypoxia due to their anatomical location and minimal glycolytic capability, making these cells an ideal candidate for IRI research and therapeutic options (Smith, Hartley, Cochemé, & Murphy, 2012; Zhan, Brooks, Liu, Sun, & Dong, 2013). Following ischemia and ATP depletion, several changes in tubular cells are observed: 1) increased intracellular calcium, 2) disruption of the apical actin cytoskeleton and loss of tight junctions, 3) loss of basolateral Na<sup>+</sup> K<sup>+</sup> ATPase, which plays an essential role in tubular sodium reabsorption, and 4) cell death, which varies between apoptosis and necrosis depending on the duration of ischemia and the damage inflicted (Jassem, Fuggle, Rela, Koo, & Heaton, 2002; Martin, Gruszczyk, Beach, Murphy, & Saeb-Parsy, 2019).

Disturbances in mitochondrial dynamics upon reperfusion are associated with increased fission and decreased fusion. Increased mitochondrial fission causes the mitochondrial permeability transition pore to open and the mitochondrial membrane potential to dissipate, both of which contribute to caspase-3 activation and apoptosis (Jiang et al., 2020). Autophagy is reportedly to be repressed by mitochondrial fission. Hence, preventing mitochondrial damage during early reperfusion can allow for tissue recovery (Brooks, Wei, Cho, & Dong, 2009).



# **Role of extracellular vesicles in ischemic/reperfusion renal injury**

The regenerative capacity of EVs is sustained by a high number of publications, and several pre-clinical studies demonstrate that stem cell-derived EVs promote tissue repair and reduce inflammation in different AKI models (Cantaluppi et al., 2013). The hallmark of AKI is the rapid reduction of renal function in parallel with tubular cell loss, resulting in increased blood urea nitrogen (BUN) and plasma creatinine (Heyman, Rosenberger, & Rosen, 2011). Various sources of MSCs have been used in preclinical results, including bone marrow, adipose tissue, and umbilical cord, with bone marrow-derived MSCs being the most commonly used (Calcatelli-Cervera, Sanz-Nogués, & O'Brien, 2021). MSC's therapeutic effects are derived from their ability to interact and respond to stimuli by releasing soluble factors and extracellular vesicles (EVs) (Figure 3). The use of EVs, has been proposed as an alternative to stem cell therapy for the regeneration of several injured organs (Elahi, Farwell, Nolte, & Anderson, 2020; Heldring, Mäger, Wood, Le Blanc, & Andaloussi, 2015). BM MSC EV source resulted in an effective ischemia/reperfusion injury (IRI) model that mimics hypoxic insult, a common feature during AKI (Gatti et al., 2011; Shen et al., 2016). UC MSC EVs also showed reduced apoptosis, improved proliferation and downregulate CXCL1 which might have protective effect in IRI (Zou et al., 2014).

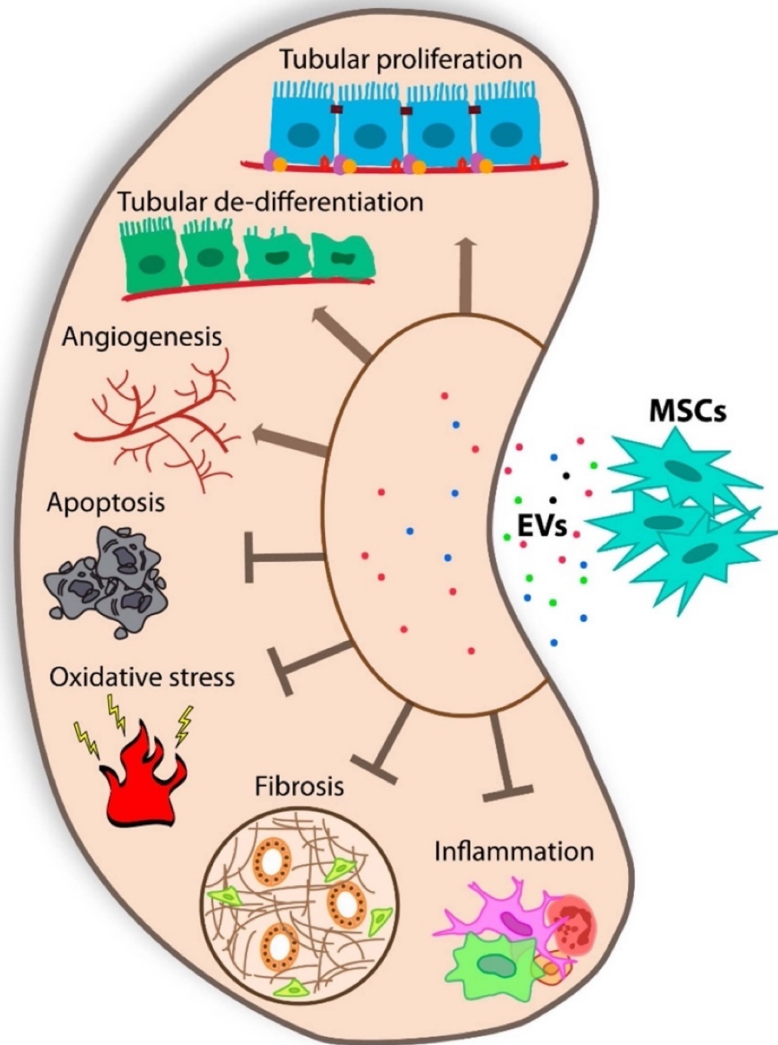


*Figure 2: Schematic representation of the effects of MSC-EVs on renal injury (Grange, Skovronova, Marabese, & Bussolati, 2019).*

I have contributed to two reviews about bioproducts of MSCs (Gebara et al., 2020) and their effects on renal injury (Grange et al., 2019). The first review explains in details the differences among the cell bioproducts such as small EVs, medium/large EVs, mitochondria and apoptotic bodies. The second review focuses on MSC EVs and their regenerative properties in acute kidney injury through tissue regeneration.



## Extracellular Vesicles, Apoptotic Bodies and Mitochondria: Stem Cell Bioproducts for Organ Regeneration

Natalia Gebara<sup>1</sup> · Andrea Rossi<sup>1</sup> · Renata Skovronova<sup>1</sup> · Justine Mariam Aziz<sup>2</sup> · Amish Asthana<sup>2</sup> · Benedetta Bussolati<sup>1,3</sup>

Published online: 27 April 2020  
© The Author(s) 2020

### Abstract

**Purpose of Review** In the current work, we will present the characterization of the main different stem cell-derived vesicular bio-products with potential application in organ regeneration.

**Recent Findings** The therapeutic effects of stem cell therapy in organ repair, specifically those utilizing mesenchymal stromal cells, are largely dependent on the cells' release of different bio-products. Among these bio-products, extracellular vesicles (EVs) appear to play a major role due to their ability to carry and deliver bioactive material for modulation of cellular pathways in recipient cells. Concurrently, mitochondria transfer emerged as a new mechanism of cell communication, in which the bioenergetics of a damaged cell are restored. Finally, apoptotic bodies released by dying apoptotic stem cells contribute to stimulation of the tissue's stem cells and modulation of the immune response.

**Summary** Exploitation of isolated extracellular vesicles, mitochondria and apoptotic bodies in preclinical models of organ damage shows promising results. Here, we describe the results of the pre-clinical applications of stem cell vesicular products, as well as the first clinical trials approaching artificial administration of extracellular vesicles and mitochondria in human subjects and their possible benefits and limitations.

**Keywords** MSC · Regenerative medicine · MicroRNA · Exosomes · Microvesicles · Mitochondrial transfer · Apoptosis

### Introduction

Organ failure is the most frequent cause of morbidity and mortality recorded in Europe and in the United States in recent decades. Organ dysfunction can be attributed to fibrosis, a pathological feature of many chronic inflammatory diseases, as its extensive remodelling of tissues leads to functional insufficiency [1]. The burden associated with fibrosis is disconcerting, representing in the United States almost half, and in

the industrialized world about 30%, of all deaths attributed to fibrotic heart, lung, kidney and liver diseases [1, 2]. In addition, episodes of acute tissue injury, especially if severe and repeated, are closely associated to development of chronic organ disease [3].

It has therefore become of increasing interest in Regenerative Medicine to limit the progression of fibrosis, promote restoration of organ function in chronic settings and support organ repair after acute injury to regain tissue integrity. In this context, increasing studies underline the role of stem cell bio-products, including secreted soluble factors and extracellular vesicles (EVs), as powerful instruments in organ regeneration. EVs, in particular, have been proposed as a new form of intracellular messaging through their ability to reach distant organs and deliver the active cargo necessary for reprogramming of the target cells. In addition, EVs released by apoptotic cells, including apoptotic bodies (ApoBDs), are recently emerging as part of the therapeutic and immune-modulating mechanisms of injected stem cells within injured tissues [4] (Fig. 1).

Finally, stem cell therapy involves the transfer of mitochondria, the organelles responsible for cellular energy production, from stem cells to damaged cells. Mesenchymal stromal cells

Natalia Gebara, Andrea Rossi and Renata Skovronova contributed equally to this work.

This article is part of the Topical Collection on *Cellular Transplants*

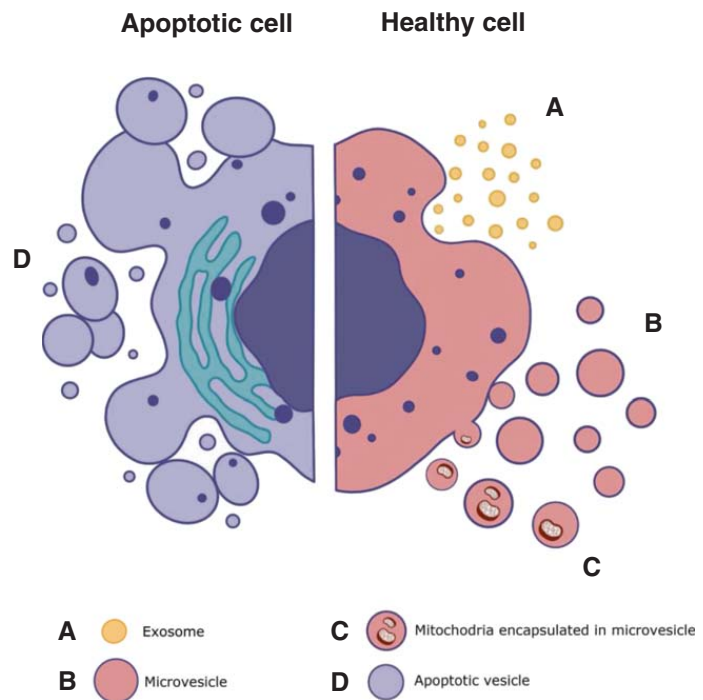
✉ Benedetta Bussolati  
benedetta.bussolati@unito.it

<sup>1</sup> Department of Molecular Biotechnology and Health Sciences, University of Torino, Torino, Italy

<sup>2</sup> Wake Forest Univ. School of Medicine, Winston-Salem, NC, USA

<sup>3</sup> Molecular Biotechnology Centre, University of Torino, via Nizza 52, 10126 Torino, Italy

**Fig. 1** Presentation of apoptotic and healthy cell secretome



(MSCs) are shown to transfer mitochondria to the recipient cells in different ways: encapsulated within EVs [5]; *via* cell-to-cell direct communication through tunnelling nanotubes; or through direct release of “naked” mitochondria into the extracellular microenvironment [6]. The organelle incorporates into the endogenous mitochondrial network of the damaged recipient cell that needs to be rescued, restoring its bioenergetic profile and health [7].

In this review, we will present the recent knowledge on mechanisms of action involved in the therapeutic effects of healthy and apoptotic EVs, as well as of mitochondria transfer, and the exploitation of these bio-products in preclinical models of organ damage. Finally, we will describe the first clinical trials approaching their use on human subjects and the possible benefits and limitations.

### Extracellular Vesicles

Since the ‘discovery’ of EVs in blood plasma in 1946 by Erwin Chargaff and Rudolph West [8], interest in those cells-to-cell communicators has risen in almost all fields of biology and chemistry. EVs have been proven to naturally occur in prokaryotes, eukaryotes, plants and cells. EVs are membrane-bound, spherical particles enclosed in a lipid bilayer. In biological samples, EVs originate

from their parental cell, taking up their internal and external composition. Guidelines from the International Society for Extracellular Vesicles (ISEV) classify three main categories of EVs; exosomes also named small EVs (~30–250 nm), large EVs or microvesicles (~100–1000 nm) and ApoBDs (>1  $\mu\text{m}$ ) [9••]. Small EVs and microvesicles are released from metabolically active cells, whereas ApoBDs are exclusively produced during cell apoptosis [10] (Fig. 1).

The content of an EV is dependent on its origin, size and the route of biogenesis. EV surface markers and cargo are specific to the three types of vesicles (Table 1) and are most commonly associated with the route of vesicle formation. The process of exosome formation begins with inward budding of early endosomes and formation of intraluminal vesicles; this involves the ESCORT complex, ALIX and tumour susceptibility gene 101 (TSG101), all of which are responsible for cargo sorting. Intraluminal vesicles mature into multi-vesicular bodies, followed by fusion with the cell membrane and release of vesicles into the extracellular environment. Alternatively, multi-vesicular bodies are degraded by lysosomes and their components recycled. Exosomes are distinguished by the presence of all three tetraspanin markers responsible for induction of membrane curvature (CD9, CD63 and CD81). Proteins that can be detected and are involved in exosome biogenesis include Rab, GTPases, annexin, flotillin,

**Table 1** Composition, size and biogenesis route of EVs

Vesicle type	Origin	Size	Markers	Components
Exosomes	Endolysosomal pathway; fusion of MVB with cell membrane	30-250 nm	CD9, CD63, CD81 ESCORT components, TSG101, flotillin, Annexin	mRNA, miRNA and other non-coding RNAs; membrane and cytoplasmic proteins, lipids, receptors
Microvesicles	Cell membrane; bud off directly from cell surface	100-1000 nm	CD40	mRNA, miRNA and other non-coding RNAs; membrane and cytoplasmic proteins, lipids, receptors
Apoptotic bodies	Cell Membrane; membrane blebbing during apoptosis	>1µm	Phosphatidylserine, Calreticulin, Calnexin	Nuclear fragments and cell organelles

ALIX, TSG101, VPS4, heat shock protein (HSP70) and the ESCORT complex [11].

Microvesicles are formed by direct budding from the cell plasma membrane with involvement of cytoskeleton components and fusion machinery, though the process is not yet fully understood. Due to their biogenesis pathway, microvesicles are primarily composed of a plasma membrane and of cytosolic-associated proteins. Other commonly found components include heat shock proteins, integrins, post-translationally modified proteins and RNA species. Several structural components are shared between exosomes and microvesicles due to their similar release pathways and origin [11].

EVs have been designated as novel cell-to-cell communicators due to their effect on cells on a paracrine and endocrine level, specifically through the direct stimulation of cell surface receptors and transfer of bioactive molecules. Indeed, EV surface receptors may act as signalling complexes and directly stimulate target cells or, alternatively, transfer functionally active receptors from one cell to another. For instance, bystander B cells can acquire antigen receptors from activated B cells becoming specific activated antigen presenting cells for CD4 T cells [12].

In addition, the presence of a complex cargo (miRNA, RNA, proteins, lipids, cytokines and mitochondria) within EVs results in a multilevel modulation of cell functions in the recipient cells [13, 14]. Small RNA species, including miRNA, are present within EVs and, interestingly, recent studies found that the overall pattern of miRNA content of small and large EVs appears similar but distinctly different from that of the originating cells [15••], implying specific mechanisms of miRNA packaging into EVs. Moreover, extensive proteomic studies on EVs originating from cell cultures, tissue cultures and isolated bio-fluids have shown a significant EV protein content. Online databases created through the collaboration of EV research groups provide us with catalogued EV components, such as Exocarta, ([www.exocarta.org](http://www.exocarta.org)), EVpedia ([www.evpedia.info](http://www.evpedia.info)) and Vesiclepedia ([www.microvesicles.org](http://www.microvesicles.org)). EVs contain many common proteins involved in vesicle trafficking and serving as part of

the cytoskeleton and the plasma membrane. Furthermore, specific protein content reflects the EV mechanism of generation and origin, as well as the cellular state of the EV originating cell. Finally, in addition to the structural functions of lipids in EV membranes, bioactive lipids such as eicosanoids, fatty acids and cholesterol are transferred by EVs to recipient cells. For instance, sphingomyelin has been shown to regulate angiogenesis in vitro and in vivo in tumour derived EVs [16].

### Apoptotic EVs

Apoptosis is commonly known as programmed cell death. An apoptotic cell undergoes several morphological changes: membrane blebbing, membrane protrusion formation and generation of ApoBDs [17–19]. The membrane of ApoBDs reflects the main changes occurring in the cell surface of the apoptotic cell. In particular, apoptotic cells express markers promoting their removal by surrounding cells or macrophages before the cell membrane ruptures [20]. For instance, Calreticulin, an “eat me” ligand is physiologically silenced by the CD47 “don’t eat me” ligand; and only expressed by cells and ApoBDs when CD47 is downregulated [21]. The size of ApoBDs ranges from 1 µm to 5 µm [22, 23]. This characteristic is similar to oncosomes (EVs secreted by cancer cells), but the biogenesis of these vesicles differs [24]. The number of ApoBDs produced per cell was quantified as  $12.87 \pm 3.23$  per hour [25••]. In comparison, the average number of released EVs by mesenchymal stem cells was found to be in the range of 2900 per cell, overnight [26].

During apoptosis, apoptotic microvesicles 0.1–1 µm in diameter and small exosome-like EVs are released [27, 28]. However, these vesicles are less characterized than the ApoBDs.

ApoBDs are characterized by the presence of externalized phosphatidylserine and by a permeable membrane. As mentioned above, they express phagocytosis-promoting signals, such as calreticulin [21] and calnexin [29]. In addition, ApoBDs express chemokines and adhesion molecules, such as CX3CL1/fractalkine and ICAM3, and MHC class II

molecules, allowing for direct antigen presentation to CD4<sup>+</sup> T cells and activation of immunological memory [30]. The cargo of ApoBDs consists of cellular components enclosed during protrusion. Due to this fact, the content of ApoEVs can be very diverse. Indeed, ApoBDs can contain microRNAs, RNA and DNA. Diversity of ApoBDs content affects their physiological properties. ApoBDs can be subdivided into two groups: DNA-carrying ApoBDs and cytoplasm-carrying ApoBDs. 5' phosphorylated blunt-ended DNA can be used as a distinctive marker of DNA-carrying ApoBDs because it is exclusively found in ApoBDs, which undergo apoptosis and contain the DNA fragments [31].

### Mitochondria

While mitochondria are widely considered the powerhouse of the cell, as they are responsible for ATP production through oxidative phosphorylation, these organelles are also involved in several other pathways. They serve a role in pluripotent stem cell maintenance [32], apoptosis and cell death regulation and proliferation capacity through complex interactions between p53 and reactive oxygen species (ROS) production [32]. Energy deprivation and mitochondria dysfunction has been strictly associated with end stage organ disease [33]. Therefore, while metabolic patterns and mitochondria contents can strictly vary among the organs, it appears evident that mitochondrial alterations are closely correlated with most of the clinical conditions that lead to organ failure [34, 35].

As mitochondria do not possess an efficient DNA-repair system [36], these organelles are typically recycled through mitophagy, a form of autophagy [37]. Moreover, the transfer of respiration-competent mitochondria from cell to cell emerged in the past few years [6] as a mechanism of damage repair or cell reprogramming [38]. The physiological mitochondria transfer is a biological phenomenon in which the organelle from a healthy donor cell is relocated into a stressed recipient cell, resulting in repair and survival of the damaged cell. During this process, the mitochondria's small size and plasticity allow it to be transported from donor to recipient cells through transporting mechanisms, such as tunneling nanotubes and microvesicles. The organelle is eventually incorporated into the endogenous mitochondrial network of the recipient cell that needs to be rescued, restoring the cell to its bio-energetic profile and health [39].

The incorporation of respiration-competent mitochondria within released microvesicles has been extensively studied in MSCs, where, once internalized, mitochondria-containing microvesicles can rescue cells from injury or act as reprogramming factors [5, 40••]. In 2012, Islam et al. demonstrated that mitochondria can be transferred in vivo through a mouse model of acute lung injury [38]. Firstly, mitochondria-labelled MSCs were administered by injection into the

damaged lungs. These MSCs homed in the damaged tissue and produced microvesicles containing the labelled mitochondria 4 h post-injection. The microvesicles were then directly transferred into the damage lung cells, resulting in the restoration of their ATP concentrations and secretory responses [38].

PMT has also been observed through the establishment of tunnelling nanotubes (TNTs) [6]. TNTs are filamentous connections formed by protrusions of a cell's membrane and are used to share organelles and contents of the cell's cytoplasm with other cells [41]. The utilization of TNTs in PMT has been observed in transfers between MSCs and macrophages, which served to enhance macrocytosis and activate antimicrobial response [42]. Moreover, Sinclair et al. demonstrated that the transfer of mitochondria via TNTs is essential due to the regenerative capacity exerted by MSCs [41]. However, the role and mechanism of PMT through the establishment of TNTs is poorly understood. The last and least known mechanism of PMT is the direct release of mitochondria in the extracellular microenvironment, usually in response to cell stress. "Naked" mitochondria can be encapsulated in a vacuole and then extruded by apoptotic cells, specifically hepatocytes [43]. Similarly, platelets can release respiration-competent mitochondria as a mediator of innate immune response [44].

### Therapeutic Effects of EVs, ApoBDs and Mitochondria for Organ Regeneration

#### EV Reprogramming of Injured Tissue

Following the emerging interest of stem cell therapy, an increasing number of research and pharmaceutical groups are focusing on stem cell derived EVs, specifically MSC-derived EVs, as a new form of therapeutic agents for organ regeneration and protection [45–48]. Due to the ability of MSC-derived EVs to transfer therapeutic molecules, such as mRNAs, miRNAs and protein, and several of their regenerating effects to MSCs, this source of EVs is one of the most studied in Regenerative Medicine. Moreover, MSCs produce a higher number of EVs in comparison with other stem cells [49]. MSC-derived EVs were proven to modulate the immune system and stimulate regeneration in a multitude of preclinical models, including graft-versus-host-disease, lung, liver, kidney and cardiovascular injury [45]. There are a significant number of studies describing the pro-regenerative effects of stem cell-EVs for organ regeneration, but it is not within the scope of this review to detail all the different preclinical models of application.

As detailed above, the therapeutic effect of stem cell-EVs on organ repair is related to transfer of pro-regenerative proteins or microRNAs. For instance, although numerous factors have demonstrated the therapeutic effects of different EV models and origins, not a single agent emerged as pivotal or

indispensable. Therefore, it can be hypothesized that not a single factor, but rather a synergic and multi-target action of EV components is responsible for the therapeutic EV results. Indeed, the common and characterizing action of therapeutic MSC-EVs can be described as a reprogramming activity on tissue expression profiles. For instance, in models of kidney and liver injury [26], the expression profile of the EV-treated diseased organ, as assessed by RNA sequencing, correlated with that of the normal tissue. Moreover, in models of chronic tissue injury, an upregulation of anti-fibrotic genes and downregulation of pro-fibrotic genes was common to the different diseases as well as stem cell sources [50, 51]. Through modulation of their phenotype and subsequent secretomes, therapeutic utilization of EVs may benefit from an *in vitro* stimulation or manipulation of the generating cell source. For instance, ischemic or hormonal stimulation may ameliorate EV activities [52–54]. In addition, EV administration for chronic diseases might require multiple administrations. The possible development of immune reactions in this setting has not yet been studied in depth.

### Regenerative Effect of Apoptotic Body Phagocytosis

Due to the rapid clearance of damaged cells by immune cells, namely phagocytes, ApoBDs play a major role in immune regulation [30, 55]. ApoBDs are emerging as a pivotal tool in cell-to-cell communication between damaged and healthy cells, therefore modulating mechanisms of organ repair. Indeed, ApoBDs may stimulate proliferation of resident stem/progenitor cells, improving tissue regeneration and replacing damaged cells [25•, 56]. For instance, phagocytosis of the ApoBDs by hepatic stellate cells can promote their differentiation and increase their cell survival [57]. Moreover, ApoBDs' engulfment may support MSC homeostasis. In particular, systemic infusion of exogenous ApoBDs was able to rescue apoptotic MSCs by transferring RNF146 and miR-328-3p and activating the Wnt/ $\beta$ -catenin signalling [58•]. In parallel, in zebrafish, dying epithelial stromal cells of the epidermis were observed to generate Wnt8a enriched ApoBDs, supporting the hypothesis of ApoBDs being biologically active vehicles in cell-to-cell communication [25••]. Neighbouring p63-positive stromal cells engulfed the ApoBDs, which caspase-dependently activated Wnt signalling and stimulated cell proliferation and tissue homeostasis over 24 h. In this model, inhibition of apoptosis significantly reduced the number of proliferating stromal cells. On the contrary, overexpression of the Wnt pathway in combination with apoptosis induced a significant increase of stromal cell proliferation [25••].

ApoBDs can deliver microRNAs, DNA and other genetic material to target cells, resulting in a multitude of different effects. For example, miRNA-126, present in endothelial ApoBDs, promoted chemokine CXCL12 expression in healthy endothelium, and repeated administration of those

ApoBDs in mice with atherosclerosis induced an atheroprotective effect [46].

Although the use of ApoBDs generated in culture as therapeutic has not yet been tested, their role appears of increasing interest in the field of Regenerative Medicine.

### Artificial Mitochondria Transfer

In recent years, artificial mitochondrial transfer (AMT) emerged as a new possible therapeutic option for tissue repair. AMT has been intensively investigated in cardiac disease models. In a rabbit model of cardiac IRI, the injection of viable respiration-competent mitochondria, isolated from donor rabbit cardiac or muscular tissues, was able to significantly reduce the infarct size area, kinase MB, cardiac troponin-I and apoptosis in the regional ischemic zone [47, 48]. AMT has also been recently tested in a mouse model of heterotopic heart transplantation: mitochondria isolated from gastrocnemius muscle were autologously administered in the heart coronary ostium before and after the transplant. Within 24 h after transplant, necrosis and neutrophil infiltration were significantly decreased compared with the vehicle-treated group. Moreover, the mitochondrial treatment significantly enhanced the beating score after transplant [59]. Interestingly, these papers demonstrated both *in vitro* and *in vivo* that fully differentiated cells can be used as a source for the mitochondrial injection.

Moreover, transfer of mitochondria, mainly derived from MSCs, has been proven effective in other pathologic models involving liver, brain and kidney. In a rat model of liver IRI, the intra-splenic administration of MSC mitochondria mitigated the necrosis of hepatocytes as well as reduced the expression of mitochondrial-induced apoptosis markers [60]. In the kidney, the effectiveness of AMT was demonstrated by rescue of damaged renal proximal tubular cells. *In vitro*, the administration of MSC-derived mitochondria reduced ROS production and increased the expression of the tubular marker megalin and mitochondrial superoxide dismutase 2, whereas *in vivo*, both the tubular basement membrane and brush border were protected [61]. Moreover, in normal mice, the administration of mitochondria improved endurance during forced swimming test. Finally, AMT has also been used *in vivo* in a murine model of Parkinson's disease and *in vitro* for the regeneration of damaged hippocampal cells [62, 63].

Although of great novelty, these therapeutic approaches have already started to be applied in the human setting.

### Clinical Trials Involving EVs and Mitochondria Transfer

All the clinical trials concerning MSC-EVs and ATM can be found at [www.clinicaltrials.gov](http://www.clinicaltrials.gov). Although the majority of listed trials focus on the diagnostic properties of EVs, there

are five trials testing the therapeutic applications of MSCs-EVs and two proposing the use of ATM (Table 2).

A first trial is designed to test the anti-inflammatory properties of umbilical cord derived MSCs-EVs to prevent the destruction of pancreatic  $\beta$ -cell islets. The MSCs-EVs will be administered intravenously in two doses, the first dose of exosomes and, after seven days, the second dose of microvesicles (NCT02138331). Two other clinical trials using EVs will involve allogeneic MSCs-EVs. One of them will administer EVs enriched by miR-124 for the treatment of acute ischemic stroke (NCT03384433). The second clinical trial will attempt to treat lesions in patients affected by dystrophic epidermolysis bullosa (NCT04173650). The last clinical trial using EVs that is in the recruiting phase focuses on promoting the healing and recovery of refractory macular holes through direct injection of MSC exosomes to the site of the injury (NCT03437759). Finally, the only concluded trial to date used umbilical cord derived MSCs-EVs to inhibit the progression of chronic kidney disease in patients with grade III-IV CKD [64]. The study showed stabilization of the disease progression, as confirmed by stable levels of glomerular filtration rate, serum creatinine and blood urea in treated patients, and an increased

level of anti-inflammatory factors (TGF- $\beta$ 1 and IL-10) in comparison with the matching placebo group.

The first clinical trial using administration of isolated mitochondria for the treatment of myocardial IRI has also been concluded with positive results [65]. Mitochondria were isolated from non-ischemic skeletal muscles and injected in the myocardium of paediatric patients with myocardial IRI. No adverse effects were detected after AMT, and four out of five patients demonstrated an enhancement in ventricular function [65].

Other clinical trials using AMT are focused on the improvement of infertility treatments (Table 2). Through autologous micro-injection of mitochondria prior to intracytoplasmic sperm injection, the patients' oocyte quality was enhanced. In the first trial, concluded in 2017, mitochondria were isolated from autologous ovarian stem cells and directly injected into the oocytes themselves. To date, no results have been published. Embryo quality has been quantified through the pregnancy rate after treatment and morphological evaluation of the treated embryos. In the second clinical trial, which is still ongoing, mitochondria will be isolated from autologous bone marrow-MSCs and administered immediately before intra-cytoplasmic sperm injection in the oocytes. Live birth

**Table 2** Current clinical trials concerning the use of EVs or AMT as therapeutic agents

	Intervention	N. pts	Follow up	State	Location	Number/Ref.
Diabetes Mellitus type 1	Two doses of MSC-EVs	20	3 months	Unknown	Sahel Teaching Hospital Sahel, Cairo, Egypt	NCT02138331
Chronic kidney disease	Two doses of umbilical cord MSC-EVs (100 $\mu$ g/kg/dose)	20	1 year	Concluded	Sahel Teaching Hospital Sahel, Cairo, Egypt	Nassar et al.
Molecular degeneration	20–50 mg of cord tissue MSC-EVs injected directly around macular hole	44	24 weeks	Recruiting	Tianjin Medical University Hospital Tianjin, China	NCT03437759
Cerebrovascular disorders acute ischemic stroke	Allogeneic MSC-EVs enriched by miR-124	5	12 months	Not recruiting yet	Shahid Beheshti University of Medical Sciences, Tehran, Iran	NCT03384433
Dystrophic Epidermolysis Bullosa	Allogeneic MSC-EVs applied directly to lesions, blisters for 60 days	30	2 months	Not recruiting yet	Aegle Therapeutics, Miami, Florida USA	NCT04173650
Repetition failure	Clinical Application of Autologous Mitochondria Transfer for Improving Oocyte Quality.	50	2-3 years	Not recruiting yet		NCT03639506
Infertility	Amelioration of oocyte quality using autologous mitochondria transfer	59	5 months	Concluded	Valencia, Spain	NCT02586298
IRI	Autologous mitochondrial transfer for dysfunction after ischemia-reperfusion injury	5	6 days	Concluded	Boston, MA, USA	Emani et al.



rate, pregnancy rate, number of oocytes retrieved and fertility rate are going to be evaluated.

## Conclusion

Numerous discoveries within the Regenerative Medicine field have highlighted the bioactivity of stem cell bio-products and their role in cell-to-cell communication. In particular, EVs are the most advanced as potential therapeutic agents due to their ability to modulate the function of targeted cells. Together with stem cell-EVs, proven to be of therapeutic effect in a large variety of pre-clinical models, ApoBDs and AMT can be utilized for selected and specific applications.

The major issue with use of EVs in clinical practice is the standardization of EVs isolation, usage and storage. However, once those issues can be overcome, using EVs as therapeutic agents provides solutions to numerous complications caused by stem-cell therapy, including immune compatibility, maldifferentiation and tumourigenicity. EV therapy allows for dosage control, evaluation of safety and potency equivalent to pharmaceutical agents. In comparison to stem cell therapy, EVs are potentially an easier option as they can be directly obtained from the medium of cultured cells, massively produced and stored without the application of toxic cryopreservative agents and/or loss of EV potency [66]. The biological properties of EV allow for modification of the EV content to obtain desired cell-specific effects. Encapsulation of effector molecules (nucleic acids, lipids and proteins) by EVs allows delivery of its cargo without the risk of degradation. Genetically modified EVs may offer a more effective and natural solution than usage of FDA-approved lipid nanoparticles, which pose a low-dose toxicity upon cell entry [67].

The application of ApoBDs is still poorly explored, as several aspects still require further investigation. For instance, apoptotic vesicles are quite heterogeneous and may have different compositions and properties depending on their size. While EVs released by primary murine aortic endothelial apoptotic cells enhanced inflammation in mice transplanted with an MHC-incompatible graft, ApoBDs did not show this behaviour [28]. Therefore, as increasing experimental evidence suggests, the therapeutic effects of stem cells are due to their clearance by the immune system [4, 68]. For this reason, therapeutic utilization of these cell products appears of interest.

Finally, the use of MSCs as a source of mitochondria for AMT is a novel, therapeutic option that shows regenerative effects in the treatment of acute cell damage. However, more studies are required for better understanding of mitochondria internalization, their fate once inside the injured cells and how mitochondria can survive in the extracellular microenvironment or the blood flow during AMT.

**Acknowledgements** We would like to thank Lola Buono for her contribution to the review by designing Figure 1.

**Funding** This project has received funding from the European Union's Horizon 2020 research and innovation programme under the Marie Skłodowska-Curie grant agreements No. 813839 and 765274.

## Compliance with Ethical Standards

**Conflict of Interest** All authors declare no conflict of interest.

**Human and Animal Rights and Informed Consent** This article does not contain any studies with human or animal subjects performed by any of the authors.

**Open Access** This article is licensed under a Creative Commons Attribution 4.0 International License, which permits use, sharing, adaptation, distribution and reproduction in any medium or format, as long as you give appropriate credit to the original author(s) and the source, provide a link to the Creative Commons licence, and indicate if changes were made. The images or other third party material in this article are included in the article's Creative Commons licence, unless indicated otherwise in a credit line to the material. If material is not included in the article's Creative Commons licence and your intended use is not permitted by statutory regulation or exceeds the permitted use, you will need to obtain permission directly from the copyright holder. To view a copy of this licence, visit <http://creativecommons.org/licenses/by/4.0/>.

## References

Papers of particular interest, published recently, have been highlighted as:

- Of importance
- Of major importance

- 1 Roesnbloom J, Castro SV, Jimenez SA. Review narrative review: fibrotic diseases: cellular and molecular mechanisms and novel therapies. *Ann Intern Med*. 2010;152(3):159–66.
- 2 Jha V, et al. Chronic kidney disease: Global dimension and perspectives. *Lancet*. 2013;382(9888):260–72.
- 3 Chawla LS, Eggers PW, Star RA, Kimmel PL. Acute kidney injury and chronic kidney disease as interconnected syndromes. *N Engl J Med*. 2014;371(1):58–66.
- 4 Galleu A, et al. Apoptosis in mesenchymal stromal cells induces in vivo recipient-mediated immunomodulation. *Sci Transl Med*. 2017;9:416.
- 5 Islam MN, et al. Mitochondrial transfer from bone-marrow-derived stromal cells to pulmonary alveoli protects against acute lung injury. *Nat Med*. 2012;18(5):759–65.
- 6 Caicedo A, Aponte PM, Cabrera F, Hidalgo C, Khoury M. Artificial mitochondria transfer: current challenges, advances, and future applications. *Stem Cells Int*. 2017;2017:7610414.
- 7 Murray LMA, Krasnodembskaya AD. Concise review: intercellular communication via organelle transfer in the biology and therapeutic applications of stem cells. *Stem Cells*. 2019;37(1):14–25.
- 8 Chargaff E, West R. The biological significance of the thromboplastic protein of blood. 1946;166(1):189–97.
- 9•• Théry C, et al. Minimal information for studies of extracellular vesicles 2018 (MISEV2018): a position statement of the International Society for Extracellular Vesicles and update of the MISEV2014

- guidelines. *J Extracell Vesicles*. 2018;7(1). **The paper provides a throughout description of minimal information needed to work with extracellular vesicles as well as their characterisation and description.**
- 10 Akers JC, Gonda D, Kim R, Carter BS, Chen CC. Biogenesis of extracellular vesicles (EV): Exosomes, microvesicles, retrovirus-like vesicles, and apoptotic bodies. *J Neurooncol*. 2013;113(1):1–11.
  - 11 Buzas EI, et al. Biological properties of extracellular vesicles and their physiological functions. 2015;1:1–60.
  - 12 Quah BJC, Barlow VP, McPhun V, Matthaai KI, Hulett MD, Parish CR. Bystander B cells rapidly acquire antigen receptors from activated B cells by membrane transfer. *Proc Natl Acad Sci U S A*. 2008;105(11):4259–64.
  - 13 Chai R, et al. Exosome secreted by MSC reduces myocardial ischemia/reperfusion injury. *Stem Cell Res*. 2010;4(3):214–22.
  - 14 Mathivanan S, Ji H, Simpson RJ. Exosomes: extracellular organelles important in intercellular communication. *J Proteomics*. 2010;73(10):1907–20.
  - 15•• Jeppesen DK, et al. Reassessment of Exosome Composition. *Cell*. 2019;177(2):428–445.e18. **The recent study shows the composition of exosomes to be different than previously thought, thus changing the ideas being exosomes and their potential applications.**
  - 16 Kim CW, Lee HM, Lee TH, Kang C, Kleinman HK, Gho YS. Extracellular membrane vesicles from tumor cells promote angiogenesis via sphingomyelin. *Cancer Res*. 2002;62(21):6312–7.
  - 17 Fadeel B, Orrenius S. Apoptosis: a basic biological phenomenon with wide-ranging implications in human disease. *Br J Cancer*. 1972;26:239–57.
  - 18 Atkin-Smith GK, et al. A novel mechanism of generating extracellular vesicles during apoptosis via a beads-on-a-string membrane structure. *Nat Commun*. 2015;6:7439.
  - 19 Alberts B, Bray D, Alexander J, Lewis J. *Základy buněčné biologie*. Espero: Partizánske; 2006.
  - 20 Depraetere V. 'Eat me' signals of apoptotic bodies. *Nat Cell Biol*. 2000;2(6):2000.
  - 21 Gardai SJ, et al. Cell-surface calreticulin initiates clearance of viable or apoptotic cells through trans-activation of LRP on the phagocyte. *Cell*. 2005;123(2):321–34.
  - 22 Hristov M, Erl W, Linder S, Weber PC. Apoptotic bodies from endothelial cells enhance the number and initiate the differentiation of human endothelial progenitor cells in vitro. *Blood*. 2004;104(9):2761–6.
  - 23 Tixeira R, et al. Defining the morphologic features and products of cell disassembly during apoptosis. *Apoptosis*. 2017;22(3):475–7.
  - 24 Jiang L, et al. Determining the contents and cell origins of apoptotic bodies by flow cytometry. *Sci Rep*. 2017;7(1):1–12.
  - 25•• Brock CK, et al. Stem cell proliferation is induced by apoptotic bodies from dying cells during epithelial tissue maintenance. *Nat Commun*. 2019;10(1):1–11. **This recent study shows that ApoBDs stimulates proliferation of stem cells improving tissue regeneration.**
  - 26 Collino F, et al. AKI recovery induced by mesenchymal stromal cell-derived extracellular vesicles carrying microRNAs. *J Am Soc Nephrol*. 2015;26(10):2349–60.
  - 27 Karpman D, Ståhl AL, Arvidsson I. Extracellular vesicles in renal disease. *Nat Rev Nephrol*. 2017;13(9):545–62.
  - 28 Dieudé M, et al. The 20S proteasome core, active within apoptotic exosome-like vesicles, induces autoantibody production and accelerates rejection. *Sci Transl Med*. 2015;7(318):1–18.
  - 29 Lunavat TR, et al. Small RNA deep sequencing discriminates subsets of extracellular vesicles released by melanoma cells – evidence of unique microRNA cargos. *RNA Biol*. 2015;12(8):810–23.
  - 30 Caruso S, Poon IKH. Apoptotic cell-derived extracellular vesicles: More than just debris. *Front Immunol*. 2018;9:1486.
  - 31 Hauser P, Wang S, Didenko VV. Apoptotic Bodies: Selective Detection in Extracellular Vesicles. *Methods Mol Biol*. 2017;1554:127–41.
  - 32 Folmes CDL, et al. Somatic oxidative bioenergetics transitions into pluripotency-dependent glycolysis to facilitate nuclear reprogramming. *Cell Metab*. 2011;14(2):264–71.
  - 33 Triolo F, Gridelli B. End-stage organ failure: Will regenerative medicine keep its promise? *Cell Transplant*. 2006;15(SUPPL. 1):S3–10.
  - 34 Červinka M. The role of mitochondria in apoptosis induced in vitro. *Gen Physiol Biophys*. 1999;18:33–40.
  - 35 Jassem W, Heaton ND. The role of mitochondria in ischemia/reperfusion injury in organ transplantation. *Kidney Int*. 2004;66(2):514–7.
  - 36 Zinovkina LA. Mechanisms of mitochondrial DNA repair in mammals. *Biochem*. 2018;83(3):233–49.
  - 37 Ding WX, Yin XM. Mitophagy: mechanisms, pathophysiological roles, and analysis. *Biol Chem*. 2012;393(7):547–64.
  - 38 Sinha P, Islam MN, Bhattacharya S, Bhattacharya J. Intercellular mitochondrial transfer: bioenergetic crosstalk between cells. *Curr Opin Genet Dev*. 2016;38(June):97–101.
  - 39 Pacak CA, et al. Actin-dependent mitochondrial internalization in cardiomyocytes: Evidence for rescue of mitochondrial function. *Biol Open*. 2015;4(5):622–6.
  - 40•• Phinney DG, et al. Mesenchymal stem cells use extracellular vesicles to outsource mitophagy and shuttle microRNAs. *Nat Commun*. 2015;6:8472. **In this study phinney et al. shed light on the complex mechanism that allow macrophages to engulf mitochondria from MSCs, in order to increase their bioenergetics after oxidative stress increase.**
  - 41 Sinclair KA, Yerkovich ST, Hopkins PMA, Chambers DC. Characterization of intercellular communication and mitochondrial donation by mesenchymal stromal cells derived from the human lung. *Stem Cell Res Ther*. 2016;7(1):1–10.
  - 42 Jackson MV, et al. Mitochondrial transfer via tunneling nanotubes is an important mechanism by which mesenchymal stem cells enhance macrophage phagocytosis in the in vitro and in vivo models of ARDS. *Stem Cells*. 2016;34(8):2210–23.
  - 43 Nakajima A, Kurihara H, Yagita H, Okumura K, Nakano H. Mitochondrial extrusion through the cytoplasmic vacuoles during cell death. *J Biol Chem*. 2008;283(35):24128–35.
  - 44 Boudreau LH, et al. Platelets release mitochondria serving as substrate for bactericidal group IIA-secreted phospholipase A to promote inflammation. *Blood*. 2014;124(14):2173–83.
  - 45 Mendt M, Rezvani K, Shpall E. Mesenchymal stem cell-derived exosomes for clinical use. *Bone Marrow Transplant*. 2019;54:789–92.
  - 46 Zemecke A, et al. Delivery of microRNA-126 by apoptotic bodies induces CXCL12-dependent vascular protection. *Sci. Signal*. 2009;2(100):1–13.
  - 47 Shi X, Zhao M, Fu C, Fu A. Intravenous administration of mitochondria for treating experimental Parkinson's disease. *Mitochondrion*. 2017;34:91–100.
  - 48 Masuzawa A, et al. Transplantation of autologously derived mitochondria protects the heart from ischemia-reperfusion injury. *Am. J Physiol Hear Circ Physiol*. 2013;304(7):966–82.
  - 49 Gatti S, et al. Microvesicles derived from human adult mesenchymal stem cells protect against ischaemia-reperfusion-induced acute and chronic kidney injury. *Nephrol Dial Transplant*. 2011;26(5):1474–83.
  - 50 Bruno S, et al. HLSC-derived extracellular vesicles attenuate liver fibrosis and inflammation in a murine model of non-alcoholic steatohepatitis. *Mol Ther*. 2020;28(2):1–11.
  - 51 Grange C, Skovronova R, Marabese F, Bussolati B. Stem cell-derived extracellular vesicles and kidney regeneration. *Cells*. 2019;8(10):1240.

- 52 Zhu J, et al. Myocardial reparative functions of exosomes from mesenchymal stem cells are enhanced by hypoxia treatment of the cells via transferring microRNA-210 in an nSMase2-dependent way. *Artif Cells Nanomed Biotechnol.* 2018;46(8):1659–70.
- 53 Lopatina T, Bruno S, Tetta C, Kalinina N, Porta M, Camussi G. Platelet-derived growth factor regulates the secretion of extracellular vesicles by adipose mesenchymal stem cells and enhances their angiogenic potential. *Cell Commun Signal.* 2014;12(1):1–12.
- 54 Zanjani ED, Banisadre M. Hormonal stimulation of erythropoietin production and erythropoiesis in anephric sheep fetuses. *J Clin Invest.* 1979;64(5):1181–7.
- 55 Caruso S, et al. Defining the role of cytoskeletal components in the formation of apoptopodia and apoptotic bodies during apoptosis. *Apoptosis.* 2019;24(11–12):862–77.
- 56 Li B, et al. Bone marrow mesenchymal stem cells protect alveolar macrophages from lipopolysaccharide-induced apoptosis partially by inhibiting the Wnt/ $\beta$ -catenin pathway. *Cell Biol Int.* 2015;39(2):192–200.
- 57 Jiang JX, Mikami K, Venugopal S, Li Y, Török NJ. Apoptotic body engulfment by hepatic stellate cells promotes their survival by the JAK/STAT and Akt/NF- $\kappa$ B-dependent pathways. *J Hepatol.* 2009;51(1):139–48.
- 58• Liu D, et al. Circulating apoptotic bodies maintain mesenchymal stem cell homeostasis and ameliorate osteopenia via transferring multiple cellular factors. *Cell Res.* 2018;28(9):918–33. **The paper shows ApoBDs activates Wnt/ $\beta$ -catenin signalling which can ameliorate MSCs in apoptosis.**
- 59 Moskowitzova K, et al. Mitochondrial transplantation prolongs cold ischemia time in murine heart transplantation. *J Heart Lung Transplant.* 2019;38(1):92–9.
- 60 Lin HC, Liu SY, Lai HS, Lai IR. Isolated mitochondria infusion mitigates ischemia-reperfusion injury of the liver in rats. *Shock.* 2013;39(3):304–10.
- 61 Konari N, Nagaishi K, Kikuchi S, Fujimiya M. Mitochondria transfer from mesenchymal stem cells structurally and functionally repairs renal proximal tubular epithelial cells in diabetic nephropathy in vivo. *Sci Rep.* 2019;9(1):1–14.
- 62 Chien L, Liang MZ, Chang CY, Wang C, Chen L. Mitochondrial therapy promotes regeneration of injured hippocampal neurons. *Biochim Biophys Acta - Mol Basis Dis.* 2018;1864(9):3001–12.
- 63 Shi X, Zhao M, Fu C, Fu A. Intravenous administration of mitochondria for treating experimental Parkinson's disease. *Mitochondrion.* 2017;34:91–100.
- 64 Nassar W, et al. Umbilical cord mesenchymal stem cells derived extracellular vesicles can safely ameliorate the progression of chronic kidney diseases. *Biomater Res.* 2016;20(21):1–11.
- 65 Emani SM, Piekarski BL, Harrild D, del Nido PJ, McCully JD. Autologous mitochondrial transplantation for dysfunction after ischemia-reperfusion injury. *J Thorac Cardiovasc Surg.* 2017;154(1):286–9.
- 66 Ohno SI, Drummen GPC, Kuroda M. Focus on extracellular vesicles: Development of extracellular vesicle-based therapeutic systems. *Int J Mol Sci.* 2016;17(2):172.
- 67 Murphy DE, et al. Extracellular vesicle-based therapeutics : natural versus engineered targeting and trafficking. *Exp Mol Med.* 2019;51:1–12.
- 68 Vagnozzi RJ, et al. An acute immune response underlies the benefit of cardiac stem-cell therapy. *Nature.* 2019;577:405–9.

**Publisher's Note** Springer Nature remains neutral with regard to jurisdictional claims in published maps and institutional affiliations.



Review

# Stem Cell-Derived Extracellular Vesicles and Kidney Regeneration

Cristina Grange <sup>1</sup>, Renata Skovronova <sup>2</sup>, Federica Marabese <sup>2,3</sup> and Benedetta Bussolati <sup>2,\*</sup>

<sup>1</sup> Department of Medical Sciences, University of Turin, via Nizza 52, 10126 Torino, Italy; cristina.grange@unito.it

<sup>2</sup> Department of Molecular Biotechnology and Health Sciences, University of Turin, via Nizza 52, 10126 Torino, Italy; renata.skovronova@unito.it (R.S.); federica.marabese@edu.unito.it (F.M.)

<sup>3</sup> Maria Pia Hospital, 10132 Turin, Italy

\* Correspondence: benedetta.bussolati@unito.it; Tel.: +39-011-6706453; Fax: +39-011-6631184

Received: 20 September 2019; Accepted: 11 October 2019; Published: 11 October 2019



**Abstract:** Extracellular vesicles (EVs) are membranous vesicles containing active proteins, lipids, and different types of genetic material such as miRNAs, mRNAs, and DNAs related to the characteristics of the originating cell. They possess a distinctive capacity to communicate over long distances. EVs have been involved in the modulation of several pathophysiological conditions and, more importantly, stem cell-derived EVs appear as a new promising therapeutic option. In fact, several reports provide convincing evidence of the regenerative potential of EVs released by stem cells and, in particular, mesenchymal stromal cells (MSCs) in different kidney injury models. Described mechanisms involve the reprogramming of injured cells, cell proliferation and angiogenesis, and inhibition of cell apoptosis and inflammation. Besides, the therapeutic use of MSC-EVs in clinical trials is under investigation. This review will focus on MSC-EV applications in preclinical models of acute and chronic renal damage including recent data on their use in kidney transplant conditioning. Moreover, ongoing clinical trials are described. Finally, new strategies to broaden and enhance EV therapeutic efficacy by engineering are discussed.

**Keywords:** AKI; CKD; exosomes; regenerative medicine; renal injury

## 1. Introduction

Renal failure is one of the most significant causes of mortality and morbidity all over the world [1]. Acute kidney injury (AKI) is a major clinical problem, affecting up to 5% of all hospitalized patients with acute illness, thus having a great impact on public health resources [2]. AKI is traditionally defined by a rapid decline of renal function, which clinically manifests as an increase of urea and creatinine in serum, associated with disruption of salt and water homeostasis. More importantly, about 8% to 16% of patients with AKI progress to chronic renal failure [3]. There is evidence that even a single episode of AKI predisposes the kidney to maladaptive response to injury leading to progressive loss of function and the development of chronic kidney disease (CKD) [4,5]. In parallel, the incidence of CKD has increased, mainly due to the enhanced prevalence of diabetes and obesity [6]. The current therapies for CKD concentrate on slowing disease progression and, despite beneficial effects, are not sufficient to counteract the disease evolution. A large proportion of patients with end-stage renal disease undergo hemodialysis and/or renal replacement therapy, the latter option with high costs and significant limitation in organ availability [7,8]. Finding new therapeutic strategies for AKI and CKD remains an ongoing quest. In the last decades, innovative stem cell therapies have been tested both as preclinical development and in pilot clinical trials, demonstrating the efficacy of these novel approaches [1,5,9]. More recently, extracellular vesicles (EVs), bioproducts released physiologically

from almost all cells, have generated great interest in Regenerative Medicine [10–13]. This review focuses on stem cell-derived EVs as a new therapeutic option for renal injury repair, with the main focus on mesenchymal stromal cell-derived EVs (MSC-EVs) from different organs.

## 2. Extracellular Vesicles

In the last decade, many studies have characterized new mechanisms of cell-to-cell communication, capable of influencing the phenotype of target cells through the release of bioactive factors [14]. Among all soluble mediators of paracrine communication, EVs possess a central role in both physiological and pathological conditions [15]. EVs are membranous vesicles released by cells of prokaryotic, eukaryotic, and plants, in an evolutionarily conserved manner. Vesicles are heterogeneous in size, sedimentation rate, flotation density, and composition [14,16]. The importance of EVs involves their ability to transfer biologically active molecules and genetic information to other target cells, influencing their function. The first study on EVs appeared many years ago, thanks to Chargaff and West [17], focusing on blood debris. Afterwards, many groups discussed the possibility to consider EVs as cellular discards or bioactive vesicles. It is now well established that EVs interact with cells, inducing target cell stimulation directly or by transferring bioactive molecules [18–20]. One of the most significant advances in the role of EVs emerged when EVs were shown to shuttle selected pattern of RNAs transferred to recipient cells and were able to modulate their protein expression pattern [19,21,22]. EVs can be isolated not only from most of the cell types but also from the majority of biological fluids, such as saliva, urine, nasal and bronchial lavage fluids, amniotic and seminal fluids, breast milk, plasma, and serum [23]. In 2011, to confirm the central role of EVs in the regulation of biological processes, the International Society for Extracellular Vesicles (ISEV) was instituted to unify nomenclatures and methodologies for EV isolation and characterization [24–27].

### *EV Composition and Biogenesis*

As described in the previous chapter, EVs are very heterogeneous and based on their origin and size; we can distinguish small-size EVs, medium-, and/or large-size EVs [28].

Small-size EVs, previously called exosomes, are vesicles between 30 to 100 nm. They derive from the multivesicular bodies by fusing with the endosomal membranes and are released into the extracellular space [29]. Medium- and/or large-size EVs, also known as microvesicles/ectosomes, are between 50 to 1000 nm. This size range includes different populations of vesicles released by healthy cells up to 200 nm and larger pre-apoptotic bodies. Medium- and/or large-size EVs develop by budding of the plasma membrane [30]. Finally, apoptotic bodies are large-size vesicles from 1 μm up to 5 μm and are shed from the blebbing of the plasma membrane of apoptotic cells [31].

EVs express surface markers specific to their cellular origin and secretion mechanisms. Markers can be distinctive for one group or common for all of them. For example, tetraspanins such as CD9, CD81, and CD63 proteins involved in membrane curvature, are particular to small-size EVs [28]. Moreover, small-size EVs are characterized by the presence of proteins involved in biogenesis, such as Rab, GTPase, annexin, flotillin, components of the endosomal sorting complex required for transport (ESCRT), auxiliary proteins, (ALIX, TSG101, VPS4) and heat shock proteins (HSP70 and HSP90). Medium- and/or large-size EVs express CD40 ligand [29,32] and Annexin A1 [33], while Annexin V is specific for apoptotic bodies [33,34]. Besides, all EV types contain different forms of lipids, such as cholesterol, diglycerides, sphingolipids (including sphingomyelin and ceramide), phospholipids, and glycerophospholipids, fundamental for EV structure [35]. Various types of genetic materials are present within EVs such as noncoding RNAs, mRNAs, miRNAs, and DNAs, each one able to regulate target gene expression at the posttranscriptional level [36]. The expression of miRNAs within EVs, compared with that of originating cells, can be significantly different, suggesting an active and still partially unknown compartmentalization process [33]. The miRNA content exhibits an important role in the biological function of EVs; in fact, it has been shown that they may modulate cell cycle, apoptosis, migration, inflammation, and angiogenesis [37,38].

### 3. MSC-EVs and Tissue Regeneration

The growing evidence in Regenerative Medicine supports the hypothesis that stem cells exert their therapeutic effect by a paracrine/endocrine manner rather than a direct repopulation of the injured tissues [39–42]. This postulate was strongly supported by numerous *in vivo* studies demonstrating that the therapeutic benefit of stem cells is orchestrated by their secretome, composed by growth factors, cytokines, chemokines, and EVs [13]. In particular, regarding renal regeneration, Bi et al. [43] showed that the injection of conditioned media from MSCs limits apoptosis and enhances proliferation of tubular cells after a toxic injury, thus promoting kidney repair. The use of EVs, and in particular stem cell-derived EVs, has been proposed as an alternative to stem cell therapy for the regeneration of several injured organs [9,41,44]. MSC-EVs may be isolated from MSCs of different adult tissues such as bone marrow, adipose tissue, peripheral blood, and neonatal birth-associated tissues including placenta, umbilical cord, and cord blood [45]. They are characterized by the expression of the typical mesenchymal stromal markers which include CD44, CD73, CD90, CD105, and CD146 [46].

Moreover, the use of EVs presents many advantages compared with their originating cells, like higher safety profile, lower immunogenicity, and the unfeasibility to maldifferentiate [47–49]. They display excellent biological tolerance, an important requirement for therapeutic applications [50]. In addition, EVs possess unique targeting and delivering features as they may be rapidly internalized into target cells [51].

### 4. MSC-EVs and Acute Kidney Injury

The regenerative capacity of EVs is sustained by a high number of publications, and several pre-clinical studies demonstrate that stem cell-derived EVs promote tissue repair and reduce inflammation in different AKI models (Table 1) [52]. The hallmark of AKI is the rapid reduction of renal function in parallel with tubular cell loss, resulting in increased blood urea nitrogen (BUN) and plasma creatinine [53]. In 2009, Bruno et al. [54] demonstrated that the effect of bone marrow (BM) MSC-EVs was superimposable to the one of the originating cells in a model of AKI induced by glycerol injection. BM MSC-EVs accelerate the recovery of injured tubular cells, promoting cell proliferation and protecting cells from apoptosis (Figure 1) [9]. Since that work, many studies have been conducted to confirm the beneficial effect of EVs in several AKI models, and related mechanisms have been explored. At present, it is well recognized that EV activity mainly involves the horizontal transfer of genetic materials [54–57]. BM MSC-EVs carry specific mRNAs that, in turn, stimulate recipient injured cells for re-entry into the cell cycle [54]. Another group demonstrated that the transfer of human IGF-1 receptor mRNA, present in BM MSC-EVs, to tubular cells is fundamental to trigger renal recovery [58].

Moreover, it has been demonstrated that Droscha-knockdown MSCs release ineffective EVs, tested in *in vivo* AKI model, sustaining a central role of miRNA cargo [57]. MSC-EVs isolated from bone marrow cells were also tested in toxic AKI models, induced by cisplatin and gentamycin [59,60]. In all toxic models, BM MSC-EVs ameliorated renal function and reduced the classical histological lesions of the disease [4]. The same EV source resulted in an effective ischemia/reperfusion injury (IRI) model that mimics hypoxic insult, a common feature during AKI [61,62]. The effect of MSC-EVs isolated from other tissues was also tested in several AKI models. Similar positive results were obtained using cord blood MSC-EVs that promoted tubular cells dedifferentiation and growth, and Warton Jelly MSC-EVs, that stimulated proliferation and reduced inflammation and apoptosis via mitochondrial protection [63–66] (Figure 1). In addition, EVs obtained from glomerular MSCs and liver MSCs, human liver stem cells (HLSCs), resulted in protection from AKI [67–69]. Altogether these data indicate that MSC-EVs, isolated from different sources, are effective in the amelioration of preclinical models of AKI, targeting multiple aspects of the disease, stimulating cell proliferation, and reducing apoptosis, inflammation, and oxidation [4,9] (Figure 1).

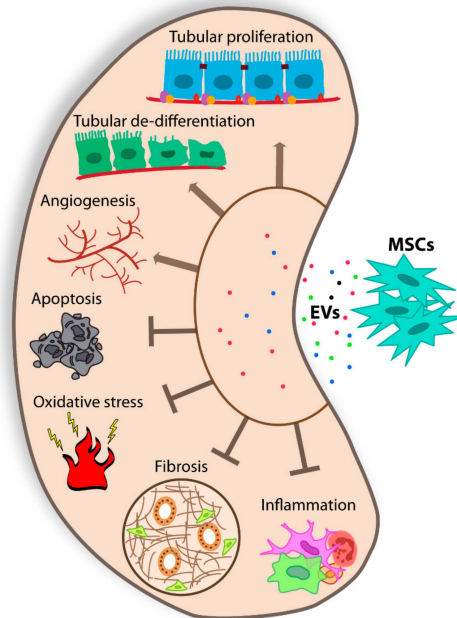


Figure 1. Schematic representation of the effects of MSC-EVs on renal injury.

### 5. Conditioning of the Kidney Transplant

Renal transplantation is significantly improving the quality of life of patients with end-stage renal disease; however, chronic allograft nephropathy limits the organ survival and more than one transplant might be required during patient life. The uses of MSCs and MSC-EVs are tested in various clinical protocols related to transplantation, to favor tolerance and to prolong allograft survival [70]. The preconditioning of a kidney with MSCs and MSC-EVs may be another interesting option to limit tissue damage due to ischemia-reperfusion injury and chronic allograft nephropathy. MSCs and MSC-EVs were tested in a rat model of kidney donation after cardiac death (DCD). DCD kidneys treated with MSC-EVs during organ cold perfusion (4 h), showed significantly lower signs of renal damage [71]. In addition, treated kidneys increased energy consumption with up-regulation of the enzymes involved in energy metabolism [71]. This approach is gaining increased interest for the pre-transplant graft perfusion in several organs, as it appears to be able to abrogate or strongly reduce ischemic injury.

### 6. MSC-EVs and Chronic Kidney Disease

Several preclinical models are available to mimic the broad range of pathologies defined as CKD. The severity of CKD can manifest itself over time depending on numerous causes. One of the trigger causes is diabetes [72]. Hyperglycemia induces a cascade of events resulting in glomerular and tubule-interstitial fibrosis, with podocyte damage/loss and mesangial cell hypertrophy, a hallmark of diabetic nephropathy. The progression of fibrosis is the leading cause of renal dysfunction not only for diabetic nephropathy but also for other CKDs [73,74]. In this scenario, several groups tested in animal models of CKD, different doses, number, and timing of EV administration, with the intent to set optimal EV regimen (Table 1). EVs isolated from urinary MSCs have been described as effective in the prevention of CKD progression by inhibiting apoptosis in a rat model of diabetic nephropathy induced by streptozotocin injection [75]. EVs induce a reduction of urine volume and apoptosis of podocyte and tubular epithelial cells (Figure 1). Urinary MSC-EVs carry transforming growth factor- $\beta$ 1, angiogenin,

and bone morphogenetic protein-7, drivers of the observed reno-protective activity [75]. In addition, the direct administration of MSC exosomes under the renal capsule generated a rapid improvement of renal morphology, demonstrated in the same animal model [76]. Recently, EVs isolated from BM MSCs and from liver MSCs have been shown to be effective in the reversion of renal fibrosis in an already established diabetic nephropathy model [8]. MSC-EVs and HLSC-EVs contain a selection of antifibrotic miRNAs able to downregulate profibrotic genes, restoring normal renal function [8]. Similar positive results were obtained by multiple injections of HLSC-EVs in a CKD model induced by aristolochic acid [77].

Other in vivo models of CKD are the surgical five-sixth resection of the kidney tissue and the obstruction of the ureter, leading to glomerulosclerosis and fibrosis [78]. In both CKD models, multiple injections of BM MSC-EVs prevented renal failure [79,80]. In a similar model, combined with diet, multiple administrations of a conditioned medium, purified from human embryonic MSCs, slowed the deterioration of renal function [81]. Moreover, in a porcine model of metabolic syndrome and renal artery stenosis, a single intrarenal administration of adipose tissue-derived MSC-EVs reduced renal inflammation and fibrosis by delivery of IL10 [82].

The robustness of preclinical data about the therapeutic efficacy of MSC-EVs in acute and chronic models is encouraging to go further towards clinical studies.

**Table 1.** Mesenchymal stromal cell-extracellular vesicle (MSC-EV) administration in animal models of renal damage. EVs released by MSCs derived from different tissues are effective in models of acute kidney injury (AKI) and chronic kidney disease (CKD). EV sources, animal models, doses, and route of administration are listed. Abbreviation: IRI Ischemia Reperfusion Injury.

MSC Origin	In vivo Models	Type of Injury	Injection	Administration	References
Bone Marrow	Glycerol	AKI	Single: 15 µg Single: $2.2 \times 10^8$	Intravenously	Bruno et al. [54] Collino et al. [57]
	IRI	AKI	Single: 30 µg	Intravenously	Gatti et al. [61]
	Cisplatin	AKI	Single: 100 µg	Intravenously	Bruno et al. [59]
	Gentamicin	AKI	Multiple: 100 µg	Intravenously	Reis et al. [60]
	IRI	AKI	Single: 200 µg	Into renal capsule	Shen B et al. [62]
	IRI	CKD	Single: 30 µg	Intravenously	Gatti et al. [61]
	Cisplatin	CKD	Multiple: 100 µg followed by 50 µg every 4 days	Intravenously	Bruno et al. [59]
	Remnant kidney	CKD	Single: 30 µg	Caudal vein	He et al. [79]
	Type 1 diabetes	CKD	Single: $5.3 \times 10$ exosomes	Renal subcapsular	Nagaishi et al. [76]
	Unilateral ureteral obstruction	CKD	Single: 30 µg	Caudal vein	He et al. [80]
Type 1 diabetes	CKD	Multiple: $1 \times 10^{10}$ /dose	Intravenously	Grange et al. [8]	
Cord blood	Cisplatin	AKI	Single: 200 µg	Caudal vein	Zhou et al. [63]
	IRI	AKI	Single: 30 µg	Caudal vein	Ju et al. [65]
Warton Jelly	IRI	AKI	Single: 100 µg	Caudal vein Caudal vein	Zou et al. [64] Gu et al. [66]
	IRI	AKI	Single: $2 \times 10^7$	Intravenously	Choi et al. [68]
Renal	IRI	AKI	Single: $400 \times 10^6$	Intravenously	Ranghino et al. [67]
	Glycerol	AKI	Single: $1.88 \pm 0.6 \times 10^9$ Single: $5.53 \pm 2.1 \times 10^9$	Intravenously Intravenously	Herrera Sanchez et al. [69]
Liver	Aristolochic acid nephropathy	CKD	Multiple	Intravenously	Kholia et al. [77]
	Type 1 diabetes	CKD	Multiple: $1 \times 10^{10}$ /dose	Intravenously	Grange et al. [9]
Urine	Type 1 diabetes	CKD	Multiple: 100 µg weekly 12 times	Intravenously	Jiang et al. [75]



Table 1. Cont.

MSC Origin	In vivo Models	Type of Injury	Injection	Administration	References
Embryonic	Remnant kidney and specific diet L-N <sup>G</sup> -nitroarginine and 6% NaCl	CKD	Multiple: 7 µg twice daily for 4 consecutive days	Intravenously	Van Koppen et al. [81]
Adipose tissue	Porcine model of metabolic syndrome and renal artery stenosis	CKD	Single: 1 × 10 <sup>10</sup>	Intra renal	Eirin et al. [82]

## 7. MSC-EVs and Clinical Trials

The translation of EV-based therapy into clinical practice requires the clarification of several critical issues [13]. The major one to be considered is the identification of optimal protocols for EV production, isolation, and storage [13]. Similarly, the determination of potency assays to test the efficacy of each EV batch is mandatory. In fact, the majority of approved clinical trials implying EVs (listed in [www.clinicaltrials.gov](http://www.clinicaltrials.gov)) focus on diagnostic purposes. However, at present, there are four clinical trials involving MSC-EVs for therapeutic use (Table 2). Two of them are designed by Nassar et al. [83] at the Sahel Teaching Hospital of the University of Cairo. Both trials imply the use of EVs isolated from cord blood MSCs [83]. The first study aims to evaluate the effect of consecutive doses of MSC-EVs in 20 patients with type 1 diabetes, with a follow up of three months [13]. The results are not available yet. The second study enrolled 20 patients with CKD and results are already published [83]. The authors observed an improvement of renal function with amelioration of glomerular filtration, proteinuria, and BUN in patients one year after EV administration (two doses). Moreover, EVs displayed an anti-inflammatory activity, decreasing TNF-α and increasing IL-10. The results of this clinical study are promising in terms of feasibility and efficacy for MSC-EV therapeutic use. Another potential application in which preclinical studies are robust and convincing is the use of MSC-EVs to promote macular regeneration. There is an ongoing clinical trial in China focusing on the safety and efficacy of exosomes isolated from cord tissue-derived MSCs in patients with refractory macular holes in the eye. Finally, a clinical trial, which involves the injection of MSC-EVs engineered with miR-124 for the treatment of patients after acute ischemic stroke, was approved in Iran,

The number of clinical trials on EVs as a therapeutic strategy will increase enormously in the next years and, hopefully, their use will enter into clinical practice.

**Table 2.** Clinical trials using MSC-EVs for therapeutic purposes. Application, dose, number of patients, and follow-up are listed. Moreover, identification number and state of trial are reported.

Disease	Intervention	N. Pats	Follow Up	State	Location	Number/Ref.
Diabetes Mellitus Type 1	Two doses of MSC-EVs	20	3 months	Unknown	Sahel Teaching Hospital Sahel, Cairo, Egypt	NCT02138331
Chronic kidney disease	Two doses of umbilical cord MSC-EVs (100 µg/kg/dose)	20	1 year	Concluded	Sahel Teaching Hospital Sahel, Cairo, Egypt	Nassar et al. [83]
Macular degeneration	20–50 mg of cord tissue MSC-EVs injected directly around macular hole	44	24 weeks	Recruiting	Tianjin Medical University Hospital Tianjin, China	NCT03437759
Cerebrovascular disorders acute ischemic stroke	Allogenic MSC-EVs enriched by miR-124	5	12 months	Not yet recruiting	Shahid Beheshti University of Medical Sciences, Teheran Iran	NCT03384433

## 8. EV Engineering and Future Strategies

In the constant quest to broaden the therapeutic applications of EVs, further approaches focused on the enhancement of EV efficacy by engineering. The natural origin of EVs, along with their spheroid shape and cargo ability, makes them ideal candidates for the efficient loading of therapeutic molecules [84]. The strategy to engineer EVs with pro-regenerative molecules or specific drugs is

currently gaining an increasing interest [85]. EVs may be engineered to potentiate their therapeutic cargo by increasing the levels of active molecules (proteins or RNAs) already present within EVs or to modify their biodistribution/stability by changing the composition of surface molecules. The strategy to deliver therapeutic RNAs possesses an excellent potential and a wide range of applicability; however, the polar RNA molecules are exposed to rapid digestion by extracellular RNases [50,86]. The use of synthetic nanoparticles has also been explored with some limitations [87,88]. For these reasons, EVs are the central point of intense research [50]. At present, the existing methods for EV engineering are divided into two categories: Direct and indirect methods, indicating the direct modification of the EVs or the engineering of the cell of origin used for EV production.

Direct EV engineering can be done with multiple techniques: Incubation, electroporation, sonication, freeze/thaw cycles, and saponin-assisted method without significantly impairing EV constitution and functionality (Figure 2) [89]. The incubation is a passive method preferred for the loading of hydrophobic compounds, with a higher efficiency compared to those obtained with liposomes. The reason may be the presence of particular domains within EV membranes, absent in artificial membranes of liposomes [90]. Sun et al. [91], for example, mixed purified EVs with curcumin, a natural compound with antioxidant and anti-inflammatory activities, and they demonstrated an increased efficacy compared with those of naive EVs when injected into mice with septic shock.

Exogenous genetic material (small RNAs or miRNAs) is generally added to EVs using electroporation, as they are hydrophilic molecules. To define the most efficient protocol, Pomatto et al. [92] tested different voltages and number of pulses and described 750 V and 10 pulses as the optimal one, with the highest RNA loading without significant EV damage [92].

As an example, a non-coding RNA (Lnc-RNA-H19) has been transfected into high-yield nano-EVs to create an effective drug delivery system for wound healing in diabetics [93]. In addition, sonication or cycles of a deep freeze and then slow thaw are two alternative methods for inserting different molecules into isolated EVs [94,95]. Moreover, it has also been shown that the saponin-assisted encapsulation method allows the highest loading efficacy and protection versus protease degradation [89]. All options mentioned above can be combined to improve final loading efficacy. The modification of the genome by CRISPR/Cas technology, which alone has low efficacy of delivery, is a new potential tool to be inserted into EVs by electroporation [96].

The second category of engineering technology is based on the modification of EV originating cells that allows subsequent isolation of EVs, which already express the desired molecule. For example, it has been demonstrated in an in vivo model of unilateral ureteral obstruction that MSCs engineered to overexpress miRlet7c selectively localize into the injured kidney and upregulate miR-let7c expression, attenuating kidney injury. Similarly, exosomes derived from engineered MSCs were able to selectively transfer miR-let7c to damaged kidney cells resulting in antifibrotic functions [97]. In a similar approach, MSCs were engineered to overexpress pro-regenerative miRNAs, such miR10a, miR127, and miR486, and deriving EVs were tested in models of acute renal injury [98]. EVs obtained from engineered MSCs were more effective than EVs derived from naive MSCs when used at low doses [98].

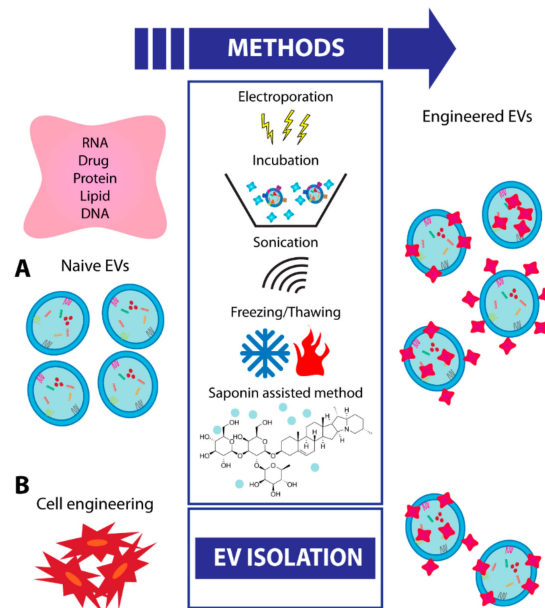


**Figure 2.** Schematic representation of different procedures for EV engineering. (A) Schematic representation of techniques for engineering EVs after their isolation (direct method). (B) Schematic representation of cell engineering followed by EV isolation (indirect method).

## 9. Conclusions

The number of studies on the use of EVs, especially those derived from MSCs, for the treatment of AKI and CKD is continuously increasing, and EVs are considered a promising approach for tissue regeneration. The pro-regenerative effect of EVs is now well established for AKI, sustained by convincing results in a large number of different experimental models. The regenerating role of MSC-EVs in the slowdown of CKD, at variance, is still limited to a restricted number of preclinical models and should be better investigated. The translation of this approach for clinical use, based on ongoing and future clinical trials, will open a new scenario in Regenerative Medicine. Finally, EVs could be further exploited as a carrier for the delivery of exogenous materials such as RNAs, proteins or existing small drugs. An accurate setting of therapeutic doses and schedule are still needed.

**Author Contributions:** All the authors read the article and approved the final version.

**Funding:** This research was funded by the IRMI “Italian Regenerative Medicine Infrastructure” program (Italian Ministry of Health CTN01 00177 88744) and by Regione Piemonte POR FESR 2014/2020—Bando Piattaforma Tecnologica Salute e Benessere—Project “Terapie Avanzate per Processi Fibrotici Cronici (EVER).” And by the European Union’s Horizon 2020 research and innovation programme under the Marie Skłodowska-Curie grant agreement No 813839, project RenalToolBox.

**Acknowledgments:** We thank Natalia Gebara for language editing.

**Conflicts of Interest:** None of the other authors has any conflict of interest.

## References

- Li, J.S.; Li, B. Renal Injury Repair: How About the Role of Stem Cells. *Adv. Exp. Med. Biol.* **2019**, *1165*, 661–670.
- Pozzoli, S.; Simonini, M.; Manunta, P. Predicting acute kidney injury: Current status and future challenges. *J. Nephrol.* **2017**, *31*, 209–223. [[CrossRef](#)] [[PubMed](#)]

3. Rewa, O.; Bagshaw, S.M. Acute Kidney injury-epidemiology, outcomes and economics. *Nat. Rev. Nephrol.* **2014**, *10*, 193–207. [[CrossRef](#)] [[PubMed](#)]
4. Grange, C.; Iampietro, C.; Bussolati, B. Stem cell extracellular vesicles and kidney injury. *Stem Cell Investig.* **2017**, *4*, 90. [[CrossRef](#)] [[PubMed](#)]
5. Tetta, C.; Weiss, S.; Grange, C.; Camussi, G. Adult Stem Cells and Extracellular Vesicles in Acute and Chronic Kidney Injury. *Curr. Regen. Med.* **2016**, *6*, 2–15. [[CrossRef](#)]
6. Cho, N.H.; Shaw, J.E.; Karuranga, S.; Huang, Y.; da Rocha Fernandes, J.D.; Ohlrogge, A.W.; Malanda, B. IDF Diabetes Atlas: Global estimates of diabetes prevalence for 2017 and projections for 2045. *Diabetes Res. Clin. Pract.* **2018**, *138*, 271–281. [[CrossRef](#)] [[PubMed](#)]
7. Abecassis, M.; Bartlett, S.T.; Collins, A.J.; Davis, C.L.; Delmonico, F.L.; Friedewald, J.J.; Hays, R.; Howard, A.; Jones, E.; Leichtman, A.B.; et al. Kidney Transplantation as Primary Therapy for End-Stage Renal Disease: A National Kidney Foundation/Kidney Disease Outcomes Quality Initiative (NKF/KDOQIM) Conference. *Clin. J. Am. Soc. Nephrol.* **2008**, *3*, 471–480. [[CrossRef](#)]
8. Grange, C.; Tritta, S.; Tapparo, M.; Cedrino, M.; Tetta, C.; Camussi, G.; Brizzi, M.F. Stem cell-derived extracellular vesicles inhibit and revert fibrosis progression in a mouse model of diabetic nephropathy. *Sci. Rep.* **2019**, *9*, 4468. [[CrossRef](#)]
9. Bruno, S.; Chiabotto, G.; Favaro, E.; Deregibus, M.C.; Camussi, G. Role of extracellular vesicles in stem cell biology. *Am. J. Physiol. Cell Physiol.* **2019**, *317*, C303–C313. [[CrossRef](#)]
10. Lai, R.C.; Yeo, R.W.; Lim, S.K. Mesenchymal stem cell exosomes. *Semin. Cell. Dev. Biol.* **2015**, *40*, 82–88. [[CrossRef](#)]
11. Ratajczak, M.Z.; Kucia, M.; Jadczyk, T.; Greco, N.J.; Wojakowski, W.; Tendera, M.; Ratajczak, J. Pivotal role of paracrine effects in stem cell therapies in regenerative medicine: Can we translate stem cell-secreted paracrine factors and microvesicles into better therapeutic strategies? *Leukemia* **2012**, *26*, 1166–1173. [[CrossRef](#)] [[PubMed](#)]
12. Ratajczak, M.Z.; Ratajczak, J. Extracellular Microvesicles as Game Changers in Better Understanding the Complexity of Cellular Interactions-From Bench to Clinical Applications. *Am. J. Med. Sci.* **2017**, *354*, 449–452. [[CrossRef](#)] [[PubMed](#)]
13. Mendt, M.; Rezvani, K.; Shpall, E. Mesenchymal stem cell-derived exosomes for clinical use. *Bone Marrow Transplant.* **2019**, *54*, 789–792. [[CrossRef](#)] [[PubMed](#)]
14. Grange, C.; Tapparo, M.; Kholia, S.; Bussolati, B.; Camussi, G. The Distinct Role of Extracellular Vesicles Derived from Normal and Cancer Stem Cells. *Current Stem Cell Reports* **2017**, *3*, 218–224. [[CrossRef](#)]
15. Borgovan, T.; Crawford, L.; Nwizu, C.; Quesenberry, P. Stem cells and extracellular vesicles: Biological regulators of physiology and disease. *Am. J. Physiol. Cell. Physiol.* **2019**, *317*, C155–C166. [[CrossRef](#)]
16. Quesenberry, P.; Goldberg, L.R. A New Stem Cell Biology: Transplantation and Baseline, Cell Cycle and Exosomes. *Adv. Exp. Med. Biol.* **2018**, *1056*, 3–9.
17. Chargaff, E.; West, R. The biological significance of the thromboplastic protein of blood. *J. Biol. Chem.* **1946**, *166*, 189–197.
18. Janowska-Wieczorek, A.; Majka, M.; Kijowski, J.; Baj-Krzyworzeka, M.; Reza, R.; Turner, A.R.; Ratajczak, J.; Emerson, S.G.; Kowalska, M.A.; Ratajczak, M.Z. Platelet-derived microparticles bind to hematopoietic progenitor cells and enhance their engraftment. *Blood* **2001**, *98*, 3143–3149. [[CrossRef](#)]
19. Deregibus, M.C.; Cantaluppi, V.; Calogero, R.; Lo Iacono, M.; Tetta, C.; Biancone, L.; Bruno, S.; Bussolati, B.; Camussi, G. Endothelial progenitor cell derived microvesicles activate an angiogenic program in endothelial cells by a horizontal transfer of mRNA. *Blood* **2007**, *110*, 2440–2448. [[CrossRef](#)]
20. Ratajczak, J.; Miekus, K.; Kucia, M.; Zhang, J.; Reza, R.; Dvorak, P.; Ratajczak, M.Z. Embryonic stem cell-derived microvesicles reprogram hematopoietic progenitors: Evidence for horizontal transfer of mRNA and protein delivery. *Leukemia* **2006**, *20*, 847–856. [[CrossRef](#)]
21. Valadi, H.; Ekström, K.; Bossios, A.; Sjöstrand, M.; Lee, J.J.; Lötvall, J.O. Exosome-mediated transfer of mRNAs and microRNAs is a novel mechanism of genetic exchange between cells. *Nat. Cell. Biol.* **2007**, *9*, 654–659. [[CrossRef](#)] [[PubMed](#)]
22. Ratajczak, M.Z.; Ratajczak, J. Horizontal transfer of RNA and proteins between cells by extracellular microvesicles: 14 years later. *Clin. Transl. Med.* **2016**, *5*, 7. [[CrossRef](#)] [[PubMed](#)]
23. Keller, S.; Ridinger, J.; Rupp, A.K.; Janssen, J.W.; Altevogt, P. Body fluid derived exosomes as a novel template for clinical diagnostics. *J. Transl. Med.* **2011**, *9*, 86. [[CrossRef](#)] [[PubMed](#)]

24. György, B.; Szabó, T.G.; Pásztói, M.; Pál, Z.; Misják, P.; Aradi, B.; László, V.; Pállinger, E.; Pap, E.; Kittel, A.; et al. Membrane vesicles, current state-of-the-art: Emerging role of extracellular vesicles. *Cell. Mol. Life Sci.* **2011**, *68*, 2667–2688. [[CrossRef](#)] [[PubMed](#)]
25. Lener, T.; Gimona, M.; Aigner, L.; Börger, V.; Buzas, E.; Camussi, G.; Chaput, N.; Chatterjee, D.; Court, F.A.; Del Portillo, H.A.; et al. Applying extracellular vesicles based therapeutics in clinical trials—an ISEV position paper. *J. Extracell. Vesicles.* **2015**, *4*, 30087. [[CrossRef](#)]
26. Lotvall, J.; Hill, A.F.; Hochberg, F.; Buzás, E.I.; Di Vizio, D.; Gardiner, C.; Gho, J.S.; Kurochkin, I.V.; Mathivanan, S.; Quesenberry, P.; et al. Minimal experimental requirements for definition of extracellular vesicles and their functions: A position statement from the International Society for Extracellular Vesicles. *J. Extracell. Vesicles* **2014**, *22*, 26913. [[CrossRef](#)]
27. Gould, S.J.; Raposo, G. As we wait: Coping with an imperfect nomenclature for extracellular vesicles. *J. Extracell. Vesicles* **2013**, *2*. [[CrossRef](#)]
28. Théry, C.; Witwer, K.W.; Aikawa, E.; Alcaraz, M.J.; Anderson, J.D.; Andriantsitohaina, R.; Antoniou, A.; Arab, T.; Archer, F.; Atkin-Smith, G.K. Minimal information for studies of extracellular vesicles 2018 (MISEV2018): A position statement of the International Society for Extracellular Vesicles and update of the MISEV2014 guidelines. *J. Extracell. Vesicles* **2018**, *7*, 1535750. [[CrossRef](#)]
29. Mathivanan, S.; Ji, H.; Simpson, R.J. Exosomes: Extracellular organelles important in intercellular communication. *J. Proteomics* **2010**, *73*, 1907–1920. [[CrossRef](#)]
30. Van der Pol, E.; Böing, A.N.; Harrison, P.; Sturk, A.; Nieuwland, R. Classification, functions, and clinical relevance of extracellular vesicles. *Pharmacol. Rev.* **2012**, *64*, 676–705. [[CrossRef](#)]
31. Théry, C.; Ostrowski, M.; Segura, E. Membrane vesicles as conveyors of immune responses. *Nat. Rev. Immunol.* **2009**, *9*, 581–593. [[CrossRef](#)] [[PubMed](#)]
32. Mobarrez, F.; Sjövik, C.; Soop, A.; Hällström, L.; Frostell, C.; Pisetsky, D.S.; Wallén, H. CD40L expression in plasma of volunteers following LPS administration: A comparison between assay of CD40L on platelet microvesicles and soluble CD40L. *Platelets* **2015**, *26*, 486–490. [[CrossRef](#)] [[PubMed](#)]
33. Jeppesen, D.K.; Fenix, A.M.; Franklin, J.L.; Higginbotham, J.N.; Zhang, Q.; Zimmerman, L.J.; Liebler, D.C.; Ping, J.; Liu, Q.; Evans, R.; et al. Reassessment of Exosome Composition. *Cell* **2019**, *177*, 428–445. [[CrossRef](#)] [[PubMed](#)]
34. Crowley, L.C.; Marfell, B.J.; Scott, A.P.; Waterhouse, N.J. Quantitation of Apoptosis and Necrosis by Annexin V Binding, Propidium Iodide Uptake, and Flow Cytometry. *Cold Spring Harb. Protoc.* **2016**, *2016*, 11. [[CrossRef](#)]
35. Record, M.; Subra, C.; Silvente-Poirot, S.; Poirot, M. Exosomes as intercellular signalosomes and pharmacological effectors. *Biochem. Pharmacol.* **2011**, *81*, 1171–1182. [[CrossRef](#)]
36. Batagov, A.O.; Kurochkin, I.V. Exosomes secreted by human cells transport largely mRNA fragments that are enriched in the 3'-untranslated regions'. *Biology Direct.* **2013**, *8*, 12. [[CrossRef](#)]
37. Di Leva, G.; Garofalo, M.; Croce, C.M. MicroRNAs in cancer. *Annu. Rev. Pathol.* **2014**, *9*, 287–314. [[CrossRef](#)]
38. Trionfini, P.; Benigni, A.; Remuzzi, G. MicroRNAs in kidney physiology and disease. *Nature Reviews Nephrology* **2015**, *11*, 23–33. [[CrossRef](#)]
39. Caplan, A.I.; Dennis, J.E. Mesenchymal stem cells as trophic mediators. *J. Cell. Biochem.* **2006**, *98*, 1076–1084. [[CrossRef](#)]
40. Humphreys, B.D.; Bonventre, J.V. Mesenchymal stem cells in acute kidney injury. *Annu. Rev. Med.* **2008**, *59*, 311–325. [[CrossRef](#)]
41. Elahi, F.M.; Farwell, D.G.; Nolte, J.A.; Anderson, J.D. Concise Review: Preclinical Translation of Exosomes Derived from Mesenchymal Stem/Stromal Cells. *Stem Cells* **2019**. [[CrossRef](#)]
42. De Jong, O.G.; Van Balkom, B.W.; Schifflers, R.M.; Bouten, C.V.; Verhaar, M.C. Extracellular vesicles: Potential roles in regenerative medicine. *Front. Immunol.* **2014**, *5*, 608. [[CrossRef](#)] [[PubMed](#)]
43. Bi, B.; Schmitt, R.; Israilova, M.; Nishio, H.; Cantley, L.G. Stromal cells protect against acute tubular injury via an endocrine effect. *J. Am. Soc. Nephrol.* **2007**, *18*, 2486–2496. [[CrossRef](#)] [[PubMed](#)]
44. Heldring, N.; Mäger, I.; Wood, M.J.; Le Blanc, K.; Andaloussi, S.E. Therapeutic Potential of Multipotent Mesenchymal Stromal Cells and Their Extracellular Vesicles. *Hum. Gene Ther.* **2015**, *26*, 506–517. [[CrossRef](#)]
45. Ferreira, J.R.; Teixeira, G.Q.; Santos, S.G.; Barbosa, M.A.; Almeida-Porada, G.; Gonçalves, R.M. Mesenchymal Stromal Cell Secretome: Influencing Therapeutic Potential by Cellular Pre conditioning. *Front. Immunol.* **2018**, *9*, 2837. [[CrossRef](#)]

46. Bruno, S.; Tapparo, M.; Collino, F.; Chiabotto, G.; Deregibus, M.C.; Soares Lindoso, R.; Neri, F.; Kholia, S.; Giunti, S.; Wen, S.; et al. Renal Regenerative Potential of Different Extracellular Vesicle Populations Derived from Bone Marrow Mesenchymal Stromal Cells. *Tissue Eng. Part. A* **2017**, *23*, 21–22. [[CrossRef](#)]
47. Lou, G.; Chen, Z.; Zheng, M.; Liu, Y. Mesenchymal stem cell-derived exosomes as a new therapeutic strategy for liver diseases. *Exp. Mol. Med.* **2017**, *49*, e346. [[CrossRef](#)]
48. Börger, V.; Bremer, M.; Ferrer-Tur, R.; Gockeln, L.; Stambouli, O.; Becic, A.; Giebel, B. Mesenchymal stem/stromal cell-derived extracellular vesicles and their potential as novel immunomodulatory therapeutic agents. *Int. J. Mol. Sci.* **2017**, *18*, 1450. [[CrossRef](#)]
49. Lai, R.C.; Tan, S.S.; Teh, B.J.; Sze, S.K.; Arslan, F.; de Kleijn, D.P.; Choo, A.; Lim, S.K. Proteolytic potential of the MSC exosome proteome: Implications for an exosome-mediated delivery of therapeutic proteasome. *Int. J. Proteom.* **2012**, *2012*, 971907. [[CrossRef](#)]
50. Murphy, D.E.; de Jong, O.G.; Brouwer, M.; Wood, M.J.; Lavieu, G.; Schiffelers, R.M.; Vader, P. Extracellular vesicle-based therapeutics: Natural versus engineered targeting and trafficking. *Exp. Mol. Med.* **2019**, *51*, 32. [[CrossRef](#)]
51. Kooijmans, S.A.A.; Schiffelers, R.M.; Zarovni, N.; Vago, R. Modulation of tissue tropism and biological activity of exosomes and other extracellular vesicles: New nanotools for cancer treatment. *Pharmacol. Res.* **2016**, *111*, 487–500. [[CrossRef](#)] [[PubMed](#)]
52. Cantaluppi, V.; Biancone, L.; Quercia, A.; Deregibus, M.C.; Segoloni, G.; Camussi, G. Rationale of mesenchymal stem cell therapy in kidney injury. *Am. J. Kidney Dis.* **2013**, *61*, 300–309. [[CrossRef](#)] [[PubMed](#)]
53. Heyman, S.N.; Rosenberger, C.; Rosen, S. Acute kidney injury: Lessons from experimental models. *Contrib. Nephrol.* **2011**, *169*, 286–296. [[PubMed](#)]
54. Bruno, S.; Grange, C.; Deregibus, M.C.; Calogero, R.A.; Saviozzi, S.; Collino, F.; Morando, L.; Busca, A.; Falda, M.; Bussolati, B.; et al. Mesenchymal stem cell-derived microvesicles protect against acute tubular injury. *J. Am. Soc. Nephrol.* **2009**, *20*, 1053–1067. [[CrossRef](#)]
55. Zhao, L.; Hu, C.; Zhang, P.; Jiang, H.; Chen, J. Genetic communication by extracellular vesicles is an important mechanism underlying stem cell-based therapy-mediated protection against acute kidney injury. *Stem Cell Res. Ther.* **2019**, *10*, 119. [[CrossRef](#)]
56. Wang, S.Y.; Hong, Q.; Zhang, C.Y.; Yang, Y.J.; Cai, G.Y.; Chen, X.M. miRNAs in stem cell-derived extracellular vesicles for acute kidney injury treatment: Comprehensive review of preclinical studies. *Stem Cell Res. Ther.* **2019**, *10*, 281. [[CrossRef](#)]
57. Collino, F.; Bruno, S.; Incarnato, D.; Dettori, D.; Neri, F.; Provero, P.; Pomatto, M.; Oliviero, S.; Tetta, C.; Quesenberry, P.J.; et al. AKI recovery induced by mesenchymal stromal cell-derived extracellular vesicles carrying microRNA. *J. Am. Soc. Nephrol.* **2015**, *26*, 2349–2360. [[CrossRef](#)]
58. Tomasoni, S.; Longaretti, L.; Rota, C.; Morigi, M.; Conti, S.; Gotti, E.; Capelli, C.; Introna, M.; Remuzzi, G.; Benigni, A. Transfer of growth factor receptor mRNA via exosomes unravels the regenerative effect of mesenchymal stem cells. *Stem Cells Dev.* **2013**, *22*, 772–780. [[CrossRef](#)]
59. Bruno, S.; Grange, C.; Collino, F.; Deregibus, M.C.; Cantaluppi, V.; Biancone, L.; Tetta, C.; Camussi, G. Microvesicles derived from mesenchymal stem cells enhance survival in a lethal model of acute kidney injury. *PLoS ONE* **2012**, *7*, e33115. [[CrossRef](#)]
60. Reis, L.A.; Borges, F.T.; Simões, M.J.; Borges, A.A.; Sinigaglia-Coimbra, R.; Schor, N. Bone marrow-derived mesenchymal stem cells repaired but did not prevent gentamicin-induced acute kidney injury through paracrine effects in rats. *PLoS ONE* **2012**, *7*, e44092. [[CrossRef](#)]
61. Gatti, S.; Bruno, S.; Deregibus, M.C.; Sordi, A.; Cantaluppi, V.; Tetta, C.; Camussi, G. Microvesicles derived from human adult mesenchymal stem cells protect against ischaemia-reperfusion-induced acute and chronic kidney injury. *Nephrol. Dial. Transpl.* **2011**, *26*, 1474–1483. [[CrossRef](#)] [[PubMed](#)]
62. Shen, B.; Liu, J.; Zhang, F.; Wang, Y.; Qin, Y.; Zhou, Z.; Qiu, J.; Fan, Y. CCR2 Positive Exosome Released by Mesenchymal Stem Cells Suppresses Macrophage Functions and Alleviates Ischemia/Reperfusion-Induced Renal Injury. *Stem Cells Int.* **2016**, *2016*, 1240301. [[CrossRef](#)] [[PubMed](#)]
63. Zhou, Y.; Xu, H.; Xu, W.; Wang, B.; Wu, H.; Tao, Y.; Zhang, B.; Wang, M.; Mao, F.; Yan, Y.; et al. Exosomes released by human umbilical cord mesenchymal stem cells protect against cisplatin-induced renal oxidative stress and apoptosis in vivo and in vitro. *Stem Cell Res. Ther.* **2013**, *4*, 34. [[CrossRef](#)] [[PubMed](#)]

64. Zou, X.; Zhang, G.; Cheng, Z.; Yin, D.; Du, T.; Ju, G.; Miao, S.; Liu, G.; Lu, M.; Zhu, Y. Microvesicles derived from human Wharton's Jelly mesenchymal stromal cells ameliorate renal ischemia-reperfusion injury in rats by suppressing CX3CL1. *Stem Cell Res. Ther.* **2014**, *5*, 40. [[CrossRef](#)]
65. Ju, G.Q.; Cheng, J.; Zhong, L.; Wu, S.; Zou, X.Y.; Zhang, G.Y.; Gu, D.; Miao, S.; Zhu, Y.J.; Sun, J.; et al. Microvesicles derived from human umbilical cord mesenchymal stem cells facilitate tubular epithelial cell dedifferentiation and growth via hepatocyte growth factor induction. *PLoS ONE* **2015**, *10*, e0121534. [[CrossRef](#)]
66. Gu, D.; Zou, X.; Ju, G.; Zhang, G.; Bao, E.; Zhu, Y. Mesenchymal Stromal Cells Derived. Extracellular Vesicles Ameliorate Acute Renal Ischemia Reperfusion Injury by Inhibition of Mitochondrial Fission through miR-30. *Stem Cells Int.* **2016**, *2016*, 2093940. [[CrossRef](#)]
67. Ranghino, A.; Bruno, S.; Bussolati, B.; Moggio, A.; Dimuccio, V.; Tapparo, M.; Biancone, L.; Gontero, P.; Frea, B.; Camussi, G. The effects of glomerular and tubular renal progenitors and derived extracellular vesicles on recovery from acute kidney injury. *Stem Cell Res. Ther.* **2017**, *8*, 24. [[CrossRef](#)]
68. Choi, H.Y.; Moon, S.J.; Ratliff, B.B.; Ahn, S.H.; Jung, A.; Lee, M.; Lee, S.; Lim, B.J.; Kim, B.S.; Plotkin, M.D.; et al. Microparticles from kidney-derived mesenchymal stem cells act as carriers of proangiogenic signals and contribute to recovery from acute kidney injury. *PLoS ONE* **2014**, *9*, e87853. [[CrossRef](#)]
69. Herrera Sanchez, M.B.; Bruno, S.; Grange, C.; Tapparo, M.; Cantaluppi, V.; Tetta, C.; Camussi, G. Human liver stem cells and derived extracellular vesicles improve recovery in a murine model of acute kidney injury. *Stem Cell Res. Ther.* **2014**, *5*, 124–135. [[CrossRef](#)]
70. Bank, J.R.; Rabelink, T.J.; de Fijter, J.W.; Reinders, M.E. Safety and Efficacy Endpoints for Mesenchymal Stromal Cell Therapy in Renal Transplant Recipients. *J. Immunol. Res.* **2015**, *2015*, 391797. [[CrossRef](#)]
71. Gregorini, M.; Corradetti, V.; Pattonieri, E.F.; Rocca, C.; Milanese, S.; Peloso, A.; Canevari, S.; De Cecco, L.; Dugo, M.; Avanzini, M.A.; et al. Perfusion of isolated rat kidney with Mesenchymal Stromal Cells/Extracellular Vesicles prevents ischaemic injury. *J. Cell. Mol. Med.* **2017**, *21*, 3381–3393. [[CrossRef](#)] [[PubMed](#)]
72. Pini, A.; Grange, C.; Veglia, E.; Argenziano, M.; Cavalli, R.; Guasti, D.; Calosi, L.; Ghè, C.; Solarino, R.; Thurmond, R.L.; et al. Histamine (H4) receptor antagonism prevents the progression of diabetic nephropathy in male DBA2/J mice. *Pharmacol. Res.* **2018**, *128*, 18–28. [[CrossRef](#)] [[PubMed](#)]
73. Simonson, M.S. Phenotypic transitions and fibrosis in diabetic nephropathy. *Kidney Int.* **2007**, *71*, 846–854. [[CrossRef](#)] [[PubMed](#)]
74. Lim, A.K. Diabetic nephropathy—complications and treatment. *Int. J. Nephrol. Renovasc. Dis.* **2014**, *7*, 361–381. [[CrossRef](#)]
75. Jiang, Z.Z.; Liu, Y.M.; Niu, X.; Yin, J.Y.; Hu, B.; Guo, S.C.; Fan, Y.; Wang, Y.; Wang, N.S. Exosomes secreted by human urine-derived stem cells could prevent kidney complications from type I diabetes in rats. *Stem Cell Res. Ther.* **2016**, *7*, 24–37. [[CrossRef](#)]
76. Nagaishi, K.; Mizue, Y.; Chikenji, T.; Otani, M.; Nakano, M.; Konari, N.; Fujimiya, M. Mesenchymal stem cell therapy ameliorates diabetic nephropathy via the paracrine effect of renal trophic factors including exosomes. *Sci. Rep.* **2016**, *6*, 34842–34858. [[CrossRef](#)]
77. Kholia, S.; Herrera Sanchez, M.B.; Cedrino, M.; Papadimitriou, E.; Tapparo, M.; Deregibus, M.C.; Brizzi, M.F.; Tetta, C.; Camussi, G. Human Liver Stem Cell-Derived Extracellular Vesicles Prevent Aristolochic Acid-Induced Kidney Fibrosis. *Front. Immunol.* **2018**, *9*, 1639. [[CrossRef](#)]
78. Heuer, J.G.; Harlan, S.M.; Yang, D.D.; Jaqua, D.L.; Boyles, J.S.; Wilson, J.M.; Heinz-Taheny, K.M.; Sullivan, J.M.; Wei, T.; Qian, H.R.; et al. Role of TGF- $\alpha$  in the progression of diabetic kidney disease. *Am. J. Physiol. Renal Physiol.* **2017**, *312*, F951–F962. [[CrossRef](#)]
79. He, J.; Wang, Y.; Sun, S.; Yu, M.; Wang, C.; Pei, X.; Zhu, B.; Wu, J.; Zhao, W. Bone marrow stem cells-derived microvesicles protect against renal injury in the mouse remnant kidney model. *Nephrology Carlton* **2012**, *17*, 493–500. [[CrossRef](#)]
80. He, J.; Wang, Y.; Lu, X.; Zhu, B.; Pei, X.; Wu, J.; Zhao, W. Micro-vesicles derived from bone marrow stem cells protect the kidney both in vivo and in vitro by microRNA-dependent repairing. *Nephrology Carlton* **2015**, *20*, 591–600. [[CrossRef](#)]
81. Van Koppen, A.; Verhaar, M.C.; Bongartz, L.G.; Joles, J.A. 5/6th nephrectomy in combination with high salt diet and nitric oxide synthase inhibition to induce chronic kidney disease in the Lewis rat. *J. Vis. Exp.* **2013**, *77*, e50398.

82. Eirin, A.; Zhu, X.Y.; Puranik, A.S.; Tang, H.; McGurran, K.A.; van Wijnen, A.J.; Lerman, A.; Lerman, L.O. Mesenchymal stem cell-derived extracellular vesicles attenuate kidney inflammation. *Kidney Int.* **2017**, *92*, 114–124. [[CrossRef](#)] [[PubMed](#)]
83. Nassar, W.; El-Ansary, M.; Sabry, D.; Mostafa, M.A.; Fayad, T.; Kotb, E.; Temraz, M.; Saad, A.N.; Essa, W.; Adel, H. Umbilical cord mesenchymal stem cells derived extracellular vesicles can safely ameliorate the progression of chronic kidney diseases. *Biomater. Res.* **2016**, *20*, 21. [[CrossRef](#)] [[PubMed](#)]
84. Wiklander, O.P.B.; Brennan, M.Á.; Lötvall, J.; Breakefield, X.O.; El Andaloussi, S. Advances in therapeutic applications of extracellular vesicles. *Sci. Transl. Med.* **2019**, *11*, 492. [[CrossRef](#)]
85. De Jong, O.G.; Kooijmans, S.A.A.; Murphy, D.E.; Jiang, L.; Evers, M.J.W.; Sluijter, J.P.G.; Vader, P.; Schiffelers, R.M. Drug Delivery with Extracellular Vesicles: From Imagination to Innovation. *Acc. Chem. Res.* **2019**, *52*, 1761–1770. [[CrossRef](#)]
86. Hung, M.E.; Leonard, J.N. A platform for actively loading cargo RNA to elucidate limiting steps in EV-mediated delivery. *J. Extracell. Vesicles* **2016**, *5*, 31027. [[CrossRef](#)]
87. Van der Meel, R.; Fens, M.H.; Vader, P.; van Solinge, W.W.; Eniola-Adefeso, O.; Schiffelers, R.M. Extracellular vesicles as drug delivery systems: Lessons from the liposome field. *J. Control. Release* **2014**, *195*, 72–85. [[CrossRef](#)]
88. Springer, A.D.; Dowdy, S.F. GalNAc-siRNA conjugates: Leading the way for delivery of RNAi therapeutics. *Nucleic Acid. Ther.* **2018**, *28*, 109–118. [[CrossRef](#)]
89. Fuhrmann, G.; Serio, A.; Mazo, M.; Nair, R.; Stevens, M.M. Active loading into extracellular vesicles significantly improves the cellular uptake and photodynamic effect of porphyrins. *J. Control. Release* **2015**, *205*, 35–44. [[CrossRef](#)]
90. Ohno, S.; Takanashi, M.; Sudo, K.; Ueda, S.; Ishikawa, A.; Matsuyama, N.; Fujita, K.; Mizutani, T.; Ohgi, T.; Ochiya, T.; et al. Systemically injected exosomes targeted to EGFR deliver antitumor microRNA to breast cancer cells. *Mol. Ther.* **2013**, *21*, 185–191. [[CrossRef](#)]
91. Sun, D.; Zhuang, X.; Xiang, X.; Liu, Y.; Zhang, S.; Liu, C.; Barnes, S.; Grizzle, W.; Miller, D.; Zhang, H.G. A novel nanoparticle drug delivery system: The anti-inflammatory activity of curcumin is enhanced when encapsulated in exosomes. *Mol. Ther.* **2010**, *18*, 1606–1614. [[CrossRef](#)] [[PubMed](#)]
92. Pomatto, M.A.C.; Bussolati, B.; D'Antico, S.; Ghiotto, S.; Tetta, C.; Brizzi, M.F.; Camussi, G. Improved Loading of Plasma-Derived Extracellular Vesicles to Encapsulate Antitumor miRNAs. *Mol. Ther. Methods Clin. Dev.* **2019**, *13*, 133–144. [[CrossRef](#)] [[PubMed](#)]
93. Tao, S.C.; Rui, B.Y.; Wang, Q.Y.; Zhou, D.; Zhang, Y.; Guo, S.C. Extracellular vesicle-mimetic nanovesicles transport LncRNA-H19 as competing endogenous RNA for the treatment of diabetic wounds. *Drug Deliv.* **2018**, *25*, 241–255. [[CrossRef](#)] [[PubMed](#)]
94. Haney, M.J.; Klyachko, N.L.; Harrison, E.B.; Zhao, Y.; Kabanov, A.V.; Batrakova, E.V. TPP1 Delivery to Lysosomes with Extracellular Vesicles and their Enhanced Brain Distribution in the Animal Model of Batten Disease. *Adv. Healthc. Mater.* **2019**, *8*, e1801271. [[CrossRef](#)]
95. Haney, M.J.; Klyachko, N.L.; Zhao, Y.; Gupta, R.; Plotnikova, E.G.; He, Z.; Patel, T.; Piroyan, A.; Sokolsky, M.; Kabanov, A.V.; et al. Exosomes as drug delivery vehicles for Parkinson's disease therapy. *J. Control. Release* **2015**, *207*, 18–30. [[CrossRef](#)]
96. Lainšček, D.; Kadunc, L.; Keber, M.M.; Bratkovič, I.H.; Romih, R.; Jerala, R. Delivery of an Artificial Transcription Regulator dCas9-VPR by Extracellular Vesicles for Therapeutic Gene Activation. *ACS Synth. Biol.* **2018**, *7*, 2715–2725. [[CrossRef](#)]
97. Wang, B.; Yao, K.; Huuskens, B.M.; Shen, H.H.; Zhuang, J.; Godson, C.; Brennan, E.P.; Wilkinson-Berka, J.L.; Wise, A.F.; Ricardo, S.D. Mesenchymal Stem Cells Deliver Exogenous MicroRNA-let7c via Exosomes to Attenuate Renal Fibrosis. *Mol. Ther.* **2016**, *24*, 1290–1301. [[CrossRef](#)]
98. Tapparo, M.; Bruno, S.; Collino, F.; Togliatto, G.; Deregis, M.C.; Provero, P.; Wen, S.; Quesenberry, P.J.; Camussi, G. Renal Regenerative Potential of Extracellular Vesicles Derived from miRNA-Engineered Mesenchymal Stromal Cells. *Int. J. Mol. Sci.* **2019**, *20*, 2381. [[CrossRef](#)]





## Study Aim

The general aim of my PhD project was to characterize and compare small and medium/large mesenchymal stromal cell (MSC) derived EVs from naïve and apoptotic conditions, in terms of phenotypic and functional properties. MSCs were obtained from three clinically relevant sources: adipose tissue, bone marrow and umbilical cord, cultured in parallel comparable conditions.

In the first part of the project the small and medium/large MSC-EVs were compared for surface marker expression using different orthogonal techniques, such as super-resolution microscopy, ExoView array and bead-based cytofluorimetric analysis. MSC-EVs were generated in naïve and apoptotic conditions

In the second part of my PhD project, their functional properties were tested using human conditionally immortalized proximal tubular epithelial cell line ischemic renal reperfusion injury model.

The third part of this PhD project was to characterize and compare properties of adipose tissue derived MSC products harvested in culture conditions suitable for a possible clinical application, such as the bioreactor.

## **MATERIALS AND METHODS**

# Materials and Methods

## Cell Culture:

### Human mesenchymal stromal cells

The MSCs were obtained in collaboration with the RenalToolBox ITN (Grant Agreement 813839). AT-MSCs from lipoaspirate adipose tissue harvested processed by the group of Prof. Karen Bieback (University of Heidelberg, Heidelberg, Germany) after informed consent. The Mannheim Ethics Commission II approved the study (vote 2011-215N-MA). For the IRI injury model we also tested BM-MSCs which were obtained from the group of Prof. Timothy O'Brien (National University of Galway, Ireland) and UC-MSCs from the group of Dr. Jon Smythe (NHS Blood and Transplant, Liverpool, UK) from three different healthy donors with informed consent obtained in accordance with Declaration of Helsinki. The MSCs were cultured using AlphaMEM with UltraGlutamine (BE02-002F, Lonza, Basal, Switzerland) and 10% Foetal Bovine Serum (10270-106, Gibco, MA, USA) in the incubator at 37 °C with 5% CO<sub>2</sub> and controlled humidity. EVs were collected from MSCs at 4-6th passage.

### Culturing in hollow Fiber Bioreactor-HFBRs

When the cells reached 80% confluency, the cells were splitted and injected in Hollow-Fiber-Bioreactors, 14x10<sup>6</sup>/cartridge (20 kD MWCO, 450 cm<sup>2</sup>, C2025D, FiberCell System-KD Bio, France). First of all, the procedure of initiation and activation of the bioreactor called "pre-culture step" (72 hours) was carried out. This phase involves the insertion of PBS inside it for 24 hours, followed by the addition of over-night fibronectin coating to help the cells attach, and adding the Alpha-MEM medium. After pre-culture process of HFBRs, each donor's ASCs have been introduced with a syringe inside the cartridge, they were placed to allow their growth

in an incubator for seven days, during which glucose levels were constantly measured. The purpose of the work is not to obtain a cellular expansion of cell lines, but to subsequently collect the EVs released in the conditional medium. After 7 days of incubation, the supernatant was collected daily, centrifuged for 5 min at 420 g to remove cell debris and apoptotic cells and stored in -80° until further use.

**Collecting the conditioned medium:** Upon reaching 80% confluency, cells were washed with 1X PBS (Gibco, ThermoFisher Scientifics, 14190094) and incubated during 24 hours in serum-free media. The supernatant was collected and centrifuged for 5 min at 400 g to remove cell debris before being transferred to Amicon Ultra-15 centrifugal units (Millipore, UFC900324) for concentration at 3,000 g for 90 min, 4°C. Concentrated conditioned media was then stored at -80 °C until further use. Conditioned media was collected from MSCs at 4-6th passage.

**EV Isolation from MSCs by ultracentrifugation:** When the cells reached 80% confluency, they were starved overnight (16 h) in RPMI medium. The supernatant was collected and centrifuged for 20 min at 3000 × g to remove cell debris and apoptotic cells on the second day. The supernatant was then ultracentrifuged for 2 h at 100,000× g, 4 °C using Beckman Coulter Optima L-100K Ultracentrifuge (Beckman Coulter, CA, USA) with the rotor type 70Ti. For the IRI injury model the EVs were obtained using sequential ultracentrifugation for 1 h at 10,000× g, 4 °C and following 1h at 100,000x g 4 °C using Beckman Coulter Optima L-100K Ultracentrifuge with the rotor type 70Ti. The EV pellet was resuspended in PBS supplemented with 0.1% DMSO. The suspension was then stored at -80°C until further use.

**SEC-qEV IZON columns isolation:** Each sample previously collected and stored at -80°C was thawed at -4°C about 2 hours before starting the isolation procedure. The conditioned medium was centrifuged for 10 min 300 g and following 2 min for 2000 g. After that the conditioned medium is filtered through 0,20 µm syringe filter and concentrated with 100kD

(Vivaspin 20, 100.000 MWCO PE, Sartorius, Sartorius AG, Germany) to final volume of 10 ml. The qEV10-IZON column 35 mm was initially washed with sterile PBS, and then 10 ml of the sample was added to concentrate it for the final volume 1,5 ml (Vivaspin 20, 100.000 MWCO PE, Sartorius), and each EV sample was collected and stored in -80°C until further use.

### **Human conditionally immortalized proximal tubular epithelial cell line**

The ciPTEC-14.4 cell line was cultured as reported previously (Wilmer et al., 2010). Briefly, cells were cultured in Dulbecco's Modified Eagle Medium/Nutrient Mixture F-12 (1:1 DMEM/F-12) (Gibco, ThermoFischer Scientific, 11039021) supplemented with 10% foetal bovine serum (FBS, Gibco, 10270-106), insulin-transferrin-sodium insulin (Sigma-Aldrich, I1884, insulin 5 µg/ml; transferrin 5 µg/ml; sodium selenite 5ng/ml), 35 ng/mL hydrocortisone (Sigma-Aldrich, H0135), 5% epidermal growth factor (Sigma-Aldrich, E9644), and 40 pg/mL tri-iodothyronine (Sigma-Aldrich, T5516), without antibiotics and up to 50 passages. Cells were cultured at 33 °C and 5% (v/v) CO<sub>2</sub> to allow proliferation and seeded at a density of 48,000 cell/cm<sup>2</sup> prior to the experiments. Following that, cells were cultured for one day at 33 °C, 5% (v/v) CO<sub>2</sub> to allow proliferation and adhesion, then for seven days at 37 °C, 5% (v/v) CO<sub>2</sub> for differentiation and maturation, with the medium refreshed every other day.

**ciPTEC ischemic model:** To mimic ischemia in vitro, ciPTECs were exposed to 10 nM of antimycin A (AA, Sigma-Aldrich, A8674), an inhibitor of mitochondrial respiration, and 20mM of 2-Deoxy-D-Glucose (2DG, Sigma-Aldrich D6134), an inhibitor of glycolysis, for 24h (in serum-free medium), at 37 °C, 5% (v/v) CO<sub>2</sub>, under normoxia (21% O<sub>2</sub>) and hypoxia (1% O<sub>2</sub>) conditions. Afterwards, ischemic cells were treated with either conditioned medium (CM) or extracellular vesicles (small and medium/large size EVs) from each of the MSC

sources for an additional 24h at 37 °C, 5% (v/v) CO<sub>2</sub>. All experiments were performed on 96-well plates (Greiner Bio-One, Frickenhausen, Germany), unless stated otherwise.

**Immunofluorescence analysis:** ciPTECs were cultured in a 96-well black/clear bottom plates (ThermoFischer, 165305) in the same conditions as stated in ‘ciPTEC ischemia model’. After exposure, the cells were washed with HBSS and fixed in 4% paraformaldehyde (ThermoFisher Scientific, 28906) for 10 mins at room temperature (RT). After fixation, ciPTECs were permeabilized with 0.3% Triton X-100 in PBS and blocked-in blocking buffer (2% (v/v) FCS, 2% (v/v) BSA, 0.1% (v/v) Tween20 in PBS). Primary and secondary antibodies were incubated for 1h at RT, and samples were washed three times in 0.1% Tween in PBS for 5mins. Nuclei were stained using 4',6-diamidino-2-phenylindole (DAPI) for 7 min, followed by three washing steps in 0.1% Tween in PBS for 5mins. Immunofluorescence was conducted using confocal microscopy (Leica TCS SP8 X) and software Leica Application Suite X. Phalloidin antibody was used in 1:1000 dilution (Invitrogen).

**Cell viability:** Cell viability was measured using PrestoBlue® cell viability reagent (ThermoFischer Scientific, A13262) before and after exposure to the conditions mentioned in ‘ciPTEC ischemic model’. Following each exposure, ciPTECs were rinsed once with Hank’s Balanced Salt Solution (HBSS; Gibco, Life Technologies) and incubated with PrestoBlue® cell viability reagent (diluted 1:10 in serum-free culture medium), in the dark. After 1 h incubation at 37 °C, 5% (v/v) CO<sub>2</sub>, the fluorescence was measured using the GloMax® Discover microplate reader (Promega, Wisconsin, United States), at excitation wavelength of 530 nm and emission wavelength of 590 nm. Data were corrected for the background, normalized to untreated cells, and presented as fold-change.

**ATP production:** To quantify the ATP production, ciPTECs were first exposed to the injury model and later the MSC therapy. Following that, 100 µl of CellTiter-Glo® 2.0 reagent

(Promega, G9242) was added to each well, and the solutions were mixed on an orbital shaker for 2 min. The plates were incubated at room temperature for 10 min to stabilize the luminescent signal before being read using the GloMax® Discover microplate reader (Promega, Wisconsin, United States). The data were corrected for the background, normalized to untreated cells, and presented as fold-change.

**Assessing mitochondrial mass:** The mitochondrial mass was quantified using MitoTracker Orange CMTMRos (Invitrogen, M7510, Invitrogen, MA, USA), a cell-permeable fluorescent dye that can diffuse across the plasma membrane and accumulate in viable mitochondria. Upon each exposure to the ischemic model, ciPTECs were rinsed once with serum-free medium, loaded with MitoTracker Orange CMTMRos (200 nM in serum-free medium), and incubated 37 °C, 5% (v/v) CO<sub>2</sub>, in the dark for 30 min. Additionally, ciPTECs were counterstained with 1 μM Hoechst 33342 for nuclei detection. Afterwards, ciPTECs were washed with HBSS and fluorescence was measuring using he GloMax® Discover microplate reader (Promega, Wisconsin, United States) at excitation/emission wavelengths of 554/576 for MitoTracker Orange CMTMRos and 361/497 for Hoechst. The data were corrected for the background, normalized to untreated cells, and presented as fold-change.

**Nanosight analysis:** After the isolation, the concentration of all the samples was measured by Nanosight NS300 (Malvern Instruments Ltd., Malvern, UK) equipped with a 488 nm laser module that utilises Brownian motion and refraction index. The particle size scatters 10 nm to 1000 nm, although the optimised size range is 70–300 nm. It uses the scattered light to detect a particle and tracks its motion as a function of time. The particles' scattered light was recorded with a light-sensitive camera under a 90° angle to the irradiation plane. This angle allows the Brownian motion of the EVs. Samples were diluted 1:100 in physiologic solution. For each sample, 3 videos of 60 s at camera level 15 and threshold 5 were captured using a syringe pump

30. All the samples were characterised with NTA 3.2.16 Analytical software. The NTA settings were kept constant between samples.

**Super-resolution microscopy:** Super-resolution microscopy pictures of EVs were obtained using a temperature-controlled Nanoimager S Mark II microscope from ONI (Oxford Nanoimaging, Oxford, UK) equipped with a 100x, 1.4NA oil immersion objective, an XYZ closed-loop piezo 736 stage, and 405 nm/150 mW, 473 nm/1 W, 560 nm/1 W, 640 nm/1 W lasers and triple emission channels split at 640 / and 568 nm. For sample preparation, EV profiler Kit (EVman, ONI) was used to perform the experiments following manufacturer's protocol. The Kit contains fluorescent antibodies anti CD9-488 and CD81-647 and the imaging buffer for amplification of the EV signalling. We further used CD44-568 (130-113-903, Miltenyi) antibody. Before each imaging session, bead slide calibration was performed for aligning the channels, to achieve a channel mapping precision smaller than 12 nm. Images were taken in dSTORM mode using 50% laser power for the 647 nm channel, 30% laser power for the 488 nm laser channel, and 30% for the 568 channel. Three-channels (2000 frames per channel) (647, 568 and 488) were acquired sequentially at 30 Hz (Hertz) in total reflection fluorescence (TIRF) mode. Single-molecule data was filtered using NimOSsoftware (v.1.18.3, ONI) based on the point spread function shape, photon count and localization precision to minimize background noise and remove low-precision and non-specific colocalization. Data has been processed with the Collaborative Discovery (CODI) online analysis platform [www.alto.codi.bio](http://www.alto.codi.bio) from ONI and the drift correction pipeline version 0.2.3 was used. Clustering analysis was performed on localizations and BD clustering constrained parameters were defined (photon count 300-max, sigma 0-200 nm, p-value 0-1, localization precision 0-20 nm). Colocalization was defined by a minimum number of localizations for each fluorophore/protein within a distance of 100 nm or distance used from the centroid position of a cluster.



**Cytofluorimetric analysis:** MACSPlex Exosome Kit (Miltenyi Biotec, Bergisch Gladbach, Germany) containing fluorescently labelled (FITC-PE) capture beads coupled to 37 exosomal surface epitopes and 2 isotope controls was used, following the manufacturer's instructions (in detail: CD3, CD4, CD19, CD8, HLA-DR, CD56, CD105, CD2, CD1c, CD25, CD49e, ROR1, CD209, CD9, SSEA-4, HLA-ABC, CD63, CD40, CD62P, CD11c, CD81, MCSP, CD146, CD41b, CD42a, CD24, CD86, CD44, CD326, CD133-1, CD29, CD69, CD142, CD45, CD31, REA control, CD20, CD14, mIgG1 control). Briefly, 15  $\mu$ L of beads were added to 120  $\mu$ L of buffer or sample, including a total of  $1 \times 10^9$  EVs, and the complex was then incubated on a rotor overnight at 4 °C. After the incubation and washing steps, a cocktail of APC fluorescent antibodies against tetraspanins (CD9, CD63 and CD81) was added (allowing the detection of beads-bound EVs) and set on the rotor for 1 h at room temperature. After washing, samples were detected using BD FACSCelesta™ Flow Cytometer (BD Bioscience, NJ, USA). Median background values of buffer control were subtracted, and samples were normalised to the median fluorescence intensity of tetraspanins.

**Angiogenesis:** Human umbilical vascular endothelial cells (HUVEC) were bought from ATCC (ATCC-PCS-100-010, Manassas, VA, USA) and cultured until the 6th passage in EndoGRO-LS Complete Culture Media Kit (SCME001, Sigma-Aldrich, St. Louis, MO, USA). In vitro formation of capillary-like structures was performed on growth factor-reduced Matrigel (356231, Corning, NY, USA). HUVEC cells were treated with EVs or CM in ration 1:2, seeded at a density of  $10 \times 10^3$  cells/well on a 48-well plate. Positive control was full EndoGro-LS medium, negative control medium without VEGF and FBS (as used for all the conditions). Cells were periodically observed with a Nikon TE2000E inverted microscope (Nikon, Tokyo, Japan), and experimental results were recorded after 16 h; 3 images were taken per well. Image analysis was performed with the ImageJ software v.1.53c, using the Angiogenesis Analyzer.

The data from three independent experiments were expressed as the mean  $\pm$  SD of tube length in arbitrary units per field.

**Statistical tests:** All statistical analyses were performed using GraphPad Prism software (v. 8.00; GraphPad, CA, USA). For multiple comparison analyses, ANOVA with Dunnett's multi-comparison test. Two-tailed  $p$  value  $<0.05$  was considered statistically significant.

# **RESULTS**

**1. CHARACTERIZATION OF SMALL AND MEDIUM/LARGE MSC-EVS FOR SURFACE MARKER EXPRESSION USING SUPER-RESOLUTION MICROSCOPY, EXOVIEW ARRAY AND BEAD-BASED CYTOFLUORIMETRIC ANALYSIS.**





The results are presented in the following published article:

Surface Marker Expression in Small and Medium/Large Mesenchymal stromal Cell-Derived Extracellular Vesicles in Naïve or Apoptotic Condition Using Orthogonal Techniques.

**Renata Skovronova**, Cristina Grange, Veronica Dimuccio, Maria Chiara Deregibus, Giovanni Camussi and Benedetta Bussolati, 10:2948, Cells, 2021

## Article

# Surface Marker Expression in Small and Medium/Large Mesenchymal Stromal Cell-Derived Extracellular Vesicles in Naive or Apoptotic Condition Using Orthogonal Techniques

Renata Skovronova <sup>1</sup>, Cristina Grange <sup>2</sup>, Veronica Dimuccio <sup>1</sup>, Maria Chiara Deregibus <sup>3</sup>, Giovanni Camussi <sup>2</sup> and Benedetta Bussolati <sup>1,\*</sup>

<sup>1</sup> Department of Molecular Biotechnology and Health Sciences, University of Turin, 10126 Turin, Italy; renata.skovronova@unito.it (R.S.); veronica.dimuccio@unito.it (V.D.)

<sup>2</sup> Department of Medical Sciences, University of Turin, 10126 Turin, Italy; cristina.grange@unito.it (C.G.); giovanni.camussi@unito.it (G.C.)

<sup>3</sup> 2i3T Business Incubator and Technology Transfer, University of Turin, 10126 Turin, Italy; mariachiara.deregibus@unito.it

\* Correspondence: benedetta.bussolati@unito.it; Tel.: +011-6706453



**Citation:** Skovronova, R.; Grange, C.; Dimuccio, V.; Deregibus, M.C.; Camussi, G.; Bussolati, B. Surface Marker Expression in Small and Medium/Large Mesenchymal Stromal Cell-Derived Extracellular Vesicles in Naive or Apoptotic Condition Using Orthogonal Techniques. *Cells* **2021**, *10*, 2948. <https://doi.org/10.3390/cells10112948>

Academic Editor: Debabrata Banerjee

Received: 5 October 2021

Accepted: 27 October 2021

Published: 29 October 2021

**Publisher's Note:** MDPI stays neutral with regard to jurisdictional claims in published maps and institutional affiliations.



**Copyright:** © 2021 by the authors. Licensee MDPI, Basel, Switzerland. This article is an open access article distributed under the terms and conditions of the Creative Commons Attribution (CC BY) license (<https://creativecommons.org/licenses/by/4.0/>).

**Abstract:** Extracellular vesicles released by mesenchymal stromal cells (MSC-EVs) are a promising resource for regenerative medicine. Small MSC-EVs represent the active EV fraction. A bulk analysis was applied to characterise MSC-EVs' identity and purity, with the assessment of single EV morphology, size and integrity using electron microscopy. We applied different methods to quantitatively analyse the size and surface marker expression in medium/large and small fractions, namely 10k and 100k fractions, of MSC-EVs obtained using sequential ultracentrifugation. Bone marrow, adipose tissue and umbilical cord MSC-EVs were compared in naive and apoptotic conditions. As detected by electron microscopy, the 100k EV size < 100 nm was confirmed by super-resolution microscopy and ExoView. Single-vesicle imaging using super-resolution microscopy revealed heterogeneous patterns of tetraspanins. ExoView allowed a comparative screening of single MSC-EV tetraspanin and mesenchymal markers. A semiquantitative bead-based cytofluorimetric analysis showed the segregation of immunological and pro-coagulative markers on the 10k MSC-EVs. Apoptotic MSC-EVs were released in higher numbers, without significant differences in the naive fractions in surface marker expression. These results show a consistent profile of MSC-EV fractions among the different sources and a safer profile of the 100k MSC-EV population for clinical application. Our study identified suitable applications for EV analytical techniques.

**Keywords:** tetraspanins; 10k MSC EVs; 100k MSC EVs; Nanosight; MACSPlex; ExoView; super-resolution microscopy

## 1. Introduction

Mesenchymal stromal cells (MSCs) are nowadays the most commonly used cell source for regenerative medicine due to their immunomodulatory, pro-regenerative and anti-inflammatory properties [1–3]. MSCs can originate from different tissues, including bone marrow (BM), adipose tissue (AT) and the umbilical cord (UC), which the ones most commonly used. As the field of extracellular vesicles (EVs) rises, so does the interest in the isolation and therapeutic application of MSC bioproducts. Indeed, MSC EVs may overlap many of the described effects of the originating cells [4], playing an essential role in cell-to-cell communication, involving stem cells and targeting injured cells [5,6].

EVs are released from cells as a heterogeneous population that can be further classified into three fractions: small EVs, large EVs and apoptotic bodies (ApoBDs) based on their size and composition, with ranges defined either as <100 nm or <200 nm for small EVs, and >200 nm for medium/large EVs as the MISEV community classified [7]. Moreover,

the classification in different EV fractions underlines distinct molecular and functional properties [8]. In addition, the EVs can also be classified into exosomes and microvesicles depending on their biogenesis from multivesicular bodies or cell surface budding, respectively [7]. However, small and medium/large EVs share many structural components. A specific surface marker expression of EV fractions lacks a strict boundary between them due to the absence of a strict boundary [9]. In particular, the classical tetraspanins, CD9, CD63 and CD81, are commonly present in different EV subpopulations [7]. However, a higher expression level on small MSC EVs was reported, in line with their possible origin in the cellular endosomal pathway [7]. At variance, the large EV surface may resemble the parental cell origin more closely, as it can be likely associated with direct budding from the plasma membrane [10]. Moreover, medium/large EVs are generally enriched with phosphatidylserine [10] and CD40 [11]. The therapeutic effect of MSC EVs was first ascribed to the entire heterogeneous EV population released by the cells under culture conditions. Subsequent studies, however, tried to identify the potentially most relevant subpopulation by fractionating MSC EVs in medium/large EVs (100–1000 nm) using a  $10,000\times g$  ultracentrifugation (10k fraction) and in small MSC EVs (<100 nm) using a subsequent  $100,000\times g$  ultracentrifugation (100k fraction). In vitro and in vivo pre-clinical experiments clearly showed that the 100k fraction was the main fraction responsible for functional and morphological tissue regeneration [12–14]. Indeed, the 10k and 100k fractions appeared biochemically and functionally distinct [12,15]. The small MSC EVs nowadays consider the proactive fraction retaining the therapeutic activity [16].

The characterisation of the small therapeutic MSC EVs required to fulfil standard EV analyses, including evaluation of morphology, size and expression of vesicular and non-vesicular markers in accordance with the minimal information for studies of extracellular vesicles 2018 (MISEV) [7], coupled with the presence of typical MSC surface antigens and lack of non-MSCs markers, reflects the identity criteria defined for the originating cells by the International Society for Cell & Gene Therapy minimal criteria [16,17]. Indeed, it is of interest and of potential relevance for clinical application to determine and quantify the expression of identity markers such as tetraspanins and mesenchymal markers, as well as of other immunological and pro-coagulative surface markers within the small MSC EV population as compared with medium/large EVs in MSCs of different origin.

Furthermore, recent studies identify that the MSC-mediated immunomodulatory effects in vivo are due to apoptosis, suggesting a therapeutic role for apoptotic EVs [18]. However, knowledge of the differences between apoptotic and naive MSC EVs is still limited. In the present work, we aimed to determine the surface marker expression of small MSC EVs isolated by sequential ultracentrifugation at  $100,000\times g$  (after removal of the  $10,000\times g$  centrifugation), defined here as 100k MSC EVs, as compared to medium/large MSC EVs isolated at  $10,000\times g$  and defined as 10k MSC EVs. In particular, we aimed to characterise and compare the profile of EVs from three different MSC sources of clinical interest, applying the same experimental conditions for MSC culture, EV isolation and analysis. For this comparison, we used different techniques following the standards and requirements of the ISEV community, including innovative single-EV analysis techniques such as ExoView chip and super-resolution microscopy, as well as bead-based cytofluorimetric analysis. Standard culture and apoptotic conditions were applied.

## 2. Materials and Methods

### 2.1. Cell Culture

The MSCs were obtained in collaboration with the RenalToolBox ITN (Grant Agreement 813839). BM-MSCs obtained by the group of Prof. Timothy O'Brien (National University of Galway, Galway, Ireland) were purchased from Lonza (Basel, Switzerland), AT-MSCs from lipoaspirate adipose tissue harvested processed by the group of Prof. Karen Bieback (University of Heidelberg, Heidelberg, Germany) after informed consent. The Mannheim Ethics Commission II approved the study (vote 2011-215N-MA). UC-MSCs were obtained from the group of Dr Jon Smythe (NHS Blood and Transplant, Liverpool, UK) from three

different healthy donors after informed consent, as per the approved protocol of the NHS Blood and Transplant Unit. MSCs were cultured and expanded under standardised protocol among the groups. In particular, all MSCs were cultured using AlphaMEM with UltraGlutamine (BE02-002F, Lonza, Basal, Switzerland) and 10% Foetal Bovine Serum (10270-106, Gibco, MA, USA) in the incubator at 37 °C with 5% CO<sub>2</sub> and controlled humidity. MSCs were checked for the expression of mesenchymal markers by cytofluorimetric analysis (data not shown). EVs were collected from MSCs at 4-6th passage.

## 2.2. EV Isolation

When the cells reached 80% confluency, they were starved overnight (16 h) in RPMI medium (Figure 1). The supernatant was collected and centrifuged for 10 min at 300 × *g* to remove cell debris on the second day. In experiments using apoptotic MSCs, the supernatant was transferred into new tubes and centrifuged 3000 × *g* for 20 min to collect apoptotic bodies. The supernatant was then ultracentrifuged for 1 h at 10,000 × *g*, 4 °C, using the Beckman Coulter Optima L-100K Ultracentrifuge (Beckman Coulter, CA, USA) with the rotor type 70Ti. At this speed, the subpopulation of 10k EVs was collected. The supernatant was further ultracentrifuged for 1 h at 100,000 × *g*, 4 °C to obtain the 100k EV subpopulation. The EV pellet was resuspended in RPMI supplemented with 0.1% DMSO. The EV suspension was then stored at −80 °C until further use.

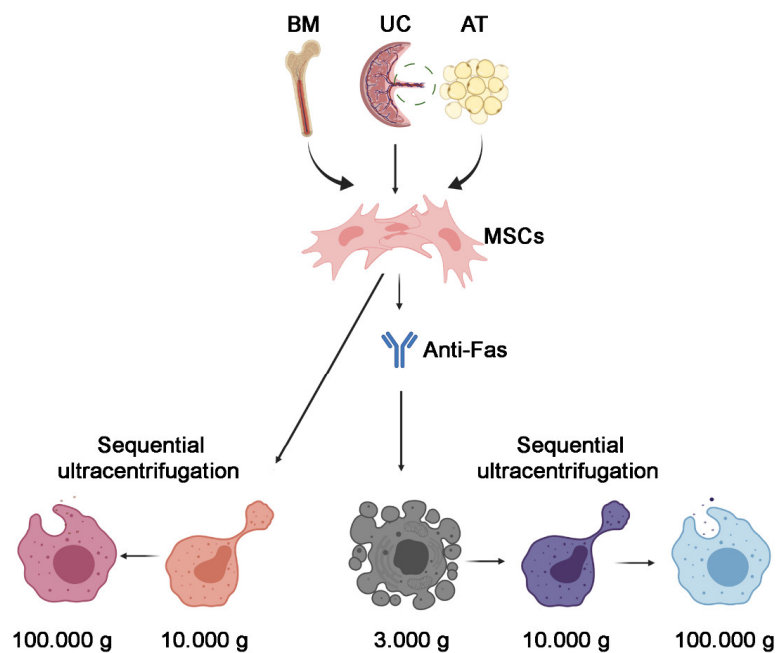


**Figure 1.** Scheme of different EV fractions used in this study. Naive and apoptotic MSC EVs, induced with anti-Fas antibody, obtained from bone marrow (BM), the umbilical cord (UC) or adipose tissue (AT) were isolated using subsequent differential ultracentrifugation. Figure was created using BioRender licence number BO233A7CUA.

Apoptotic vesicles were isolated from MSCs undergoing apoptosis for 24 h using 500 ng/mL of an Anti-Fas Ab (3510771, Merck, NY, USA) diluted in RPMI medium. Isolation of the apoptotic EVs followed the same ultracentrifugation protocol of the naive MSC EVs. The ApoBDs were re-suspended in RPMI supplemented with 1% DMSO.

### 2.3. Nanoparticle Tracking Analysis

After the isolation, the concentration of all the samples was measured by Nanosight NS300 (Malvern Instruments Ltd., Malvern, UK) equipped with a 488 nm laser module that utilises Brownian motion and refraction index. The particle size scatters 10 nm to 1000 nm, although the optimised size range is 70–300 nm. It uses the scattered light to detect a particle and tracks its motion as a function of time. The particles' scattered light was recorded with a light-sensitive camera under a 90° angle to the irradiation plane. This angle allows the Brownian motion of the EVs. Samples were diluted 1:100 in physiologic solution. For each sample, 3 videos of 60 s at camera level 15 and threshold 5 were captured using a syringe pump 30. All the samples were characterised with NTA 3.2 Analytical software. The NTA settings were kept constant between samples.

### 2.4. Transmission Electron Microscopy

The transmission electron microscopy (TEM) was performed on EVs placed on 200-mesh nickel formvar carbon-coated grids (Electron Microscopy Science) for 20 min to promote adhesion. The grids were then incubated with 2.5% glutaraldehyde plus 2% sucrose. EVs were negatively stained with NanoVan (Nanoprobes, Yaphank, NY, USA) and observed using a Jeol JEM 1400 Flash electron microscope (Jeol, Tokyo, Japan).

### 2.5. Cytofluorimetric Analysis

MACSPlex Exosome Kit (Miltenyi Biotec, Bergisch Gladbach, Germany) containing fluorescently labeled (FITC-PE) capture beads coupled to 37 exosomal surface epitopes and 2 isotope controls was used, following the manufacturer's instructions (in detail: CD3, CD4, CD19, CD8, HLA-DR, CD56, CD105, CD2, CD1c, CD25, CD49e, ROR1, CD209, CD9, SSEA-4, HLA-ABC, CD63, CD40, CD62P, CD11c, CD81, MCSP, CD146, CD41b, CD42a, CD24, CD86, CD44, CD326, CD133-1, CD29, CD69, CD142, CD45, CD31, REA control, CD20, CD14, mIgG1 control). Briefly, 15 µL of beads were added to 120 µL of buffer or sample, including a total of  $1 \times 10^9$  EVs, and the complex was then incubated on a rotor overnight at 4 °C. After the incubation and washing steps, a cocktail of APC fluorescent antibodies against tetraspanins (CD9, CD63 and CD81) was added (allowing the detection of beads-bound EVs) and set on the rotor for 1 h at room temperature. After washing, samples were detected using BD FACSCelesta™ Flow Cytometer (BD Bioscience, NJ, USA). Median background values of buffer control were subtracted, and samples were normalised to the median fluorescence intensity of tetraspanins.

### 2.6. ExoView Chip-Based Analysis

NanoView Biosciences (Boston, MA, USA) customised silicone chips coated with tetraspanins, CD44 and CD105 were incubated overnight with  $1 \times 10^8$  MSC EVs suspension diluted in a final volume of 35 µL of incubation buffer A at room temperature. After the incubation, chips were washed 3 times for 3 min on an orbital plate shaker with wash solution B. The chips were scanned with the ExoView™ R100 reader (NanoView Biosciences) by the ExoScanner software (3.0, NanoView Biosciences, Boston, MA, USA). The particle size scatters 50 nm to 200 nm. The data were analysed using ExoViewer software (3.0, NanoView Biosciences, Boston, MA, USA). The number of captured EVs for each surface epitope were compared between the samples.

### 2.7. Super-Resolution Microscopy

Super-resolution microscopy pictures of EVs were obtained using a temperature-controlled Nanoimager S Mark II microscope from ONI (Oxford Nanoimaging, Oxford, UK) equipped with a 100x, 1.4NA oil immersion objective, an XYZ closed-loop piezo 736 stage, and 405 nm/150 mW, 473 nm/1 W, 560 nm/1 W, 640 nm/1 W lasers, as well as dual/triple emission channels split at 640 / and 555 nm. The samples were prepared using 10 µL of 0.01% Poly-L-Lysine (Sigma-Aldrich, St. Louis, MO, USA) placed on high-precision coverslips cleaned in sonication bath 2 times in dH<sub>2</sub>O and once in KOH, in silicon



gasket (Sigma-Aldrich, St. Louis, MO, USA). The coated coverslips were placed at 37 °C in a humidifying chamber for 2 h. Excess of Poly-L-Lysine was removed. Then, 1 µL of EVs ( $1 \times 10^{10}$ ) resuspended in 9 µL of blocking solution (PBS-5% Bovine Serum Albumin) were pipetted into a previously coated well to attach overnight at +4 °C. The next day, the sample was removed, and 10 µL of blocking solution was added into the wells for 30 min. Antibodies were directly conjugated as follows: 2.5 µg of purified mouse anti-CD9 was conjugated with Atto 488 dye (ONI, Oxford, UK), and anti-CD63, CD40 and Annexin V antibodies (Santa Cruz, CA, USA: SC-5275, SC-13128, SC-8300) were conjugated with Alexa Fluor 555 dye. Anti-CD81, Annexin A1 and Anti-Phosphatidylserine antibodies (Santa Cruz, CA, USA; SC-31234, SC-12740. Merck, NY, USA; 05-719) were conjugated with Alexa Fluor 647 dye using the Apex Antibody Labelling Kit (Invitrogen, Carlsbad, CA, USA) according to the manufacturer's protocol. Samples were incubated with 1 µL of each antibody, added into blocking buffer at a final dilution 1:10, under light protection, overnight at +4 °C. The day after, samples were washed twice with PBS, and 10 µL of the mixed ONI B-Cubed Imaging Buffer (Alfatest, Rom, Italy) was added for amplifying the EV imaging. Two-channel (647 and 555) dSTORM data (5000 frames per channel) or three channels (2000 frames per channel) (647, 555 and 488) were acquired sequentially at 30 Hertz in total reflection fluorescence (TIRF) mode. Before each imaging session, beads slide calibration was performed to align fluorescent channels, achieving a channel mapping precision smaller than 12 nm. Single-molecule data was filtered using NimOS (Version 1.18.3, ONI, Oxford, UK) based on the point spread function shape, photon count and localisation precision to minimise background noise and remove low-precision and non-specific co-localisation. All pictures were analysed using algorithms developed by ONI via their CODI website platform (<https://alto.codi.bio/>, 3 October 2021). The filtering and drift correction were used as in NimOS software. The BDScan clustering tool was applied to merged channels, and co-localised EVs were also counted in separate channels.

### 2.8. Statistical Analysis

Data are shown as mean  $\pm$  SD. At least three independent replicates were performed for each experiment. Statistical analysis was carried out on Graph Pad Prism version 8.04 (GraphPad Software, Inc., San Diego, CA, USA) by using the two-way ANOVA followed by Turkey's multiple comparisons test, where appropriate. A *p* value < 0.05 was considered significant.

## 3. Results

### 3.1. Isolation of 100k and 10k MSC EVs and Size Analysis

Two MSC EV fractions were isolated using sequential centrifugations, as detailed in Methods; in particular, medium/large MSC EVs were isolated by a  $10,000 \times g$  ultracentrifugation (10k fraction), followed by the small MSC EV isolation from the remaining supernatant by a  $100,000 \times g$  ultracentrifugation (100k fraction) (Figure 1). MSCs were obtained from bone marrow, adipose tissue and the umbilical cord from three different donors for each cell source. To allow comparison among MSC EVs of different origin, we cultured MSCs in standardised superimposable conditions.

The 100k and 10k MSC EV fractions were first analysed using Nanoparticle tracking analysis (Figure 2A), which confirmed that 100k MSC EVs was a homogenous population. At variance, 10k EVs showed a multi-peak profile, indicating the presence of fractions with a highly variable size (Figure 2A). Transmission electron microscopy analysis showed the 100k EV morphology, as spherical, membrane-encapsulated particles with a characteristic cup-shaped aspect (Figure 2B). In contrast, the 10k EVs represented a heterogeneous population of EVs, differing greatly in size, shape and electron-density (Figure 2B). Quantitative size analysis using Nanoparticle tracking analysis showed that EV size (mode size) was superimposable between the different MSC EV sources (Table 1).

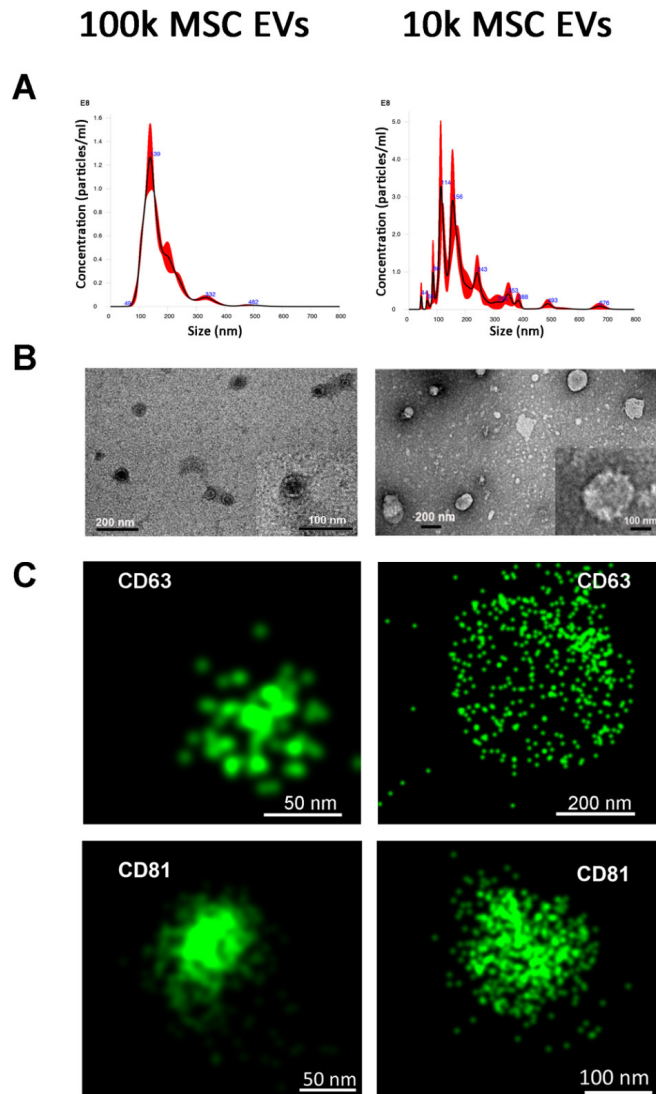


**Figure 2.** Characterisation of 100k and 10k naive MSC EVs. (A) Representative graphs of nanoparticle tracking analysis of 100k MSC EVs (left panel) and 10k MSC EVs (right panel). (B) Representative images of transmission electron microscopy of 100k MSC EVs (left panel) and 10k MSC EVs. The corresponding scale bar is below each EV image. (C) Representative super-resolution microscopy images of 100k MSC EVs (left panel) and 10k MSC EVs (right panel) stained with CD63 or CD81 tetraspanins.

In addition, no differences were detected in the size of the 100k EVs in respect to the 10k EV fractions using this technique. In contrast, by electron microscopy, the majority of 100k EVs were smaller than 100 nm, whereas the majority of 10k EVs were in a size range of 100–300 nm (Table 2).

**Table 1.** Average size and EVs concentration in 1 mL measured by Nanosight.

		100k				10k			
Naive	Mode (nm)	SD	Concentration (Particles/mL)	SD	Mode (nm)	SD	Concentration (Particles/mL)	SD	
BM	187.70	14.31	$5.1 \times 10^8$	$2.4 \times 10^8$	188.83	2.73	$5.8 \times 10^8$	$3.1 \times 10^8$	
UC	184.23	19.63	$3.6 \times 10^8$	$2.1 \times 10^8$	197.07	8.54	$6.8 \times 10^8$	$4.9 \times 10^8$	
AT	208.53	26.44	$6.2 \times 10^8$	$2.5 \times 10^8$	238.61	25.38	$6.2 \times 10^8$	$2.7 \times 10^8$	
		100k				10k			
Apoptotic	Mode (nm)	SD	Concentration (Particles/mL)	SD	Mode (nm)	SD	Concentration (Particles/mL)	SD	
BM	183.67	15.63	$1.4 \times 10^9$	$1.1 \times 10^9$	169.10	18.71	$1.4 \times 10^9$	$1.1 \times 10^9$	
UC	179.57	16.24	$7.8 \times 10^9$	$9.0 \times 10^9$	211.03	14.61	$1.2 \times 10^9$	$1.4 \times 10^9$	
AT	170.90	35.94	$1.1 \times 10^9$	$6.7 \times 10^8$	202.77	22.80	$7.9 \times 10^9$	$1.0 \times 10^9$	

**Table 2.** Mean size of EVs measured by transmission electron microscopy, super-resolution microscopy and ExoView.

	Sample	TEM	Super-Resolution Microscopy	ExoView (50–200 nm Detection)
SIZE 100k EVs [nm]	BM	40–100	$88.00 \pm 7.94$	$61.85 \pm 3.64$
	UC	40–100	$88.00 \pm 3.46$	$59.14 \pm 2.03$
	AT	40–100	$98.00 \pm 2.11$	$59.92 \pm 2.72$
SIZE 10k EVs [nm]	BM	100–300	$140.00 \pm 5.77$	$90.00 \pm 1.73$
	UC	100–300	$120.00 \pm 5.77$	$90.33 \pm 2.34$
	AT	100–300	$120.00 \pm 8.42$	$92.83 \pm 5.08$

Using super-resolution microscopy based on tetraspanin staining (CD63 and CD81) on intact unfixed MSC EVs, we also confirmed the size of tetraspanin-expressing EV fractions (Figure 2C), being 100k EVs quantified, as around 90 nm median size for all MSC sources using an automatic size analysis software, whereas 10k EVs have a median size of around 130 nm (see Table 2). Single molecule analysis of CD63 expression also indicated its differential distribution on the EV surface, as 10k EVs showed a discrete surface expression, whereas 100k EVs showed a more condensed tetraspanin localisation, possibly due to the small size (Figure 2C). The patchy distribution of tetraspanins was more evident on larger EVs within the 10k fraction (>500 nm) (Supplementary Figure S1).

#### Variable Tetraspanin Expression on 100k and 10k Single MSC EVs by Super-Resolution Microscopy

Transmembrane tetraspanin proteins CD63, CD9 and CD81 are a major class of EV-expressed molecules previously reported to be enriched in 100k in respect to 10k EV fraction [19,20]. We first took advantage of super-resolution microscopy to assess tetraspanin co-expression at a single EV level on 100k and 10k MSC EVs (Figure 3). Advanced three-colour staining was performed using the anti-tetraspanin Abs dyed in red (CD81), green (CD63) and blue (CD9) using dSTORM single-molecule analysis with super-resolution microscopy. Tetraspanin single-molecule surface analysis highlighted an uneven tetraspanins distribution on the EV surface. Moreover, we observed a heterogeneous tetraspanin distribution of EVs variably positive for single, double or triple tetraspanins (Figure 3). We also took advantage of an automated software analysis for the quantification of tetraspanin co-expression on single EVs (Figure 3C,D).

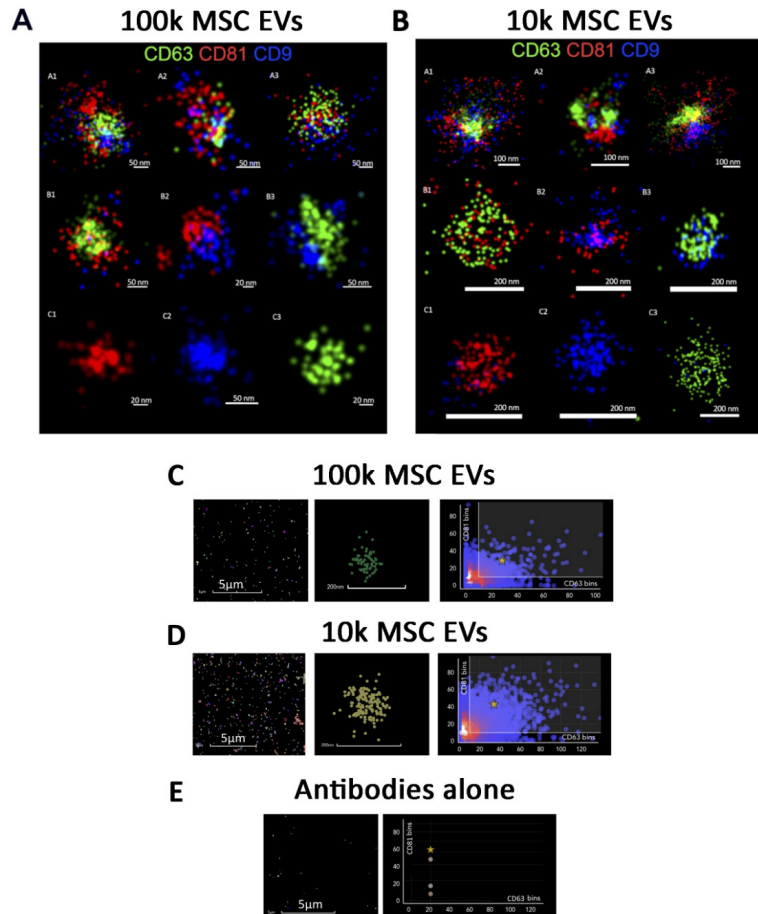


**Figure 3.** Super-resolution microscopy images. Representative super-resolution microscopy images of 100k EVs (**A**) and 10k EVs (**B**) stained with tetraspanins: CD81 red, CD63 green, and CD9 blue. Both panels (**A,B**) show triple positive, double positive and single positive MSC EVs. The corresponding scale bar is below each EV image. (**C**) Representative clustering strategy of MSC 100k EVs with large field of view (left panel), a selected cluster (central panel) and graph (right panel) showing CD81/CD63 cluster distribution. (**D**) Representative clustering strategy of MSC 10k EVs with large field of view (left panel), a selected cluster (central panel) and graph (right panel) showing the proportion of CD81 and CD63 antibodies/cluster. (**E**) Representative clustering strategy of negative control using antibodies alone without EVs showing large field of view and graph demonstrating the proportion of CD81 and CD63 antibodies.

In particular, the triple tetraspanin expression only represented a fraction of the entire EV population, as the other EVs were variably positive for the different markers (Figure 4). The 100k MSC EV fraction, in general, did not show increased tetraspanin expression in respect to the 10k fraction. CD63 was the most expressed marker in the single positive EV population in AT- and UC-MSC EVs, but not in BM-MSC EVs (Figure 4). The 10k fraction of UC-MSC EVs showed the largest population of EVs co-expressing CD81, CD63 and CD9 (Figure 4B). These results show a variable co-expression of the tetraspanins on MSC EV sources, without significant differences in the 10k and 100k fractions.

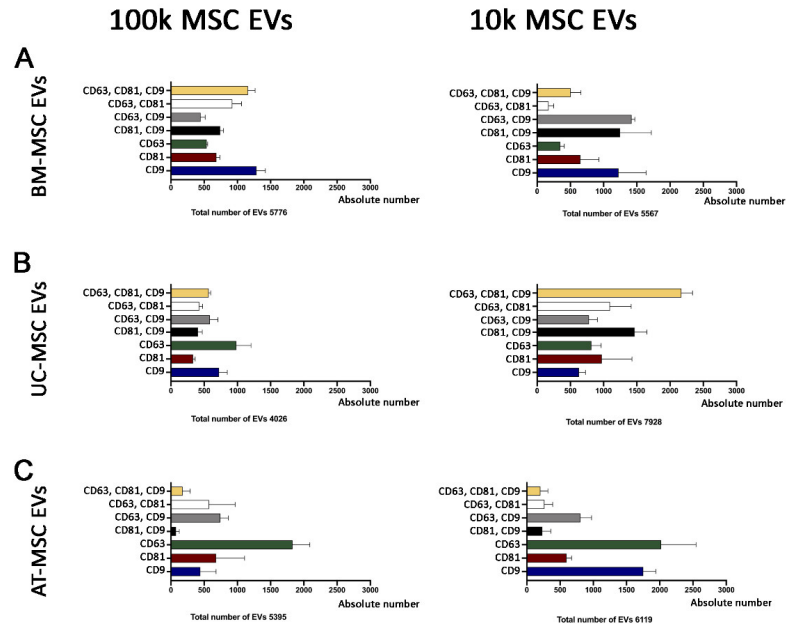


**Figure 4.** Super-resolution microscopy analysis of 100k and 10k MSC EVs. The graphs show triple positive, double positive and single positive EVs of 100k and 10k MSC EVs. (A) BM-MSC EVs, (B) UC-MSC EVs, (C) AT-MSC EVs. The total number of single EVs analysed is reported below each graph.

### 3.2. Isolation of 100k and 10k MSC EVs from Apoptotic Cells

We also generated 100k and 10k EVs from MSCs undergoing apoptosis using an anti-Fas Ab, as described [21,22], for further comparison with the naive fractions. Fas triggered MSC apoptosis induction was confirmed by Annexin V staining (Supplementary Figure S2 and Supplementary Table S1). Moreover, apoptosis induction was also assessed by the generation of large apoptotic bodies (size range 1–5  $\mu\text{m}$ ), showing positivity for the apoptotic marker Annexin V by flow cytometry and by super-resolution microscopy (Supplementary Figure S2). Moreover, apoptotic bodies also showed positivity for Phosphatidylserine (Supplementary Figure S2C), as previously described [7].

The size and number of apoptotic MSC EVs were analysed by nanoparticle tracking analysis and by electron microscopy, showing a similar size of the naive MSC EVs for both the 100k and 10k fractions (Table 1 and Figure 5). However, apoptotic 100k EVs showed a less homogeneous profile than the naive ones in the nanoparticle tracking analysis (Figure 5A). Interestingly, the average concentration of both 100k and 10k EVs from apoptotic cells was significantly higher than that obtained from naive cells using the same originating cell number (Table 1). Superimposable results were obtained for the three MSC sources. Using super-resolution microscopy, we detected the expression of Phosphatidylserine and Annexin V on apoptotic 100k and 10k and not on naive MSC EVs, confirming that these markers are able to specifically characterise the apoptotic EVs (Figure 5C,D) [23].

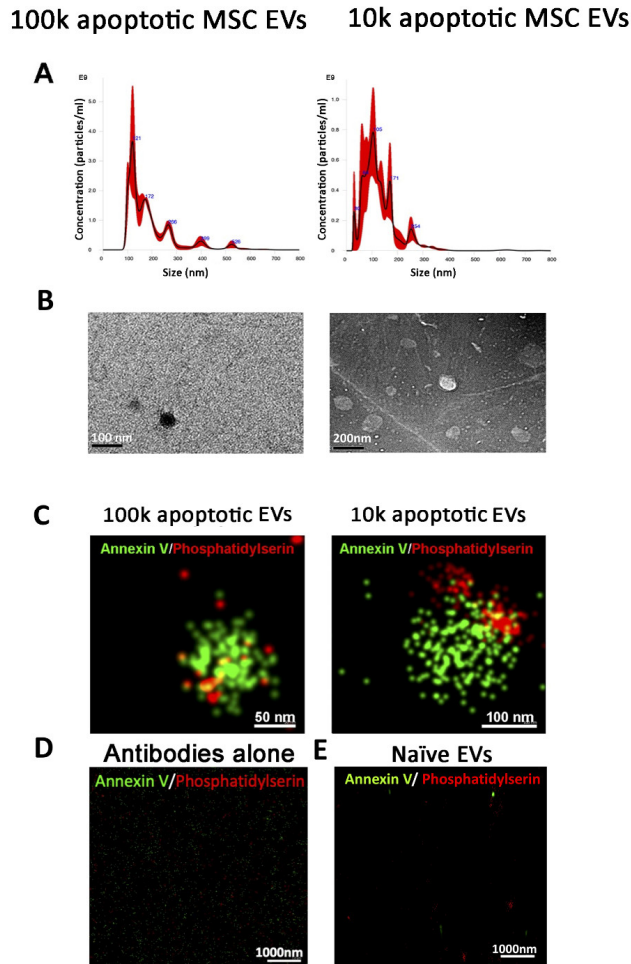


**Figure 5.** Characterisation of 100k and 10k apoptotic MSC EVs. (A) Representative graphs of nanoparticle tracking analysis of 100k apoptotic MSC EVs (left panel) and 10k apoptotic MSC EVs (right panel). (B) Representative images of transmission electron microscopy of 100k apoptotic MSC EVs (left panel) and 10k apoptotic MSC EVs (right panel). (C) Representative super-resolution microscopy images of 100k apoptotic MSC EVs (left panel) and 10k apoptotic MSC EVs (right panel) stained with Annexin V (green) and Phosphatidylserine (red). (D) Representative super-resolution microscopy image of Annexin V (green) and Phosphatidylserine (red) as a negative control without EVs. (E) Representative super-resolution microscopy image of 100k MSC EVs isolated from naïve MSCs and stained with Annexin V (green) and Phosphatidylserine (red).

### 3.2.1. Quantitative Tetraspanin Evaluation of Naïve and Apoptotic 100k and 10k MSC EVs

We therefore used cytofluorimetric analysis and ExoView to gain quantitative results for the comparison of tetraspanin level expression in MSC EV fractions from all different sources, in naïve and apoptotic MSC EVs.

Semiquantitative analysis of tetraspanin levels in all MSC EV subsets was performed using the MACSPlex exosome kit, a bead-based cytofluorimetric analysis. This technique

did not detect differences among MSC sources, MSC EV fractions and naive or apoptotic conditions (Figure 6).

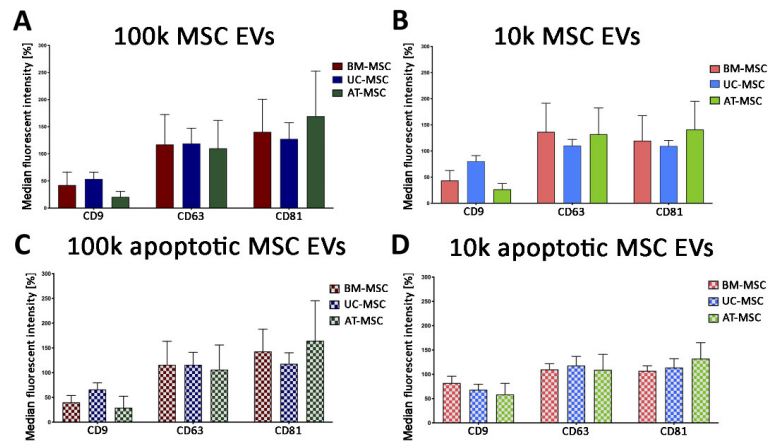


**Figure 6.** MACSPlex tetraspanin analysis of 100k MSC EVs and 10k MSC EVs of naive and apoptotic MSCs. Histograms represent the median fluorescence intensity of CD9, CD63 and CD81 tetraspanins for 100k MSC EVs (A,C) and 10k MSC EVs (B,D) isolated from naive (A,B) and apoptotic (C,D) MSCs. BM-MSC EVs, UC-MSC EVs and AT-MSC EVs were compared. Data are expressed as mean  $\pm$  SD of three different experiments.

ExoView chip-based analysis was then used to obtain an evaluation of the number of the particles captured on a specific chip coated with tetraspanins and negative mouse IgG control (MIgG). The number of EVs loaded onto each chip was normalised based on their concentration, as evaluated with the nanoparticle tracking analysis. The results showed that the apoptotic EV fractions showed a higher number of tetraspanin-captured EVs than the naive ones, and that the 10k fractions showed a higher number of tetraspanin-captured EVs than the 100k fractions for all MSC sources used (Figure 7). Among the different sources the tetraspanin levels were significantly different, and UC-MSC EVs had the highest expression of most markers (Figure 7).

Comparing different techniques, CD9 expression by MACSPlex appeared lower than other tetraspanins for all MSC sources and fractions, at the variance of the results obtained using ExoView or super-resolution microscopy. These data highlight that ExoView provides a better quantitative analysis regarding the bead-based cytofluorimetric assay, performing a semiquantitative analysis. Moreover, different antibody affinities could be present.

### 3.2.2. Mesenchymal, and Immunological Marker Expression on Naive and Apoptotic 100k and 10k MSC EVs

Mesenchymal markers are usually assessed to characterise MSC EVs [24]. The MACSPlex exosome kit allowed the evaluation of CD56, CD44, CD29, CD49e, CD146 and CD105 mesenchymal marker expression on all EV fractions, from the three MSC sources in naive and apoptotic conditions (Figure 8).

Mesenchymal markers were expressed from all MSC sources and MSC EV fractions in the naive and apoptotic EV conditions, but higher levels were generally observed in the 10k fraction with respect to the 100k fraction. We confirmed the expression of the mesenchymal CD105 and CD44 markers on the 100k naive and apoptotic MSC EVs (Figure 9A,B). CD44 and CD105 had a wider size range by size distribution of captured EVs, which is especially evident in the 100k apoptotic MSC EVs (Figure 9C,D).

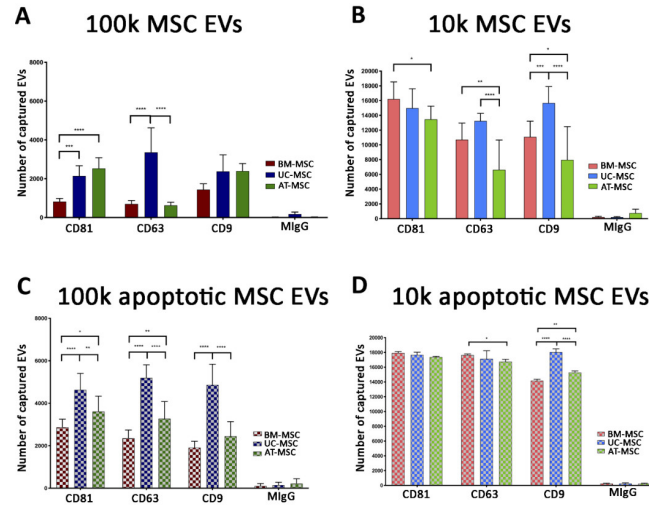


**Figure 7.** ExoView tetraspanin analysis of 100k and 10k MSC EVs of naive and apoptotic MSCs. Histograms represent the number of captured EVs for CD9, CD63 and CD81 tetraspanins and negative control. 100k MSC EVs (A,C) and 10k MSC EVs (B,D) isolated from naive (A,B) and apoptotic (C,D) MSCs were analysed. BM-MSC EVs, UC-MSC EVs and AT-MSC EVs were compared. Data are expressed as mean  $\pm$  SD of three different experiments. A  $p$  value  $< 0.05$  was considered significant (\*  $p < 0.05$ , \*\*  $p < 0.001$ , \*\*\*  $p < 0.001$ , \*\*\*\*  $p < 0.0001$ ).

**Mesenchymal markers**

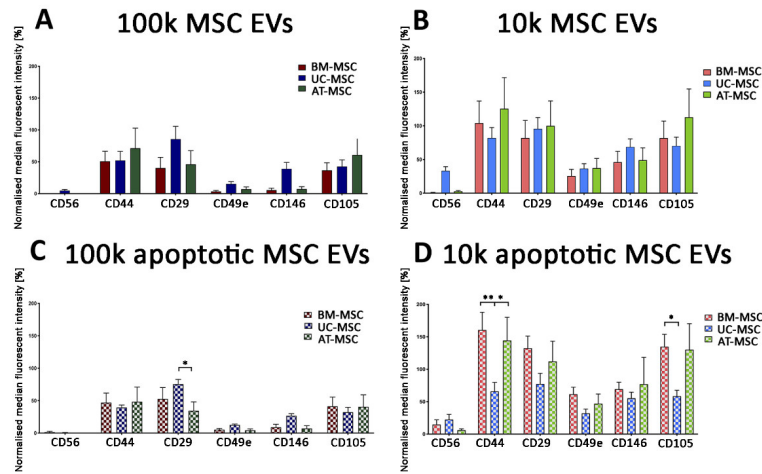


**Figure 8.** MACSPlex mesenchymal marker analysis of 100k and 10k MSC EVs of naive and apoptotic MSCs. (A–D) Histograms represent normalised fluorescence intensity of mesenchymal markers (CD56, CD44, CD29, CD49e, CD146, CD105) for 100k MSC EVs (A,C) and 10k MSC EVs (B,D) isolated from naive (A,B) and apoptotic (C,D) MSCs. BM-MSC EVs, UC-MSC EVs and AT-MSC EVs were compared. Data are expressed as median fluorescence intensity normalised to the median fluorescence intensity of tetraspanins  $\pm$  SD of three different experiments. A  $p$  value  $< 0.05$  was considered significant (\*  $p < 0.05$ , \*\*  $p < 0.001$ ).



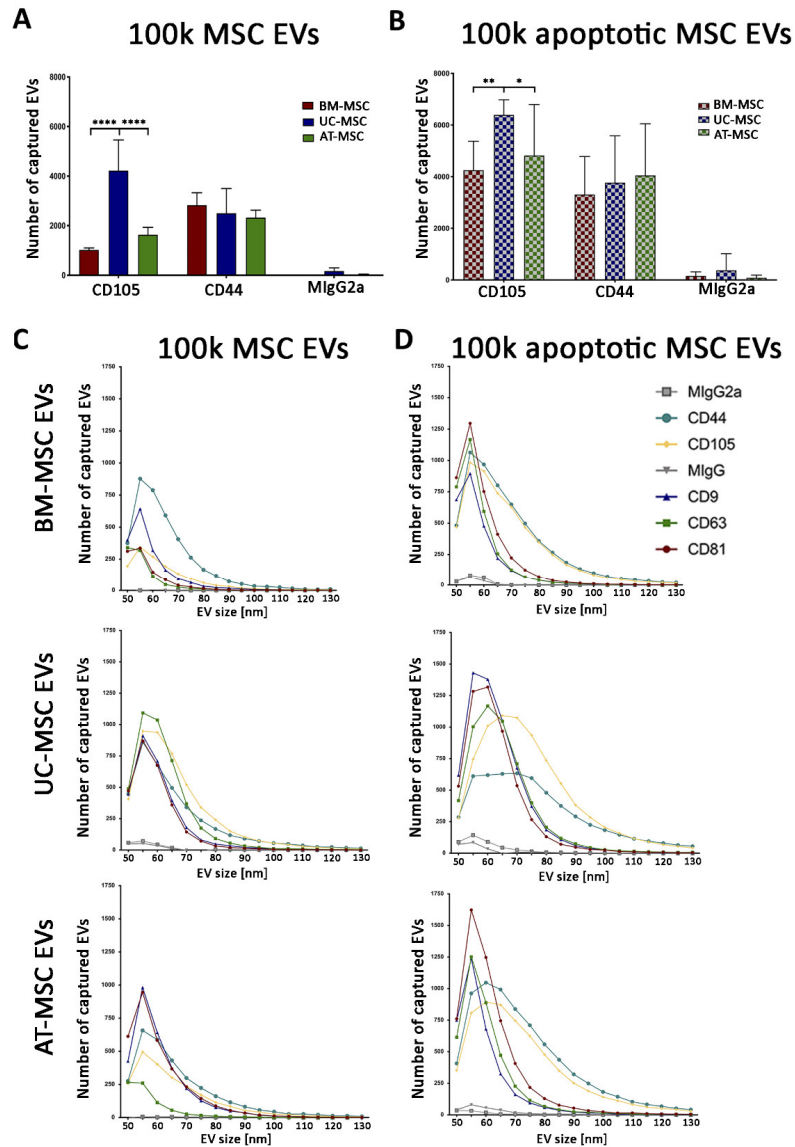


**Figure 9.** ExoView mesenchymal marker analysis of 100k of naive and apoptotic MSC EVs. (A,B) Histograms showing the number of captured EVs for mesenchymal markers (CD44, CD105) and negative control for 100k MSC EVs (A) and 100k apoptotic MSC EVs (B). Data are mean  $\pm$  SD of three different experiments. A  $p$  value  $<0.05$  was considered significant (\*  $p < 0.05$ , \*\*  $p < 0.001$ , \*\*\*\*  $p < 0.0001$ ). (C,D) Size of naive (C) and apoptotic (D) 100k MSC EVs from BM-MSC EVs, UC-MSC EVs and AT-MSC EVs.

Moreover, as demonstrated by the MACSPlex exosome kit, all EVs were negative for CD14, CD19, CD31 and CD45, as were the originating cells (data not shown). Interestingly, the 100k fractions were constantly negative for immunological markers, selectively expressed by the 10k EVs (Figure 10A–D). In particular, the fraction enriched for 10k EVs both in naive and apoptotic conditions was selectively expressing HLA-class I and CD40

co-stimulatory molecule. Moreover, tissue factor (TF), known to be involved in platelet activation, was expressed by 10k EVs of AT- and UC-MSC EVs, and not from those of BM-MSC EVs (Figure 10B,D).

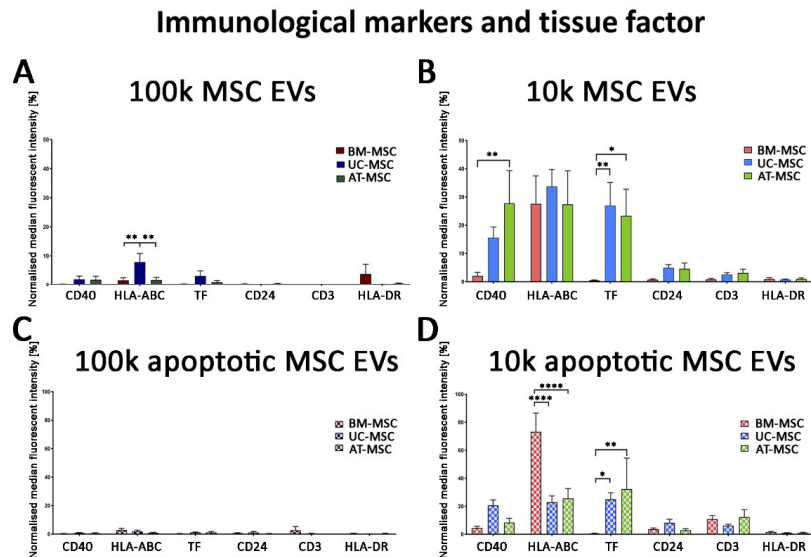


**Figure 10.** MACSplex immunological marker analysis of 100k and 10k MSC EVs of naive and apoptotic MSCs. (A–D) Histograms represent normalised fluorescence intensity of immunity markers (CD40, HLA-ABC, CD24, CD3 and HLA-DR) and tissue factor (TF) for 100k MSC EVs (A,C) and 10k MSC EVs (B,D) isolated from naive (A,B) and apoptotic (C,D) MSCs. BM-MSC EVs, UC-MSC EVs and AT-MSC EVs were compared. Data are expressed as median fluorescence intensity normalised to the median fluorescence intensity of tetraspanins  $\pm$  SD of three different experiments. A  $p$  value  $< 0.05$  was considered significant (\*  $p < 0.05$ , \*\*  $p < 0.001$ , \*\*\*\*  $p < 0.0001$ ).

#### 4. Discussion

Small MSC EVs appear to be the most promising EV type for therapeutic application, and the information on the surface marker expression characterising the different MSC sources and fractions is of importance. This study presents a quantitative analysis of the surface expression profile of tetraspanins at a single EV level, showing variable tetraspanin coexpression in all EV fractions and sources by super-resolution microscopy. Moreover, using bead-based cytofluorimetric analysis and chip-based arrays, tetraspanins, as well as other clinically relevant markers (mesenchymal, immunological and pro-coagulative markers), were compared in MSC EVs from three sources in naive or apoptotic condition. The results highlight a similar characterisation profile of MSC EVs from the different MSC sources, with variable but consistent tetraspanin expression. Moreover, we observed an increased expression of mesenchymal surface markers and the restricted expression of HLA-class I, the co-stimulatory molecule CD40 and tissue factor by 10k MSC EVs, with respect to 100k MSC EVs. Finally, apoptotic conditions only modified the number, not the characterisation profile, of MSC EVs. Further functional analysis will be required to fully compare the properties of the different EV fractions and sources.

Thanks to an extensive effort of the EV community, the minimal criteria for EV characterisation have been set in open-access publication MISEV 2018 [7]. The analysis of the EV preparation includes a bulk analysis of protein expression demonstrating the EV identity and purity together with qualitative and quantitative analysis using a particle counter and electron microscopy [25]. The development of new nanotechnological instruments in recent

years may allow the assessment of EV identity at a single EV level using affinity-based chips, super-resolution microscopy and high-resolution flow cytometry.

Here, we compared different orthogonal methods to provide a single EV analysis of 100k and 10k MSC EVs, highlighting their potential contribution and utility for 100k MSC EVs characterisation. The analysis of the EV size appeared discordant between the commonly used nanoparticle tracking analysis and the other methods. In fact, nanoparticle tracking analysis clearly showed a differential profile of 100k and 10k EVs, but the mean size of the 100k fraction was higher than that detected with other quantitative methods, as previously described [12]. This could be due to phenomena of EV aggregation, or to the influence of both temperature and Brownian motion incorporated in the nanoparticle tracking method of EV characterisation. In addition, particle size using this method can result in non-consistent data; similar analyses were reported with a difference of 15–50% in size [26].

Electron microscopy analysis clearly showed that the 100k MSC EVs and 10k MSC EVs had distinct size. Interestingly, this observation was in line with that obtained by the specific analysis of tetraspanin expressing EVs, acquired with super-resolution microscopy on more than 10,000 analysed fresh, unfixed EVs. In addition, quantitative single-vesicle imaging by super-resolution microscopy revealed a heterogeneous pattern of tetraspanin expressions (single, double and triple) in variable proportions in 100k and 10k MSC EVs. Recently, a single-vesicle imaging and co-localisation analysis of tetraspanins were investigated in EVs derived from HEK397, breast cancer and melanoma cell line, showing distinct fractions of single, double or triple co-expressing EVs, depending on the analysed EV type [27]. This is consistent with the observation that CD9- and CD81-positive EVs did not correlate with distinct EV populations using a size-based EV separation technique [28]. Another relevant feature was the patchy distribution of tetraspanins on the EV surface, usually characteristic of 10k EVs. Indeed, tetraspanins are known to homodimerize and form large complexes [29]. This may suggest the ability of tetraspanins on EV surface to move within the lipidic membrane, as described for the cell membrane, with capping after antibody binding [30].

Different MSC sources can be identified for clinical application of deriving EVs, the BM-MSC EVs being the first and most commonly used in clinical trials. However, EVs from adipose tissue and the umbilical cord might display advantages for easier cell isolation from adipose tissue, reduced impact of donor diseases or enhanced potency for umbilical cord [31]. We therefore compared 100k and 10k EVs from MSCs cultured in completely identical culture conditions (media and serum, expansion number and passages) for the expression of clinically relevant markers using a standard semiquantitative cytofluorimetric assay commonly used to assess MSC EV profile [32]. Interestingly, mesenchymal markers were present in both 100k MSC EVs and 10k MSC EVs, but with higher expression in the apoptotic EV fractions. At variance, HLA class I, co-stimulatory molecule and tissue factor expression were selectively expressed on 10k MSC EVs. These data suggest that the 100k MSC EV fractions are safe for clinical application, avoiding the possible development of anti-HLA antibodies and rejection. Moreover, 10k EVs from AT- or UC-MSCs also showed the expression of tissue factor. This is more in line with the increased coagulative capacity of 10k than that of the 100k MSC EV fractions previously reported [33]. Moreover, 10k BM-MSC EVs appeared to display the lowest expression of tissue factor, in analogy with reports showing higher thrombogenic activity of UC- or AT-MSCs in respect to BM-MSC EVs [34,35].

Finally, in the present study, we also compared naive MSC EVs and apoptotic MSC EVs from the different MSC sources. Indeed, apoptotic EVs are considered to display peculiar functions and are now considered an additional but distinct MSC product with potent immunoregulatory ability [18]. The EVs were released by apoptotic cells after Fas receptor triggering [21,22], and apoptosis was confirmed by the detection of apoptotic bodies and by expression of Phosphatidylserin [10] and Annexin V by apoptotic EVs [36]. The most relevant feature observed was the increase in number of both 100k and 10k MSC EVs released

from all MSC types under apoptotic conditions. Moreover, apoptotic EVs expressed higher tetraspanin levels and mesenchymal markers with respect to the normal counterpart, as evaluated by ExoView and MACSPlex analysis, respectively.

## 5. Conclusions

In conclusion, our results show that the characterisation profile of MSC EV fractions is consistent among different MSC sources, with an increased number of EVs released under apoptotic condition. Moreover, the 100k MSC EV population displays a safer profile than the 10k MSC EV population for immunological and pro-coagulative marker expression. Finally, our study identified advantages of the different EV analytical techniques for specific applications. In particular, super-resolution microscopy was useful to characterise a large number of EVs at a single EV level, whereas ExoView analysis allowed an easy quantitative comparison of marker expression among fractions of different origins and conditions. In addition, bead-based cytofluorimetric analysis appeared to be of utility for its large variety of markers of clinical applicability, although it can only provide semiquantitative results. These results suggest that quantitative EV analysis methods are useful and reliable enough to be applied for the characterisation of MSC EV fractions.

**Supplementary Materials:** The following are available online at <https://www.mdpi.com/article/10.3390/cells10112948/s1>, Figure S1: Representative super-resolution microscopy images of a single EV from the 10k BM-MSC fraction, showing CD81 tetraspanin surface distribution along the membrane, with areas of condensed expression. Figure S2: Induction of apoptosis and characterization of apoptotic bodies using MUSE flow cytometry and super-resolution microscopy. (A) MSCs viability profile after 24 h in RPMI with 500 ng of anti-Fas antibody (A1), RPMI (A2) and AlphaMEM with 10% FBS (A3). (B) Representative images of flow cytometric analysis showing Annexin V expression. (B1) flow cytometry gating strategies, P4: apoptotic bodies (ApoBDs), P2: 4 µm latex beads, P3: apoptotic cells. Representative images of flow cytometric analysis showing (B2) unstained ApoBDs and (B3) ApoBDs stained with Annexin V. (C) Representative super-resolution microscopy image of ApoBD fraction stained (C1) with Annexin V (red), (C2) with Annexin V (red) and Phosphatidylserine (green). (D1) Representative bright field microscopy image of ApoBDs realised by MSCs undergoing apoptosis. Table S1: MUSE assay used to set up the apoptotic induction. Cells were analysed after 6, 16 and 24 h in full condition medium, RPMI or RPMI with 500 ng of anti-Fas antibody. Graphical visualization is in Supplementary Figure S2A.

**Author Contributions:** Conceptualization, R.S. and B.B.; methodology, R.S., G.C. and M.C.D.; software, R.S. and C.G.; validation, V.D. and R.S.; formal analysis, R.S.; investigation, R.S.; data curation, R.S.; writing—original draft preparation, R.S.; writing and editing, R.S., C.G. and B.B.; supervision, B.B.; project administration, B.B.; funding acquisition, B.B. All authors have read and agreed to the published version of the manuscript.

**Funding:** This project has received funding from the European Union's Horizon 2020 research and innovation programme under the Marie Skłodowska-Curie Grant agreement No. 813839.

**Institutional Review Board Statement:** The use of AT-MSCs was approved by the Mannheim Ethics Commission II (vote 2011-215N-MA).

**Data Availability Statement:** Data supporting reported results can be obtained by the corresponding author under request.

**Acknowledgments:** The authors thank Natalia Gebara for her support in preparing and analysing the experiments; Eleonora Scaccia, Erika Erika, Francesco Amadeo and Sandra Calcat for isolating and providing MSCs; Pradeep Kumar for helping with super-resolution microscopy acquisition and analysis. The authors also thank Marco Sassoe Pognetto of the Department of Neurosciences at the University of Turin for the use of the electron microscopy facility.

**Conflicts of Interest:** The authors declare no conflict of interest.

## References

- Flemming, A.; Schallmoser, K.; Strunk, D.; Stolk, M.; Volk, H.D.; Seifert, M. Immunomodulative efficacy of bone marrow-derived mesenchymal stem cells cultured in human platelet lysate. *J. Clin. Immunol.* **2011**, *31*, 1143–1156. [[CrossRef](#)]
- Humphreys, B.D.; Bonventre, J.V. Mesenchymal stem cells in acute kidney injury. *Annu. Rev. Med.* **2008**, *59*, 311–325. [[CrossRef](#)] [[PubMed](#)]
- Bussolati, B.; Hauser, P.; Carvalhosa, R.; Camussi, G. Contribution of Stem Cells to Kidney Repair. *Curr. Stem Cell Res. Ther.* **2009**, *4*, 2–8. [[CrossRef](#)] [[PubMed](#)]
- Lener, T.; Gimona, M.; Aigner, L.; Börger, V.; Buzas, E.; Camussi, G.; Chaput, N.; Chatterjee, D.; Court, F.A.; del Portillo, H.A.; et al. Applying extracellular vesicles based therapeutics in clinical trials—An ISEV position paper. *J. Extracell. Vesicles* **2015**, *4*. [[CrossRef](#)] [[PubMed](#)]
- Chargaff, E.; West, R. The biological significance of the thromboplastic protein of blood. *J. Biol. Chem.* **1946**, *166*, 189–197. [[CrossRef](#)]
- Park, K.S.; Bandeira, E.; Shelke, G.V.; Lässer, C.; Lötvall, J. Enhancement of therapeutic potential of mesenchymal stem cell-derived extracellular vesicles. *Stem Cell Res. Ther.* **2019**, *10*, 1–15. [[CrossRef](#)]
- Théry, C.; Witwer, K.W.; Aikawa, E.; Alcaraz, M.J.; Anderson, J.D.; Andriantsitohaina, R.; Antoniou, A.; Arab, T.; Archer, F.; Atkin-Smith, G.K.; et al. Minimal information for studies of extracellular vesicles 2018 (MISEV2018): A position statement of the International Society for Extracellular Vesicles and update of the MISEV2014 guidelines. *J. Extracell. Vesicles* **2018**, *7*, 1535750. [[CrossRef](#)] [[PubMed](#)]
- Willms, E.; Johansson, H.J.; Mäger, I.; Lee, Y.; Blomberg, K.E.M.; Sadik, M.; Alaarg, A.; Smith, C.I.E.; Lehtio, J.; El Andaloussi, S.; et al. Cells release subpopulations of exosomes with distinct molecular and biological properties. *Sci. Rep.* **2016**, *6*, 22519. [[CrossRef](#)] [[PubMed](#)]
- Yáñez-Mó, M.; Siljander, P.R.-M.; Andreu, Z.; Zavec, A.B.; Borrás, F.E.; Buzas, E.I.; Buzas, K.; Casal, E.; Cappello, F.; Carvalho, J.; et al. Biological properties of extracellular vesicles and their physiological functions. *J. Extracell. Vesicles* **2015**, *4*, 27066. [[CrossRef](#)] [[PubMed](#)]
- Leventis, P.A.; Grinstein, S. The Distribution and Function of Phosphatidylserine in Cellular Membranes. *Annu. Rev. Biophys.* **2010**, *39*, 407–427. [[CrossRef](#)] [[PubMed](#)]
- Mobarrez, F.; Sjövik, C.; Soop, A.; Hällström, L.; Frostel, C.; Pisetsky, D.S.; Wallén, H. CD40L expression in plasma of volunteers following LPS administration: A comparison between assay of CD40L on platelet microvesicles and soluble CD40L. *Platelets* **2014**, *26*, 486–490. [[CrossRef](#)] [[PubMed](#)]
- Bruno, S.; Tapparo, M.; Collino, F.; Chiabotto, G.; Deregibus, M.C.; Lindoso, R.S.; Neri, F.; Kholia, S.; Giunti, S.; Wen, S.; et al. Renal Regenerative Potential of Different Extracellular Vesicle Populations Derived from Bone Marrow Mesenchymal Stromal Cells. *Tissue Eng. Part A* **2017**, *23*, 1262–1273. [[CrossRef](#)]
- Aliotta, J.M.; Pereira, M.; Wen, S.; Dooner, M.S.; Del Totto, M.; Papa, E.; Goldberg, L.R.; Baird, G.L.; Ventetuolo, C.; Quesenberry, P.J.; et al. Exosomes induce and reverse monocrotaline-induced pulmonary hypertension in mice. *Cardiovasc. Res.* **2016**, *110*, 319–330. [[CrossRef](#)]
- Wen, S.; Dooner, M.; Cheng, Y.; Papa, E.; del Totto, M.; Pereira, M.; Deng, Y.; Goldberg, L.; Aliotta, J.; Chatterjee, D.; et al. Mesenchymal stromal cell derived extracellular vesicles rescue radiation damage to murine marrow hematopoietic cells Sicheng. *Physiol. Behav.* **2016**, *176*, 139–148.
- Xu, R.; Greening, D.W.; Rai, A.; Ji, H.; Simpson, R.J. Highly-purified exosomes and shed microvesicles isolated from the human colon cancer cell line LIM1863 by sequential centrifugal ultrafiltration are biochemically and functionally distinct. *Methods* **2015**, *87*, 11–25. [[CrossRef](#)] [[PubMed](#)]
- Witwer, K.W.; van Balkom, B.W.M.; Bruno, S.; Choo, A.; Dominici, M.; Gimona, M.; Hill, A.F.; de Kleijn, D.; Koh, M.; Lai, R.C.; et al. Defining mesenchymal stromal cell (MSC)-derived small extracellular vesicles for therapeutic applications. *J. Extracell. Vesicles* **2019**, *8*. [[CrossRef](#)]
- Gimona, M.; Brizzi, M.F.; Choo, A.B.H.; Dominici, M.; Davidson, S.M.; Grillari, J.; Hermann, D.M.; Hill, A.F.; de Kleijn, D.; Lai, R.C.; et al. Critical considerations for the development of potency tests for therapeutic applications of mesenchymal stromal cell-derived small extracellular vesicles. *Cytotherapy* **2021**, *23*, 373–380. [[CrossRef](#)]
- Caruso, S.; Poon, I.K.H. Apoptotic cell-derived extracellular vesicles: More than just debris. *Front. Immunol.* **2018**, *9*, 1486. [[CrossRef](#)] [[PubMed](#)]
- Crescitelli, R.; Lässer, C.; Szabó, T.G.; Kittel, A.; Eldh, M.; Dianzani, I.; Buzás, E.I.; Lötvall, J. Distinct RNA profiles in subpopulations of extracellular vesicles: Apoptotic bodies, microvesicles and exosomes. *J. Extracell. Vesicles* **2013**, *2*, 1–10. [[CrossRef](#)]
- Kowal, J.; Arras, G.; Colombo, M.; Jouve, M.; Morath, J.P.; Prindl-Bengtson, B.; Dingli, F.; Loew, D.; Tkach, M.; Théry, C. Proteomic comparison defines novel markers to characterize heterogeneous populations of extracellular vesicle subtypes. *Proc. Natl. Acad. Sci. USA* **2016**, *113*, E968–E977. [[CrossRef](#)]
- Adachi, K.; Osaki, M.; Kase, S.; Takeda, A.; Ito, H. Anti-Fas antibody-induced apoptosis and its signal transduction in human gastric carcinoma cell lines. *Int. J. Oncol.* **2003**, *23*, 713–719. [[CrossRef](#)] [[PubMed](#)]
- Wang, Y.; Xia, C.; Lv, Y.; Li, C.; Mei, Q.; Li, H.; Wang, H.; Li, S. Crosstalk Influence between P38MAPK and Autophagy on Mitochondria-Mediated Apoptosis Induced by Anti-Fas Antibody/Actinomycin D in Human Hepatoma Bel-7402 Cells. *Molecules* **2017**, *22*, 1705. [[CrossRef](#)] [[PubMed](#)]

23. Tixeira, R.; Caruso, S.; Paone, S.; Baxter, A.A.; Atkin-Smith, G.K.; Hulett, M.D.; Poon, I.K.H. Defining the morphologic features and products of cell disassembly during apoptosis. *Apoptosis* **2017**, *22*, 475–477. [[CrossRef](#)]
24. Giebel, B.; Kordelas, L.; Börger, V. Clinical potential of mesenchymal stem/stromal cell-derived extracellular vesicles. *Stem Cell Investig.* **2017**, *4*, 84. [[CrossRef](#)] [[PubMed](#)]
25. EV-TRACK Consortium; Van Deun, J.; Mestdagh, P.; Agostinis, P.; Akay, A.; Anand, S.; Anckaert, J.; Martinez, Z.A.; Baetens, T.; Beghein, E.; et al. EV-TRACK: Transparent reporting and centralizing knowledge in extracellular vesicle research. *Nat. Methods* **2017**, *14*, 228–232. [[CrossRef](#)]
26. Rohde, E.; Pachler, K.; Gimona, M. Manufacturing and characterization of extracellular vesicles from umbilical cord-derived mesenchymal stromal cells for clinical testing. *Cytotherapy* **2019**, *21*, 581–592. [[CrossRef](#)]
27. Han, C.; Kang, H.; Yi, J.; Kang, M.; Lee, H.; Kwon, Y.; Jung, J.; Lee, J.; Park, J. Single-vesicle imaging and co-localization analysis for tetraspanin profiling of individual extracellular vesicles. *J. Extracell. Vesicles* **2021**, *10*, e12047. [[CrossRef](#)] [[PubMed](#)]
28. Jeong, H.; Han, C.; Cho, S.; Gianchandani, Y.; Park, J. Analysis of Extracellular Vesicles Using Coffee Ring. *ACS Appl. Mater. Interfaces* **2018**, *10*, 22877–22882. [[CrossRef](#)] [[PubMed](#)]
29. Kovalenko, O.V.; Yang, X.; Kolesnikova, T.V.; Hemler, M.E. Evidence for specific tetraspanin homodimers: Inhibition of palmitoylation makes cysteine residues available for cross-linking. *Biochem. J.* **2004**, *377*, 407–417. [[CrossRef](#)]
30. Hadjiargyrou, M.; Kaprielian, Z.; Kato, N.; Patterson, P.H. Association of the Tetraspan Protein CD9 with Integrins on the Surface of S-16 Schwann Cells. *J. Neurochem.* **2002**, *67*, 2505–2513. [[CrossRef](#)]
31. Kern, S.; Eichler, H.; Stoeve, J.; Klüter, H.; Bieback, K. Comparative Analysis of Mesenchymal Stem Cells from Bone Marrow, Umbilical Cord Blood, or Adipose Tissue. *Stem Cells* **2006**, *24*, 1294–1301. [[CrossRef](#)] [[PubMed](#)]
32. Wiklander, O.P.B.; Bostancioglu, R.B.; Welsh, J.A.; Zickler, A.M.; Murke, F.; Corso, G.; Felldin, U.; Hagey, D.W.; Evertsson, B.; Liang, X.; et al. Systematic methodological evaluation of a multiplex bead-based flow cytometry assay for detection of extracellular vesicle surface signatures. *Front. Immunol.* **2018**, *9*. [[CrossRef](#)] [[PubMed](#)]
33. Gamperl, H.; Plattfaut, C.; Freund, A.; Quecke, T.; Theophil, F.; Gieseler, F. Extracellular vesicles from malignant effusions induce tumor cell migration: Inhibitory effect of LMWH tinzaparin. *Cell Biol. Int.* **2016**, *40*, 1050–1061. [[CrossRef](#)]
34. Chance, T.C.; Rathbone, C.R.; Kamucheka, R.M.; Peltier, G.C.; Cap, A.P.; Bynum, J.A. The effects of cell type and culture condition on the procoagulant activity of human mesenchymal stromal cell-derived extracellular vesicles. *J. Trauma Acute Care Surg.* **2019**, *87* (Suppl. 1), S74–S82. [[CrossRef](#)]
35. Silachev, D.; Goryunov, K.; Shpilyuk, M.; Beznoschenko, O.; Morozova, N.; Kraevaya, E.; Popkov, V.; Pevzner, I.; Zorova, L.; Evtushenko, E.; et al. Effect of MSCs and MSC-Derived Extracellular Vesicles on Human Blood Coagulation. *Cells* **2019**, *8*, 258. [[CrossRef](#)]
36. Atkin-Smith, G.K.; Tixeira, R.; Paone, S.; Mathivanan, S.; Collins, C.; Liem, M.; Goodall, K.; Ravichandran, K.; Hulett, M.; Poon, I.K. A novel mechanism of generating extracellular vesicles during apoptosis via a beads-on-a-string membrane structure. *Nat. Commun.* **2015**, *6*, 7439. [[CrossRef](#)] [[PubMed](#)]

## 2. FUNCTIONAL PROPERTIES OF MSC-EVs FROM DIFFERENT SOURCES ON ISCHEMIC RENAL REPERFUSION INJURY.

The functional properties of the characterized MSC-EVs described above on renal proximal tubular cell repair were tested in vitro, in a model of IRI.

The study was performed at University of Utrecht in a collaboration with Sandra Calcat i Cervera and João Faria, and the publication of our results is on-going.

### IRI ciPTEC injury model

Ischemic injury ciPTEC model was used. The ciPTEC cells (Figure 4) were obtained by Cell4Pharma (Oss, The Netherlands). The ciPTEC is a human renal cell line (Wilmer et al., 2010) that mimics the proximal tubule cells of the kidney. The cells are main locus of AKI. Due to their partial immortalisation the ciPTEC cells have unlimited proliferation capacity and highly resemblance with human kidney. The cells expressed most relevant protein transporters involved in the functional processes.

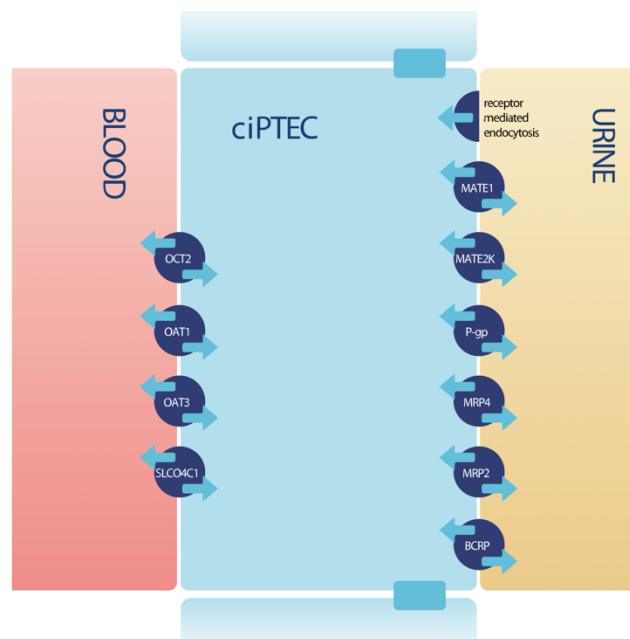


Figure 3: ciPTEC cell illustration <https://cell4pharma.com/technology/ciptec>.

The ischemic injury induced morphological changes, including loss of cytoskeleton and nuclei fragmentation (Figure 5), with increased effects under hypoxic conditions (Figure 5 right panel). At a molecular level, we observed a significant decrease of metabolic activity, ATP production and significant reduction in mitochondrial mass, typical features of IRI (Figure 6).

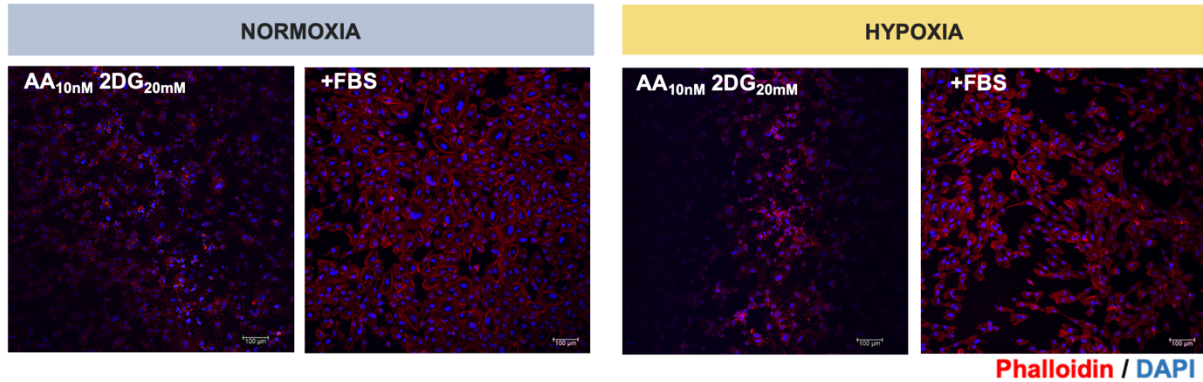


Figure 4: Morphological changes observed by Phalloidin/DAPI staining on ciPTEC cells with ischemic injury and the reperfusion with FBS in normoxia and hypoxia.

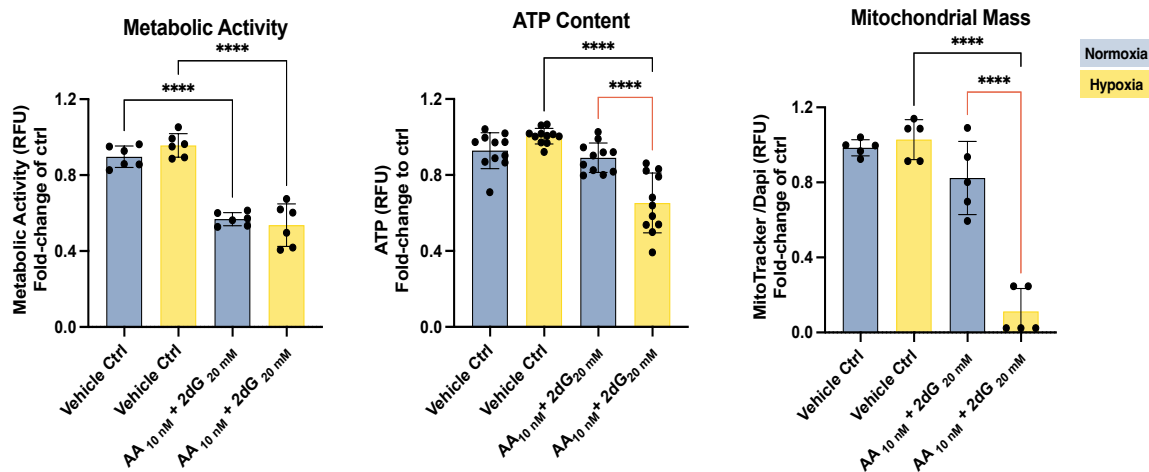


Figure 5: Functional changes observed by assessing metabolic activity, ATP content or mitochondrial mass on ciPTEC cells with ischemic injury in normoxia and hypoxia. Vehicle control are cells without ischemic injury.

During the reperfusion phase, ciPTECs were treated either with Conditioned Medium or with EV fractions from MSC obtained from adipose tissue (AT), bone marrow (BM) or umbilical cord (UC).

BM and UC by-products partially reverted the morphological alterations (Figure 7), specially under normoxia conditions. No differences in metabolic activity or mitochondrial mass were observed after treatment with all MSC conditioned, in respect to the injured cells alone (Figure 6). At



variance, a significant restoration of ATP production was induced by treatment with conditioned medium, with no differences regarding cell source (Figure 8).

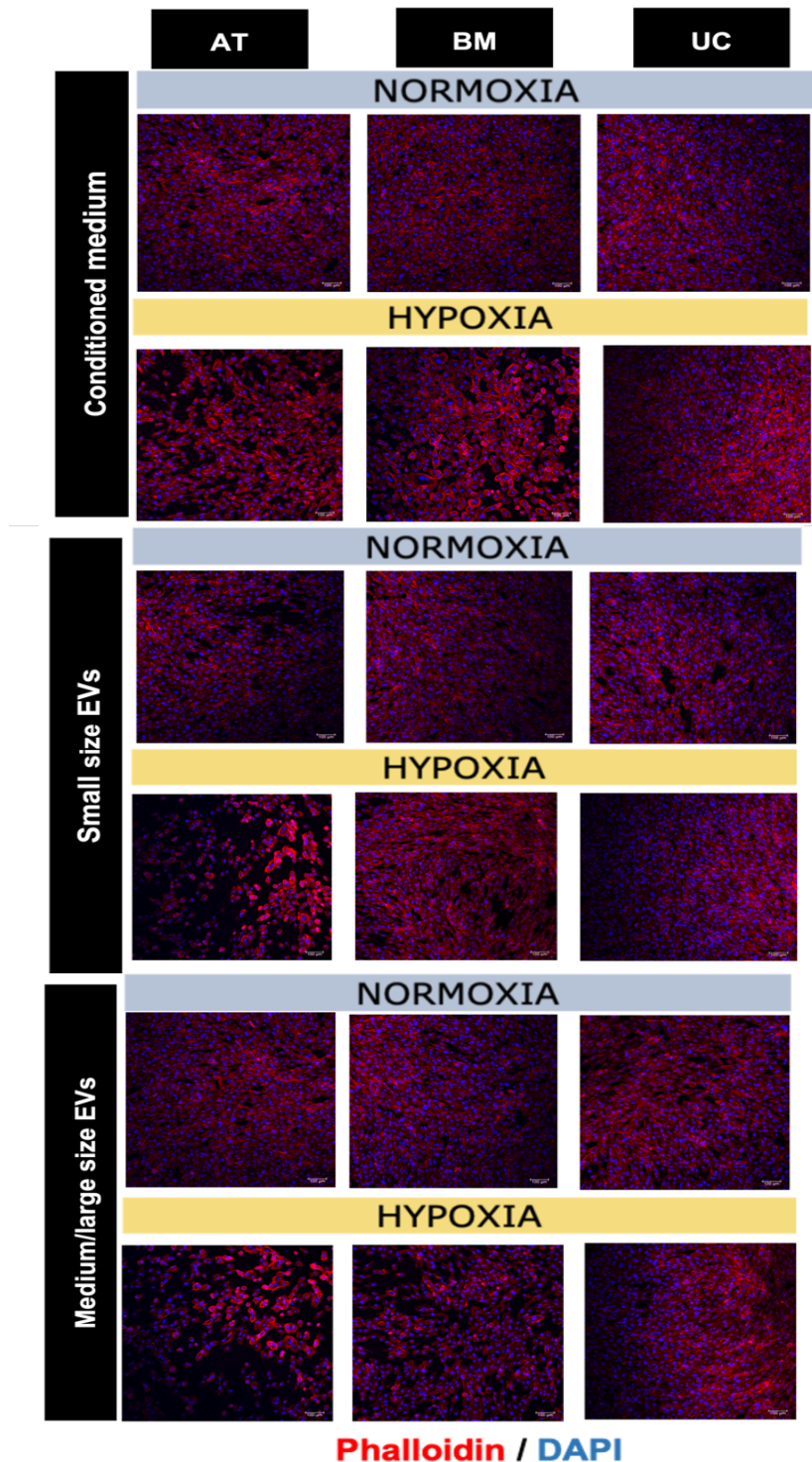
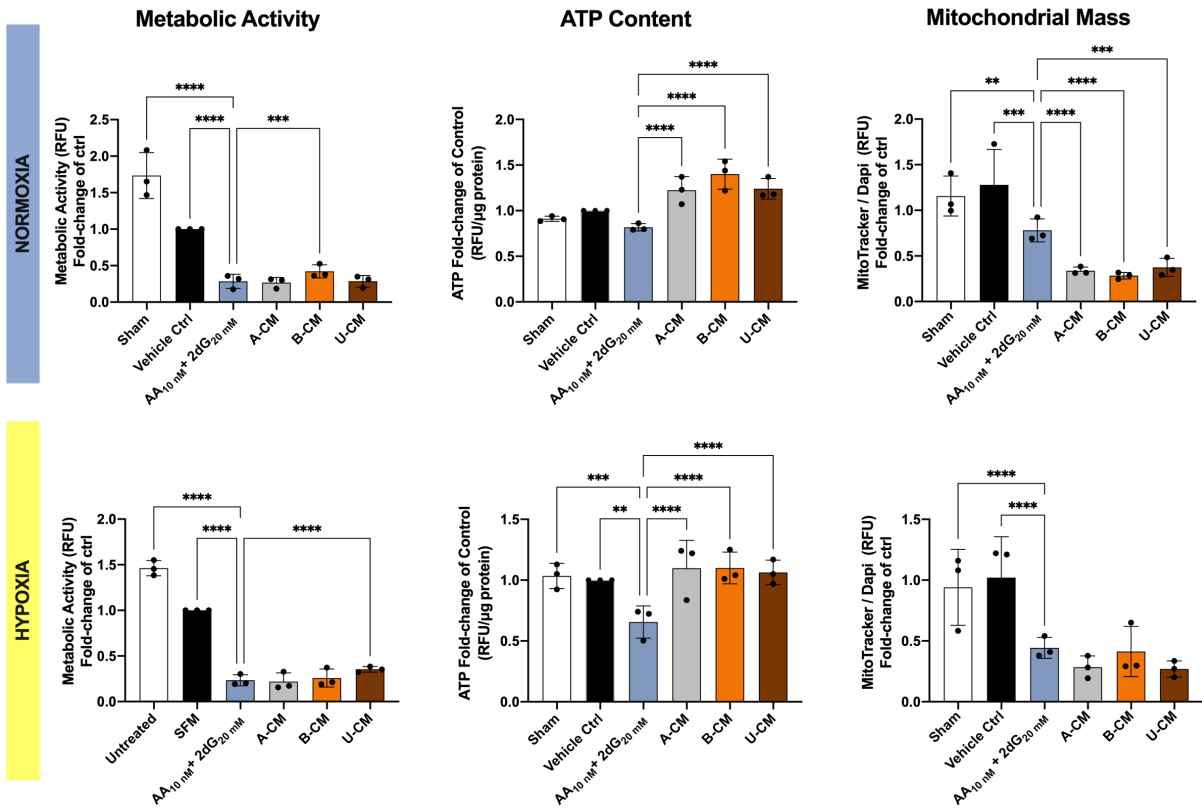
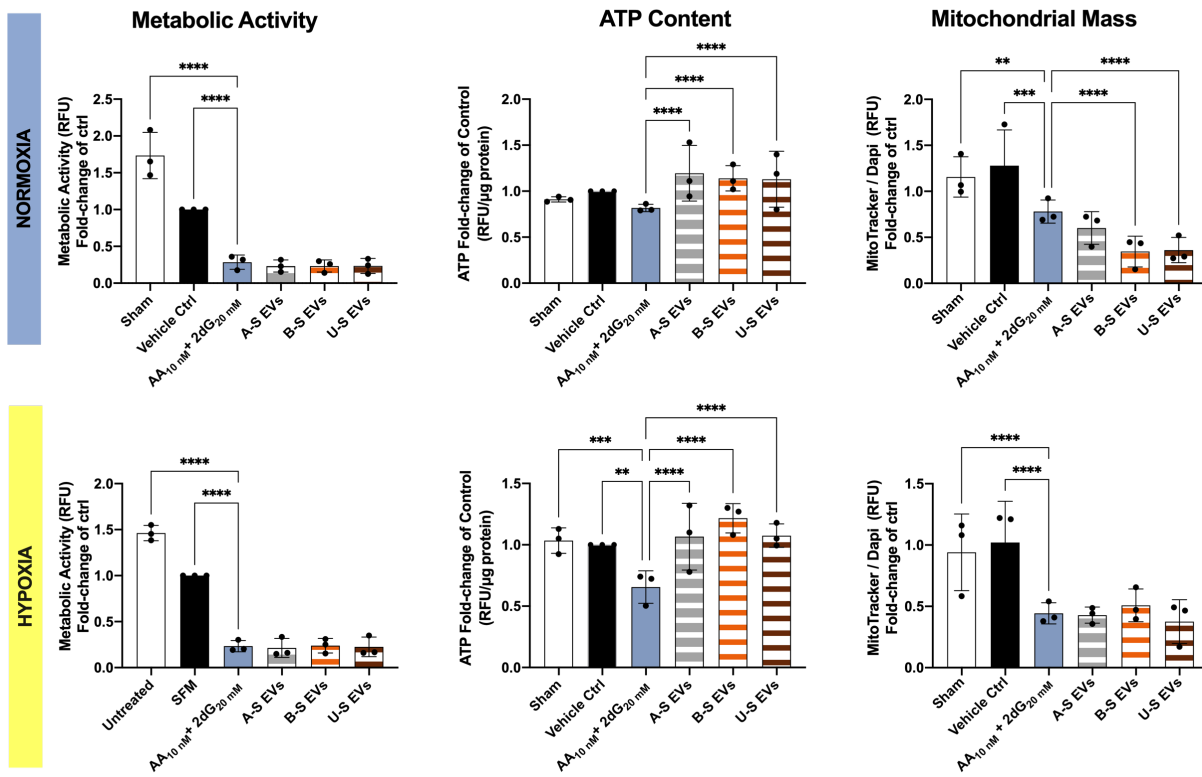


Figure 6: Illustrative images of morphological changes observed by Phalloidin/DAPI staining on ciPTEC cells with ischemic injury after the reperfusion with conditioned medium, small size EVs or medium/large size EVs in normoxia and hypoxia.

CONDITIONED MEDIA



Small size EVS



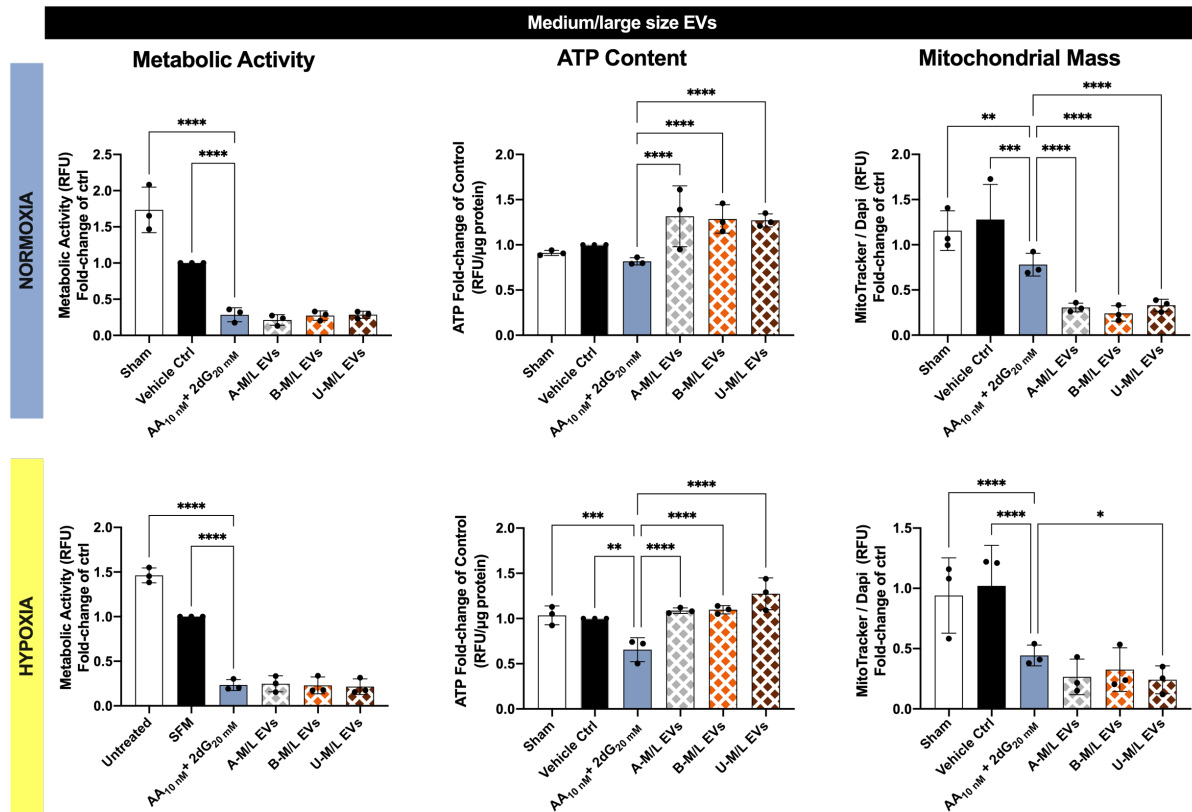


Figure 7: Functional assays performed after the reperfusion phase in IRI ciPTEC model. Among the treatment with conditioned media, small size EVs or medium/large size EVs we did not observe significant amelioration in the metabolic activity or mitochondrial mass. The significant restoration was observed for ATP production by all the treatments.

The effect of the conditioned medium in toto was then compared with the effect of small and large MSC-EVs from the three different sources. The results confirmed the observation obtained with the conditioned medium, showing a specific effect on ATP levels of the three MSC-EV sources, with no differences on originating cell type or EV fraction.

## Conclusions

Our findings showed that our in vitro model was capable of replicating in vivo-like morphological and molecular changes observed during IRI. Following MSC treatment with condition media, small size EVs or medium/large size EVs, a specific effect on ATP production was induced, demonstrating MSC's ability to ameliorate proximal tubule damage caused by ischemic/reperfusion conditions.

### 3. CHARACTERIZATION AND FUNCTIONAL PROPERTIES OF ADIPOSE TISSUE DERIVED MSC PRODUCTS UNDER CULTURE IN 2D AND IN A BIOREACTOR.

The aim of this collaborative project was to compare different MSCs culturing conditions and their EVs or conditioned medium.

#### i. Bioproducts generation

AT MSCs were cultured in parallel in three independent laboratories using the same medium, in standard 2D culture conditions or in a bioreactor (Figure 9). From the cells cultured on plastic adhesion, we collected the conditioned medium, that was either concentrated (10x) or used to isolate EVs by ultracentrifugation. At variance, from the MSCs cultured in the bioreactor, the EVs were isolated using size-exclusion chromatography.

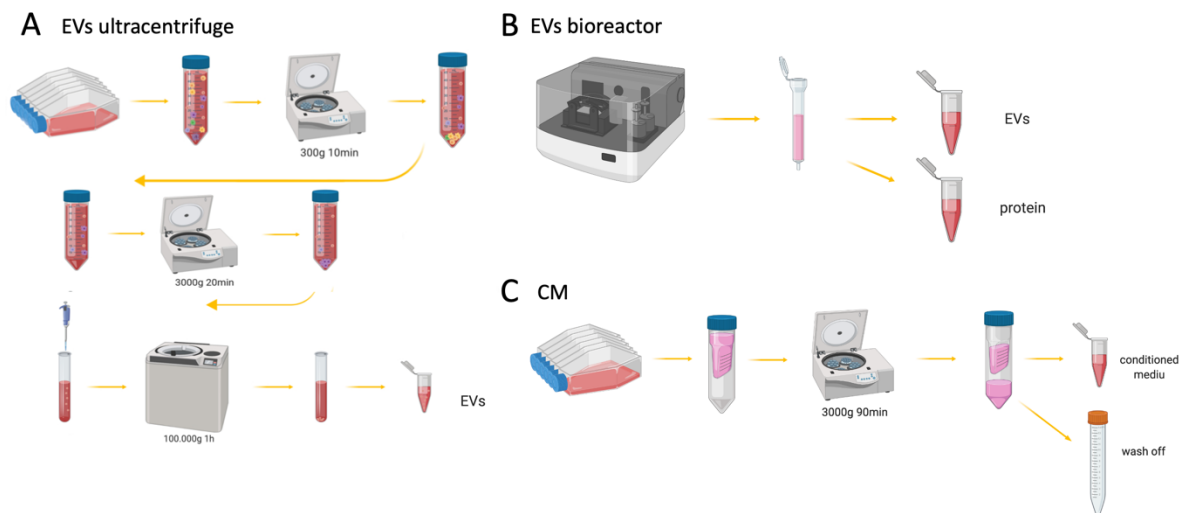


Figure 8: Scheme of bioproducts generation. (A) EVs extracted by ultracentrifugation. (B) EVs from bioreactor extracted by size-exclusion chromatography. (C) Extraction and concentration of conditioned medium.

#### ii. Characterization of AT-MSC EVs

We compared products from three different MSCs donors (sample code 31, 87, 95). As measured by nanoparticle tracking analysis, particle concentration was observed in all samples, including the isolated EVs from 2D plastic or bioreactor culture condition, and conditioned

medium. However, a high particle concentration was also observed in the wash-off (negative control) obtained during the processing of conditioned medium (Table 1).

Table 1: Concentration of AT MSC particles measured by Nanosight. Values shown are particles/ml of a sample.

Sample code	Ultracentrifuged 2D EVs	SEC bioreactor EVs	Protein from bioreactor	Conditioned medium 2D	wash-off 2D
31	$2.60 \times 10^8$	$5.33 \times 10^9$	$9.72 \times 10^8$	$6.27 \times 10^8$	$4.24 \times 10^9$
87	$2.68 \times 10^8$	$3.02 \times 10^8$	$2.34 \times 10^8$	$5.12 \times 10^8$	$1.36 \times 10^9$
95	$2.58 \times 10^8$	$2.16 \times 10^9$	$1.52 \times 10^9$	$7.24 \times 10^8$	$1.15 \times 10^9$

Due to the fact that this technique appears quite unspecific, we proceeded with flow cytometry analysis of the samples to better understand the composition.

The flow cytometry revealed variable expression of tetraspanins (Figure 10). Higher expression of the CD9 and CD63 was observed in the samples from bioreactor and conditioned medium from 2D plastic (CM). The graphs also show no expression of the EV markers in the negative control (WO) which demonstrate non specificity of the particle count obtained by Nanosight (Table 1).

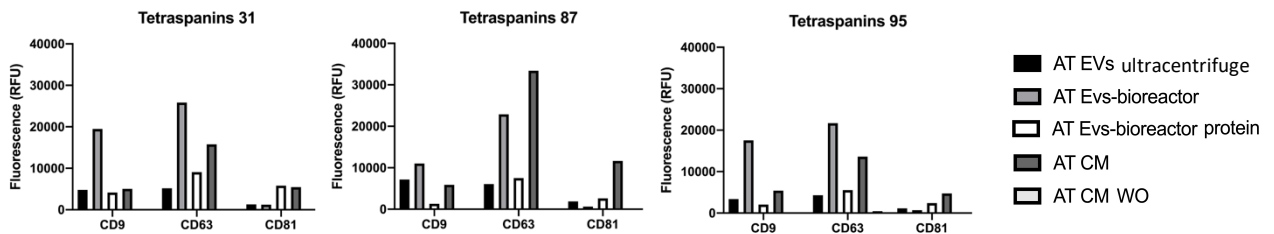


Figure 9: Flow cytometric analysis of tetraspanin surface marker expression on AT MSC EVs. Data are shown divided into 3 graphs depending on the origin of the samples. Each graph demonstrates the differences between the type of EVs from the same donor.

We next assessed the expression of the typical mesenchymal marker by the different MSC-bioproducts (Figure 11). The expression the CD44 and CD29 showed similar levels among the bioproduct samples. Instead CD49e, CD146 and CD105 were almost exclusively present on the EVs from ultracentrifuge.

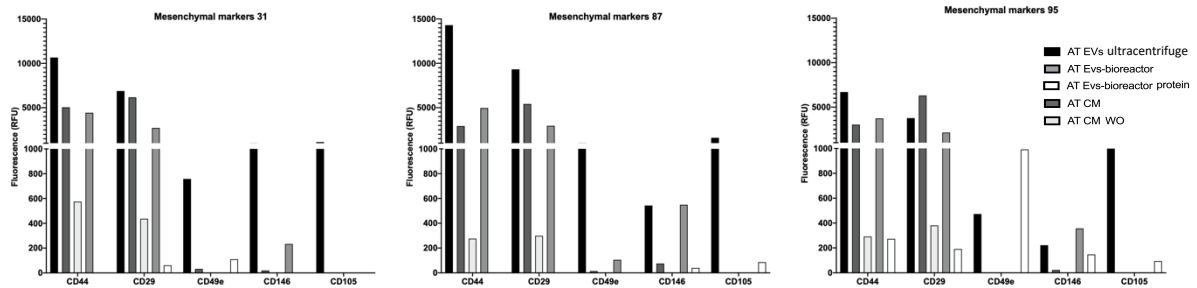


Figure 10: Flow cytometric analysis of mesenchymal marker expression on AT MSC EVs. Data are shown divided into 3 graphs depending on the origin of the samples. Each graph demonstrates the differences between the type of EVs from the same donor.

Analysing the immunological markers (Figure 12), we observed similar levels of CD29, MCSP, ROR1 for all bioproduct samples from all three donors. Instead CD142 (tissue factor) is exclusively present on the EVs isolated by ultracentrifuge and CD133-1 on bioreactor EVs. All these data will be confirmed by single EV flow cytometry performed by the other institute of the interlab comparison.

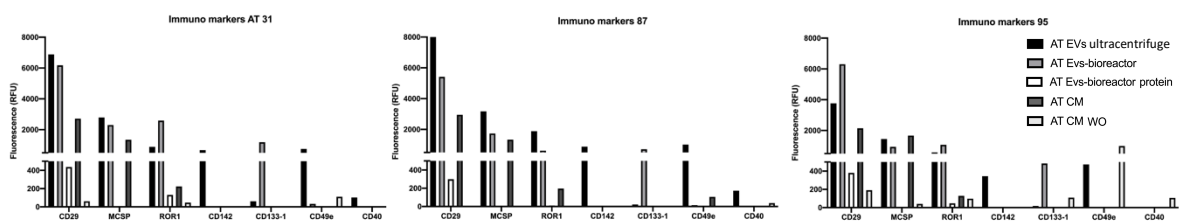


Figure 11: Flow cytometric analysis of immune surface marker expression on AT MSC EVs. Data are shown divided into 3 graphs depending on the origin of the samples. Each graph demonstrates the differences between the type of EVs.

Characterisation of the surface markers and size of the particles was confirmed by super-resolution microscopy (Figure 13 B). We decided to test CD44 marker which showed high expression in the flow cytometry assay. All three bioproducts were positive to tetraspanin and

CD44 expression. The bioreactor EVs showed different marker composition compared to ultracentrifuge EVs and to conditioned medium. Most of the particles were single tetraspanin positive, being the ultracentrifuge EVs and those in the conditioned medium mainly CD81 positive, whereas the bioreactor EVs mainly CD9 positive.

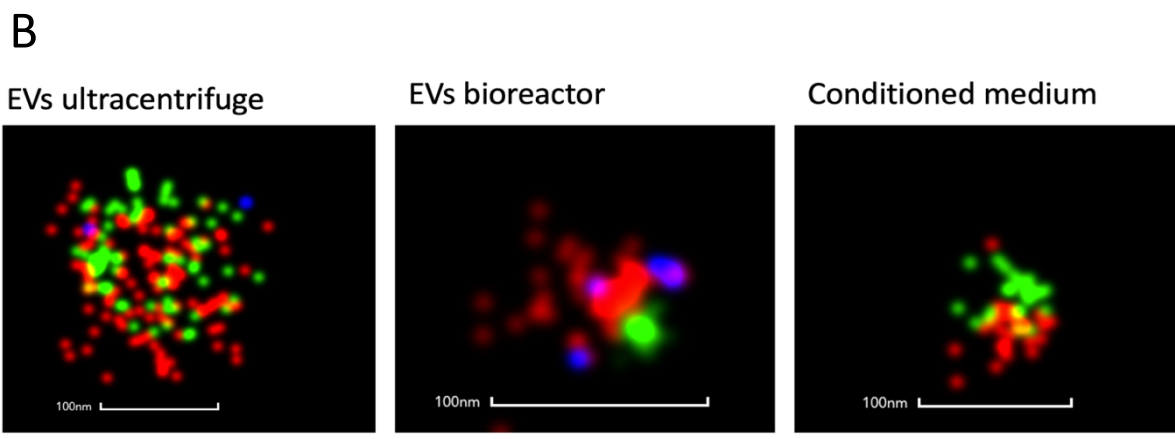
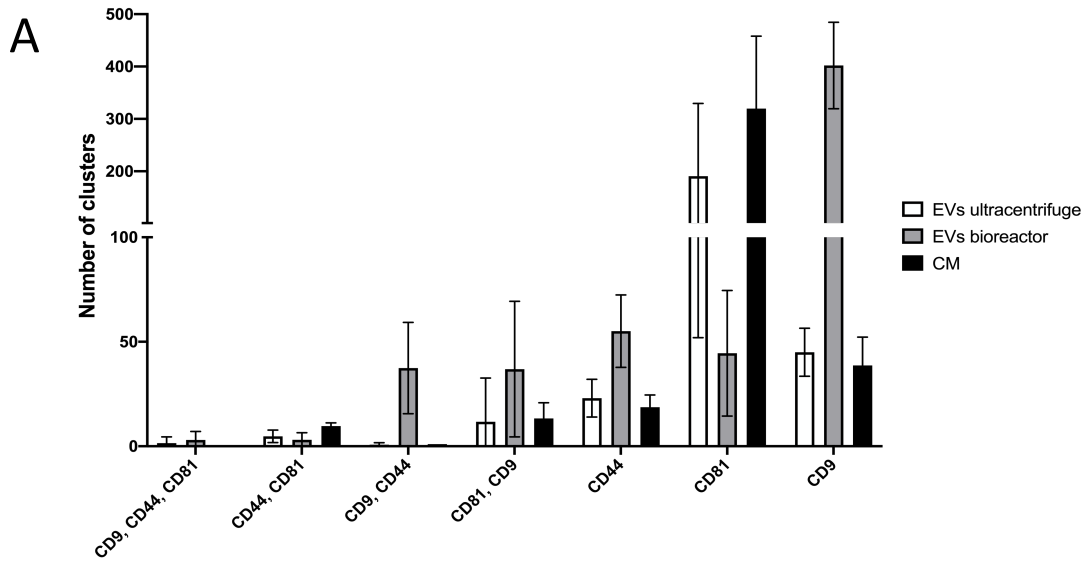


Figure 12: Super-resolution microscopy analysis of tetraspanins expression in AT MSC EVs from different preparation. A) Clustering analysis of super-resolution microscopy images showing the single, double and triple positive EV fractions expressing the tetraspanin markers. The analyses were performed using a CODI software; the graph shows the mean±SD of a cumulative analysis of 3 fields for each preparation. B) Representative super-resolution microscopy images of AT MSC EVs showing triple or double expression of CD44 (green), CD81 (red), CD9 (blue). The corresponding scale bare is below each EV image.

iii. Functional comparison of AT-MSC-EVs using an angiogenic assay.

As a functional analysis the HUVEC tubule formation was performed. The complete conditioned medium showed the highest tubule formation with the highest number of the branches. Also in this assay, the wash off showed negative results and confirmed that the samples were deprived of any functional molecules. In analogy, the protein extract obtained from bioreactor showed high induction for the tubule formation (Figure 14). As expected, EVs had the lowest potential to form the tubules, being EVs isolated with SEV the less angiogenic. These data will be confirmed in both collaboration laboratories to confirm the results.

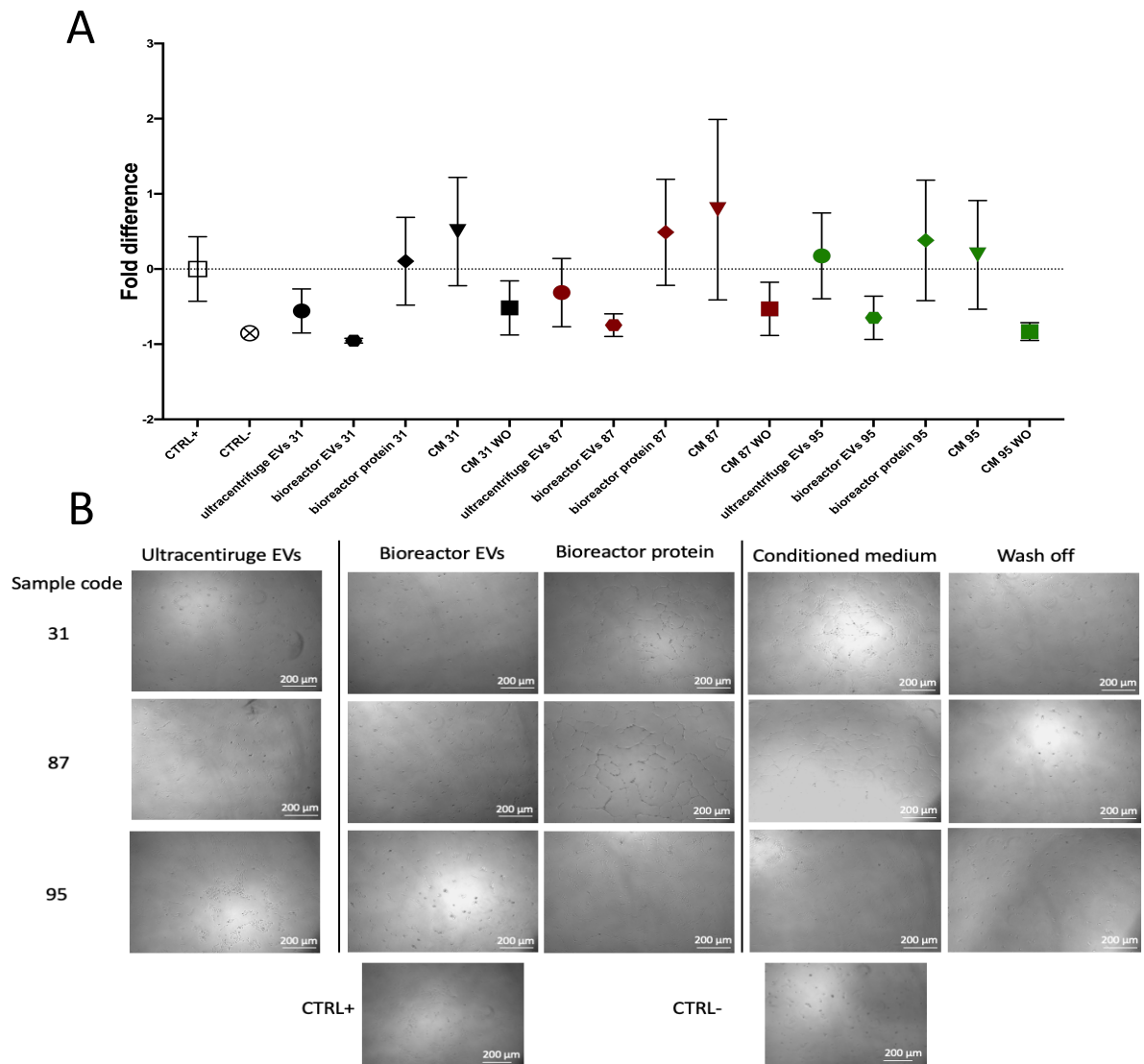


Figure 13: Effect of ultracentrifuge EVs, bioreactor EVs, bioreactor protein, conditioned medium or wash-off on HUVEC tube formation. A) Quantification of tube lengths of HUVEC treated by samples derived from double concentration of cells (HUVEC:MSCs - 1:2). Positive control: EndoGROW medium with 10ng of VEGF and 5% of serum; negative control: EndoGROW medium without FBS and VEGF. B) Representative micrographs of the tube formation assay.



## **Conclusions**

We compared the three different bioproducts derived from the same donor and passage number of adipose tissue mesenchymal cells. The cells were shipped across the three sites, this might add some variable in this project because the shipment cannot be additionally controlled than using the standard methods of cell shipment. From the cells cultured traditionally in the 2D setting we obtained the EVs by ultracentrifugation and whole concentrated conditioned medium. Instead from the 3D culture condition in bioreactor the EVs were successfully isolated using size exclusion chromatography.

The results reveal different surface marker proportion between the bioproducts, possibly due to different isolation technique. Tissue factor and CD105 markers were exclusively present on the EVs from ultracentrifuge. Finally, our data confirmed previous results showing that the angiogenic properties of EVs are associated with growth factors present in the conditioned medium of the plastic culture/proteins of the bioreactor (Shabbir, Cox, Rodriguez-Menocal, Salgado, & Van Badiavas, 2015), and indicate that SEC isolation generates purer EVs. Other functional assay to compare EVs from cells cultured in the different conditions will be performed.

#### 4. CHARACTERISATION OF EVs AT SINGLE EV LEVEL

In my PhD study, I dedicated extensively to the set-up of super-resolution microscopy and ExoView array-based analyses for a surface marker characterisation of single EVs derived from different sources. I characterized several EV preparations from biofluids and from cell cultures.

In particular, my results contributed to the characterization amniotic fluid EVs and of spike-expressing EVs.

**Article: ‘Single extracellular vesicle analysis in human amniotic fluid shows evidence of phenotype alterations in preeclampsia’** Natalia Gebara, Julia Scheel, **Renata Skovronova**, Cristina Grange, Luca Marozio, Shailendra Gupta, Veronica Giorgione, Federico Caicci, Chiara Benedetto, Asma Khalil, Benedetta Bussolati, *Journal of Extracellular Vesicles*, 2022

We used ONi super-resolution microscope to analyse EVs derived from amniotic fluid. The aim was to understand the possible differences between HLA-G and tetraspanins expression on EVs derived from amniotic fluid of normal pregnancy (Gebara et al., 2022). The figure shows the heterogeneous population of triple, double and single positive EVs for tetraspanins with the majority of CD81, CD9 double positive (Figure 15). We also demonstrated the CD63, HLA-G double positivity of most of the EVs from the stained population (Figure 16).

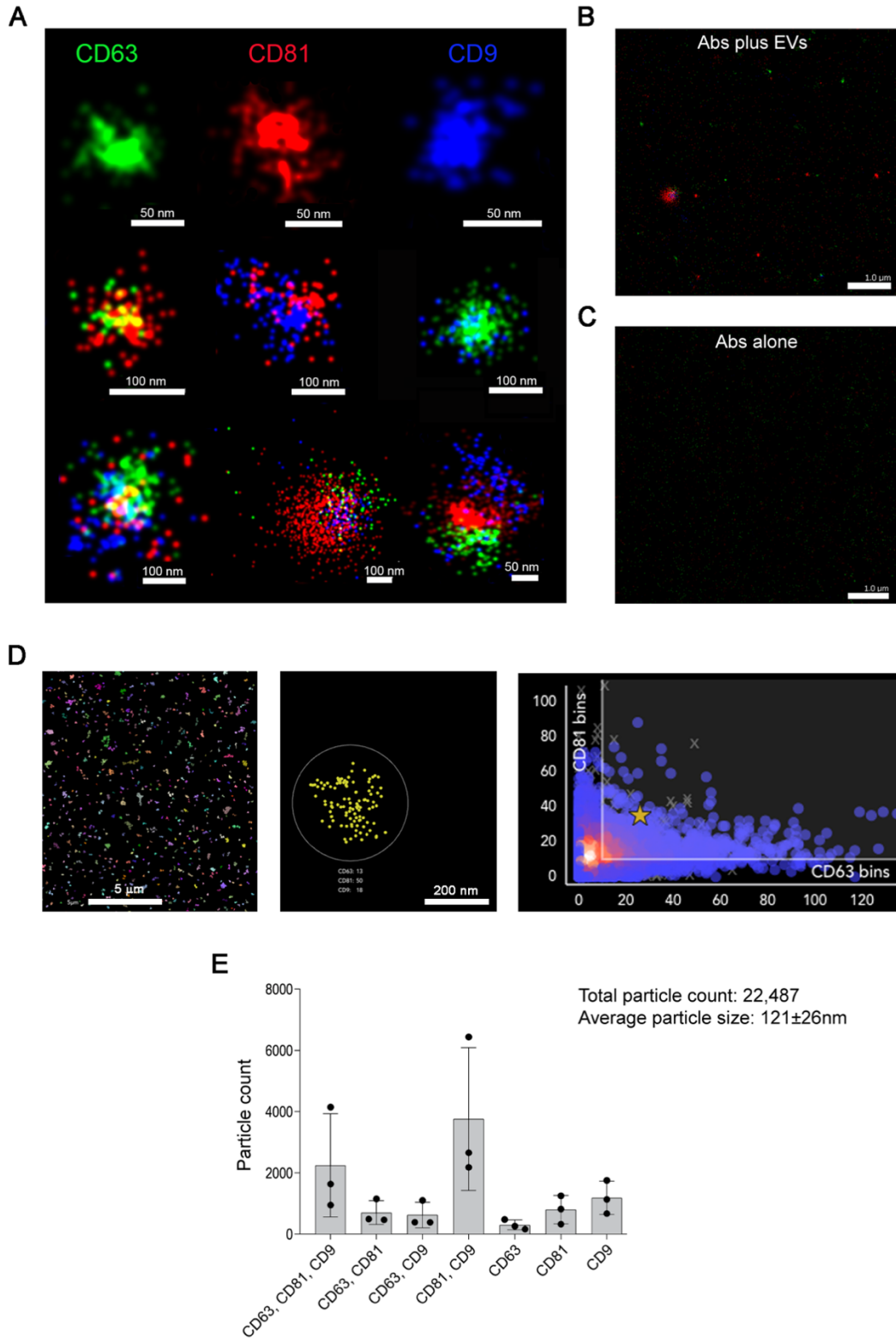


Figure 15: Super-resolution microscopy analysis of tetraspanins expression in NP-EVs. (A) Representative super-resolution microscopy images of NP-EVs showing single, double, and triple expression of CD63 (green), CD81 (red), CD9 (blue). The corresponding scale bare is below each EV image. (B) Representative super-resolution images, at low magnification, showing staining with anti-tetraspanin antibodies in the presence of EVs (EVs plus Abs) or (C) in the absence of EVs (Abs alone). (D) Representative clustering strategy of NP-EV analysis showing a large field of view (left panel), a

selected cluster (right panel) and a graph (bottom panel) of CD81/CD63 cluster distribution. (E) Clustering analysis of super-resolution microscopy images showing the single, double, and triple positive EV fractions expressing the tetraspanin markers. The analyses were performed in three NP-EV preparations using a CODI software; the graph shows the mean  $\pm$  SD of a cumulative analysis of 10 fields for each preparation.

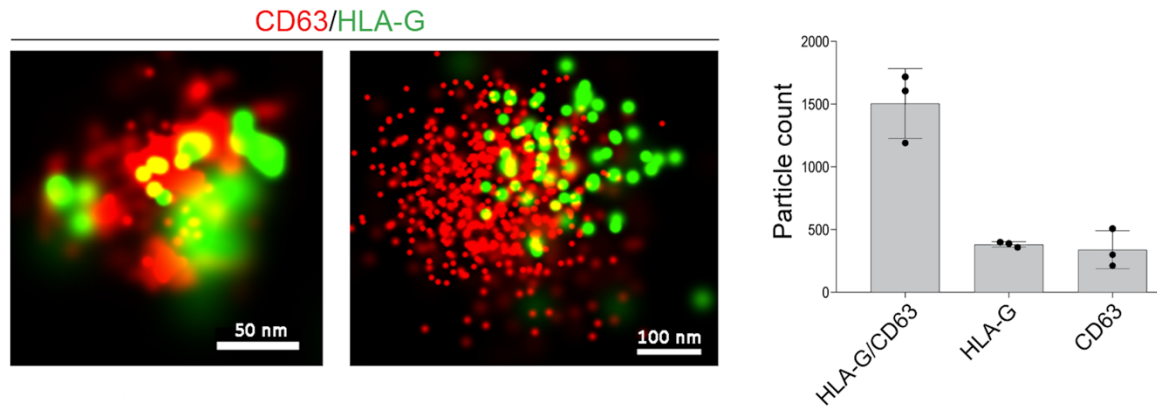


Figure 16: Representative super-resolution microscopy images of single amniotic fluid-derived EVs expressing CD63 (red) and HLA-G (green). The number of single and double positive EVs for CD63 and HLA-G was analysed in three NP-EV preparations using the CODI software; the graph shows the mean  $\pm$  SD of a cumulative analysis of 10 fields for each preparation, total EV number: 6676.

We subsequently used chip based ExoView technology to confirm the co-expression of HLA-G, Tie-2, CD105 or CD117 with tetraspanins (Figure 17A). Samples used were from normal pregnancy (NP-EVs) and from preeclampsia (PE-EVs). The analysis confirmed the presence of HLA-G, as shown by super-resolution microscopy, and revealed the presence of the angiogenic marker Tie-2 and of the stem cell marker CD117 on both NP- and PE-EVs (Figure 17B). The analysis showed that the HLA-G expressing EVs displayed similar CD105 and c-kit markers levels, suggesting that the increased CD105 expressing EVs present in PE were not of placental origin (Figure 17C). At variance, Tie-2 levels were significantly lower in placental EVs of PE pregnancies. Results were confirmed using amniotic fluid stem cells (Figure 18).

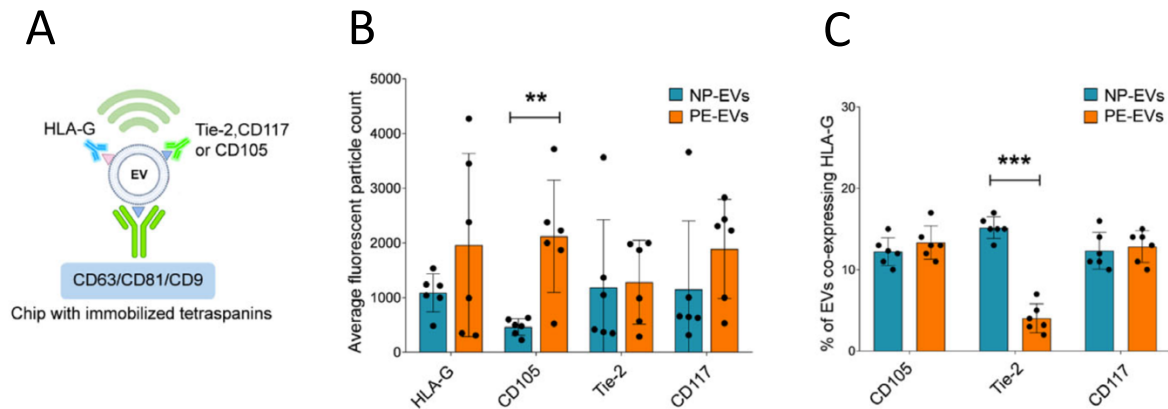


Figure 17: (A) Diagram explaining the experimental method behind ExoView technology in relation to the graphs in panel B. (B and C) ExoView analysis of amniotic fluid-derived NP-EVs ( $n = 6$ ) and PE-EVs ( $n = 6$ ). (B) Comparison of the expression of HLA-G, Tie-2, CD105 and CD117 (c-kit) shown as average fluorescent particle count in NP-EVs vs PE-EVs from combined tetraspanins capture of CD63, CD81 and CD9. (C) Normalized expression of HLA-G positive EVs co-expressing other angiogenic (CD105 and Tie-2) and stem cell (CD117) markers.  $5.8 \times 10^8$  EVs in final volume of 35  $\mu$ l of buffer were used for all samples. Unpaired student's t-test: \* =  $P < 0.05$ , \*\* =  $P < 0.01$ , \*\*\* =  $P < 0.001$ .

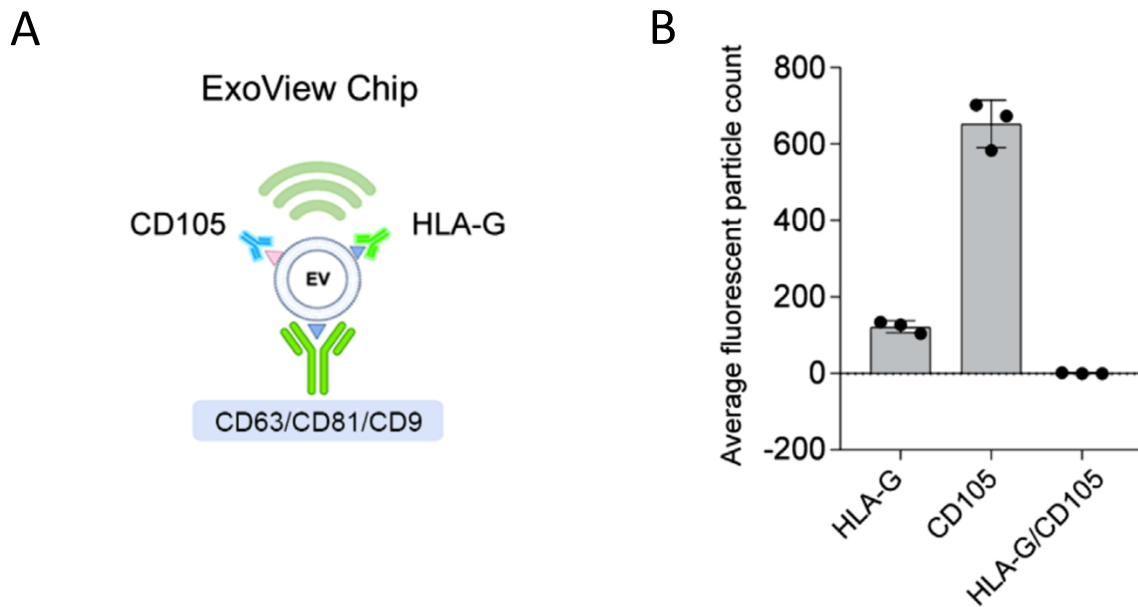


Figure 18: Characterization of HLA-G expressing EVs from term AFSCs. (A) Diagram explaining the experimental method in relation to the graph in panel b. (B) Fluorescent particle count of AFSC-EVs captured on tetraspanin-coated chip analysed by ExoView, showing expression of HLA-G+ and CD105+ EVs, but lack of co-expression of the markers.

**Article: ‘Generation of Spike-Extracellular Vesicles (S-EVs) as a Tool to Mimic SARS-CoV-**

**2 Interaction with Host Cells’** Roberta Verta, Cristina Grange, **Renata Skovronova**, Adele Tanzi,

Licia Peruzzi, Maria Chiara Deregibus, Giovanni Camussi and Benedetta Bussolati, Cells, 2022

We also used super-resolution nanoimager ONi to characterise the engineered Spike-Extracellular Vesicles. The aim was to confirm the engineering process with Spike vector and to further understand the percental positivity of the spike expression in the single EV population from spike transfected cells (Verta et al., 2022). We confirmed the spike expression coupled with one or two tetraspanins and by software analysis we quantified the total number of spike positive EVs in the population between 35-43% (Figure 19).

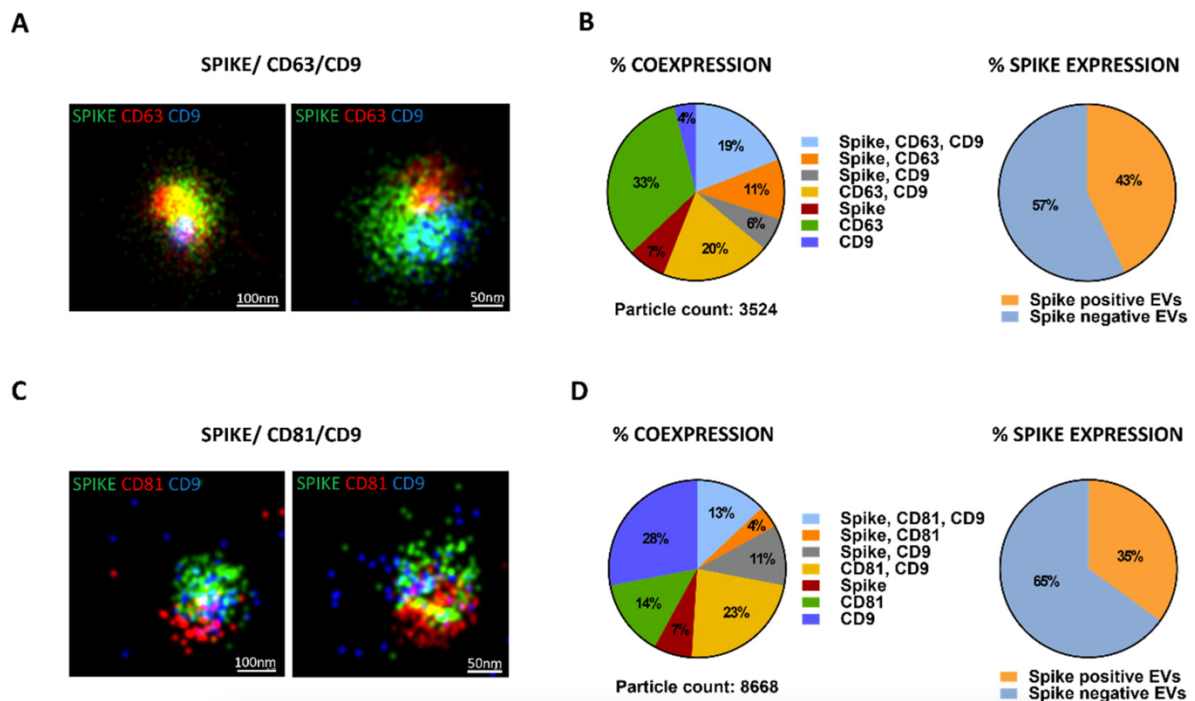


Figure 19: Super-resolution microscopy analysis of EVs isolated from H-S. (A) The percentage of EVs in triple, double or single positivity for spike, CD63, CD9 markers and the total percentage of EVs positive or negative for spike protein was reported. (B) Super-resolution microscopy micrographs showing the pattern distribution of spike in green, CD63 in red and CD9 in blue for S-EVs. (C) The percentage of EVs in triple, double or single positivity for spike, CD81, CD9 markers and the total percentage of EVs positive or negative for spike protein was reported. (D) Super-resolution microscopy micrographs showing the pattern distribution of spike in green, CD81 in red and CD9 in blue for S-EVs.

The spike co-expression with CD9, CD63 and CD81, on the EVs surface, was further confirmed using ExoView analysis, with similar expression levels on the single tetraspanin-affinity chips (Figure 20B).

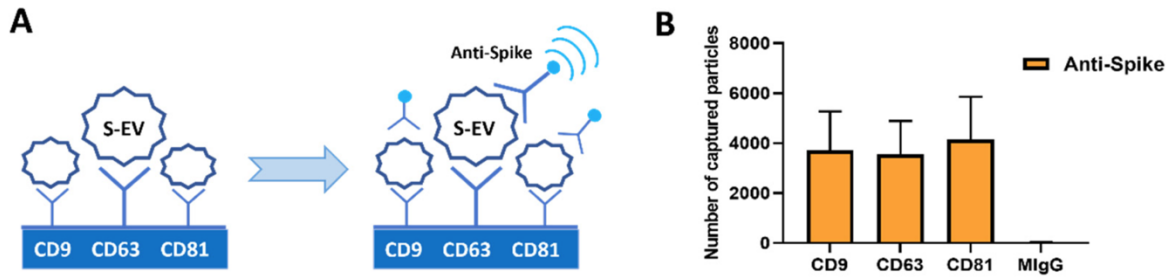


Figure 20: ExoView analysis of S-EVs. (A) Schematic representation of S-EVs detection process for ExoView technique. (B) Number of S-EVs captured on CD9, CD63, CD81 or MIgG spots fluorescently labelled by anti-spike ab in APC obtained by ExoView analysis. The graph shows the average of three independent experiments  $\pm$  SD.

## **LIMITATIONS AND CONCLUSION**



### **Limitations of the study**

The study was limited by the number of MSCs donors due to Covid-19 limitations. In case of MSCs working with primary cells gave us a unique opportunity to examine their properties but also gave us the limitations of passage numbers before the cells change their behaviour. The EVs were stored maximum for 3 months in -80°C which oblige us to collect all the samples shortly before starting the experiments.

### **Conclusion**

The study is divided into 3 separates but well-connected studies from which two of them are performed in collaboration within the consortium. It brings deep morphological characterisation of ultracentrifuge isolated EVs at single EV level from diverse MSCs culture. From phenotypic and functional analyses, the MSC-EVs appeared heterogeneous but consistent among the different sources and fractions for dimension, surface marker expression and functional properties.

**Bibliography:**

- Abebe, A., Kumela, K., Belay, M., Kebede, B., & Wobie, Y. (2021). Mortality and predictors of acute kidney injury in adults: a hospital-based prospective observational study. *Scientific Reports*, *11*(1), 1–8. <https://doi.org/10.1038/s41598-021-94946-3>
- Agarwal, A., Dong, Z., Harris, R., Murray, P., Parikh, S. M., Rosner, M. H., ... Ronco, C. (2016). Cellular and molecular mechanisms of AKI. *Journal of the American Society of Nephrology*, *27*(5), 1288–1299. <https://doi.org/10.1681/ASN.2015070740>
- Brooks, C., Wei, Q., Cho, S. G., & Dong, Z. (2009). Regulation of mitochondrial dynamics in acute kidney injury in cell culture and rodent models. *Journal of Clinical Investigation*, *119*(5), 1275–1285. <https://doi.org/10.1172/JCI37829>
- Calcat-i-Cervera, S., Sanz-Nogués, C., & O'Brien, T. (2021). When Origin Matters: Properties of Mesenchymal Stromal Cells From Different Sources for Clinical Translation in Kidney Disease. *Frontiers in Medicine*, *8*(September). <https://doi.org/10.3389/fmed.2021.728496>
- Cantaluppi, V., Biancone, L., Quercia, A., Deregibus, M. C., Segoloni, G., & Camussi, G. (2013). Rationale of mesenchymal stem cell therapy in kidney injury. *American Journal of Kidney Diseases*, *61*(2), 300–309. <https://doi.org/10.1053/j.ajkd.2012.05.027>
- Charles, C., & Ferris, A. H. (2020). Chronic Kidney Disease. *Primary Care: Clinics in Office Practice*, *47*(4), 585–595. <https://doi.org/https://doi.org/10.1016/j.pop.2020.08.001>
- Doyle, J. F., & Forni, L. G. (2016). Acute kidney injury: Short-term and long-term effects. *Critical Care*, *20*(1), 1–7. <https://doi.org/10.1186/s13054-016-1353-y>
- Elahi, F. M., Farwell, D. G., Nolte, J. A., & Anderson, J. D. (2020). Preclinical translation of exosomes derived from mesenchymal stem/stromal cells. *Stem Cells*, *38*(1), 15–21. <https://doi.org/10.1002/stem.3061>
- Eltzschig, H. K., & Eckle, T. (2011). Ischemia and reperfusion—from mechanism to translation. *Nature Medicine*, *17*(11), 1391–1401. <https://doi.org/10.1038/nm.2507>
- Gatti, S., Bruno, S., Deregibus, M. C., Sordi, A., Cantaluppi, V., Tetta, C., & Camussi, G. (2011). Microvesicles derived from human adult mesenchymal stem cells protect against ischaemia-reperfusion-induced acute and chronic kidney injury. *Nephrology Dialysis Transplantation*, *26*(5), 1474–1483. <https://doi.org/10.1093/ndt/gfr015>
- Gebara, N., Rossi, A., Skovronova, R., Aziz, J. M., Asthana, A., & Bussolati, B. (2020). Extracellular Vesicles, Apoptotic Bodies and Mitochondria: Stem Cell Bioproducts for Organ Regeneration. *Current Transplantation Reports*, *7*(2), 105–113. <https://doi.org/10.1007/s40472-020-00282-2>
- Gebara, N., Scheel, J., Skovronova, R., Grange, C., Marozio, L., Gupta, S., ... Bussolati B., (2022). Single extracellular vesicle analysis in human amniotic fluid shows evidence of phenotype alterations in preeclampsia. *Journal of Extracellular Vesicles*, *2022.02.14.480331*. <https://doi.org/10.1002/jev2.12217>
- Grange, C., Skovronova, R., Marabese, F., & Bussolati, B. (2019). Stem cell-derived extracellular vesicles and kidney regeneration. *Cells*, *8*(10), 1–13. <https://doi.org/10.3390/cells8101240>
- Heldring, N., Mäger, I., Wood, M. J. A., Le Blanc, K., & Andaloussi, S. E. L. (2015). Therapeutic Potential of Multipotent Mesenchymal Stromal Cells and Their Extracellular Vesicles. *Human Gene Therapy*, *26*(8), 506–517. <https://doi.org/10.1089/hum.2015.072>
- Heyman, S. N., Rosenberger, C., & Rosen, S. (2011). Acute kidney injury: Lessons from experimental models. *Contributions to Nephrology*, *169*, 286–296.

- <https://doi.org/10.1159/000313957>
- Jassem, W., Fuggle, S. V., Rela, M., Koo, D. D. H., & Heaton, N. D. (2002). The role of mitochondria in ischemia/reperfusion injury. *Transplantation*, *73*(4), 493–499. <https://doi.org/10.1097/00007890-200202270-00001>
- Jiang, M., Bai, M., Lei, J., Xie, Y., Xu, S., Jia, Z., & Zhang, A. (2020). Mitochondrial dysfunction and the AKI-to-CKD transition. *American Journal of Physiology - Renal Physiology*, *319*(6), F1105–F1116. <https://doi.org/10.1152/AJPRENAL.00285.2020>
- Li, X., Liu, C., Mao, Z., Li, Q., & Zhou, F. (2021). Timing of renal replacement therapy initiation for acute kidney injury in critically ill patients: a systematic review of randomized clinical trials with meta-analysis and trial sequential analysis. *Critical Care*, *25*(1), 1–15. <https://doi.org/10.1186/s13054-020-03451-y>
- Lv, J. C., & Zhang, L. X. (2019). Prevalence and Disease Burden of Chronic Kidney Disease. In *Advances in Experimental Medicine and Biology* (Vol. 1165). [https://doi.org/10.1007/978-981-13-8871-2\\_1](https://doi.org/10.1007/978-981-13-8871-2_1)
- Malek, M., & Nematbakhsh, M. (2015). Renal ischemia/reperfusion injury; from pathophysiology to treatment. *Journal of Renal Injury Prevention*, *4*(2), 20–27. <https://doi.org/10.12861/jrip.2015.06>
- Martin, J. L., Gruszczuk, A. V., Beach, T. E., Murphy, M. P., & Saeb-Parsy, K. (2019). Mitochondrial mechanisms and therapeutics in ischaemia reperfusion injury. *Pediatric Nephrology*, *34*(7), 1167–1174. <https://doi.org/10.1007/s00467-018-3984-5>
- Rabb, H. (2012). The promise of immune cell therapy for acute kidney injury. *Journal of Clinical Investigation*, *122*(11), 3852–3854. <https://doi.org/10.1172/JCI66455>
- Selby, N. M., Fluck, R. J., Kolhe, N. V., & Taal, M. W. (2016). International Criteria for Acute Kidney Injury: Advantages and Remaining Challenges. *PLoS Medicine*, *13*(9), 1–8. <https://doi.org/10.1371/journal.pmed.1002122>
- Shabbir, A., Cox, A., Rodriguez-Menocal, L., Salgado, M., & Van Badiavas, E. (2015). Mesenchymal Stem Cell Exosomes Induce Proliferation and Migration of Normal and Chronic Wound Fibroblasts, and Enhance Angiogenesis in Vitro. *Stem Cells and Development*, *24*(14), 1635–1647. <https://doi.org/10.1089/scd.2014.0316>
- Shen, B., Liu, J., Zhang, F., Wang, Y., Qin, Y., Zhou, Z., ... Fan, Y. (2016). CCR2 Positive Exosome Released by Mesenchymal Stem Cells Suppresses Macrophage Functions and Alleviates Ischemia/Reperfusion-Induced Renal Injury. *Stem Cells International*, *2016*. <https://doi.org/10.1155/2016/1240301>
- Shiva, N., Sharma, N., Kulkarni, Y. A., Mulay, S. R., & Gaikwad, A. B. (2020). Renal ischemia/reperfusion injury: An insight on in vitro and in vivo models. *Life Sciences*, *256*, 117860. <https://doi.org/10.1016/J.LFS.2020.117860>
- Smith, R. A. J., Hartley, R. C., Cochemé, H. M., & Murphy, M. P. (2012). Mitochondrial pharmacology. *Trends in Pharmacological Sciences*, *33*(6), 341–352. <https://doi.org/10.1016/j.tips.2012.03.010>
- Verta, R., Grange, C., Skovronova, R., Tanzi, A., Peruzzi, L., Deregibus, M. C., ... Bussolati, B. (2022). Generation of Spike-Extracellular Vesicles (S-EVs) as a Tool to Mimic SARS-CoV-2 Interaction with Host Cells. *Cells*, *11*(1), 1–16. <https://doi.org/10.3390/cells11010146>
- Wilmer, M. J., Saleem, M. A., Masereeuw, R., Ni, L., Van Der Velden, T. J., Russel, F. G., ... Levtchenko, E. N. (2010). Novel conditionally immortalized human proximal tubule cell line expressing functional influx and efflux transporters. *Cell and Tissue Research*, *339*(2), 449–457. <https://doi.org/10.1007/s00441-009-0882-y>
- Zhan, M., Brooks, C., Liu, F., Sun, L., & Dong, Z. (2013). Mitochondrial dynamics: Regulatory mechanisms and emerging role in renal pathophysiology. *Kidney International*, *83*(4), 568–581. <https://doi.org/10.1038/ki.2012.441>

Zou, X., Zhang, G., Cheng, Z., Yin, D., Du, T., Ju, G., ... Zhu, Y. (2014). Microvesicles derived from human Wharton's Jelly mesenchymal stromal cells ameliorate renal ischemia-reperfusion injury in rats by suppressing CX3CL1. *Stem Cell Research and Therapy*, 5(2), 1–13. <https://doi.org/10.1186/scrt428>